BESSY

Highlights 2004

Berliner Elektronenspeicherring-Gesellschaft für Synchrotronstrahlung m.b.H.

Member of the Leibniz Association

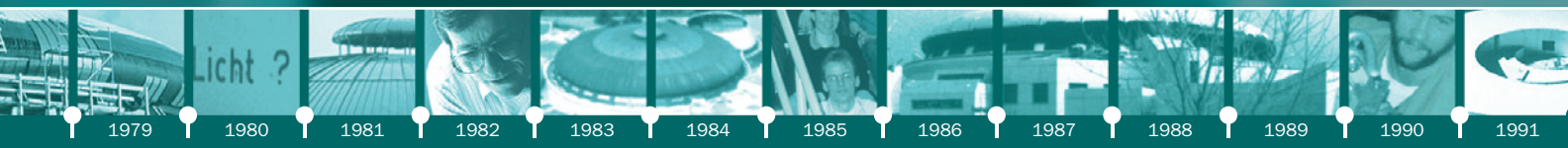

Published by:
Berliner Elektronenspeicherring-Gesellschaft für
Synchrotronstrahlung m.b.H. – BESSY

Albert-Einstein-Straße 15
12489 Berlin, Germany
phone +49 (0)30 / 6392 2999
fax +49 (0)30 / 6392 2990
www.bessy.de
info@bessy.de

Board of Directors:
Prof. Dr. Dr. h.c. Wolfgang Eberhardt,
Prof. Dr. Eberhard Jaeschke,
Thomas Frederking

Editors:
Gabriele André, Dr. Heike Henneken,
Dr. Markus Sauerborn

Layout:
Annette Weber, Stitz & Betz GmbH, Dortmund

ISSN Number: 1611-6127

BESSY

Berliner Elektronenspeicherring-Gesellschaft für Synchrotronstrahlung m.b.H.

Member of the Leibniz Association

1 BESSY Inside 04

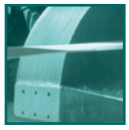

2 Scientific Highlights 06

Surface Sciences 08
Solid State Physics 14
Magnetism 18
Nanosciences 22
Atomic Physics 26
Life Sciences 28
Archeometry 32
Astronomy 34
Micro Engineering 36

3 News & Events 38

4 Optics Special 44

High Precision Optics:
Mirrors, Mounts and Drives

5 Facility Report 50

Maschine Status 51
Beamline Developments 52
BESSY Soft X-ray
FEL Project 54
Metrology Light Source
of the PTB 55

6 User Pages 56

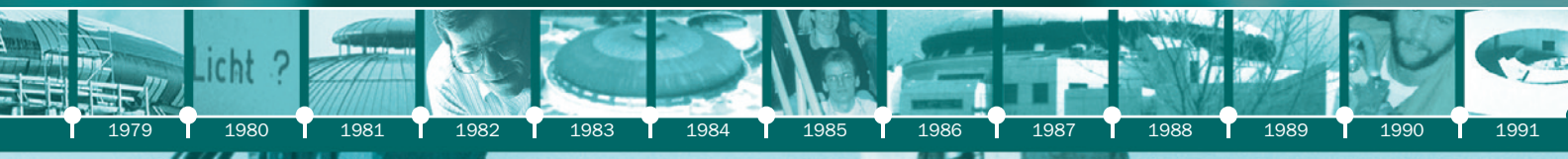

1

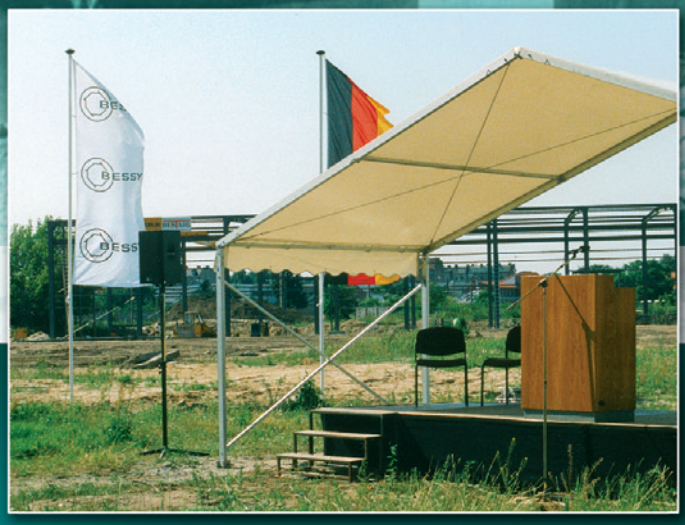

An engineer's way of ground breaking for BESSY II, 1994

Introduction

BESSY Inside

Dear colleagues and friends,

the activities of a new and exciting year often supersede the events of the past year very quickly. However, 2004 was truly a memorable year. Not only due to the 25th anniversary of BESSY but also due to several outstanding events concerning BESSY's future.

In early summer, BESSY was evaluated by Leibniz-Gemeinschaft for the first time since BESSY II went into operation and we all await the results with great interest. Almost in parallel the FEL team finalised the Technical Design Report for our second generation Free Electron Laser Facility and handed it over to Staatssekretär Dr. Husung from the Berlin government. Shortly thereafter the Standing Committee for Science and Technology of the Berlin State Assembly (Abgeordnetenhaus) met at BESSY to discuss this project. Across all party boundaries the BESSY-FEL project received the full support of all committee members and the Berlin Senate asked the German Science Council (Wissenschaftsrat) for an evaluation of the technical design of this facility, which will take place in 2005.

The 25th anniversary celebration was a great success (except for the weather and most regrettably the cream). Alex Bradshaw reflected on the past quarter century: the 'good old days' when BESSY was established as the first dedicated SR source in Germany, the 'wavy' times during the planning and decision making process leading to the funding of BESSY II, as well as the realisation and growth of BESSY II and its user community into one of the worlds foremost synchrotron radiation centres for the VUV and soft X-ray spectral region. Additionally, the festivities included a glance into the future with the ground breaking of the Willy-Wien-Laboratory, the new Metrology Light Source of the PTB, which is realised in collaboration with BESSY, and with Joe Stöhr's exciting lecture on femtosecond research in magnetism which will be enabled by Free Electron Lasers delivering controlled and synchronised fs-pulses in the soft X-ray spectral region.

Talking about exciting research... All together five user groups were able to publish their results in high-ranking journals such as Science and Nature in 2004 (see for example the Highlights of Erdélyi et al. and Sørensen et al.).

The variety of research taking place at BESSY is still expanding and we have chosen fifteen articles for the Highlights to represent a truly diverse range of topics from atomic physics to life sciences and archaeometry. Since the creation of the 'BESSY-Highlights' in 2001, we have encouraged authors to introduce their special field of research to a more general public. This approach seems to be successful since non-scientists keep us asking for a 'German Highlights' version. We have not abandoned this idea but for the present we had to postpone it once more.

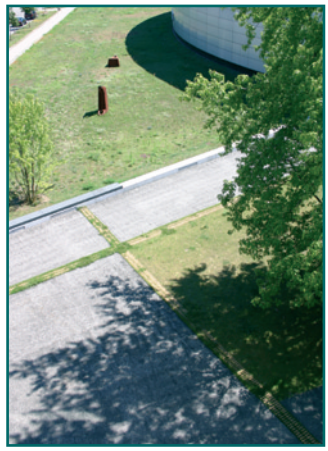

Among some 8,000 visitors (5,500 alone at the 'Lange Nacht der Wissenschaften') in 2004, we have had the honour to welcome the German Chancellor Gerhard Schröder, the Federal Minister of Commerce and Labour Wolfgang Clement, and the Federal Minister of Research and Education Edelgard Bulmahn together with several prominent CEO's of leading German industries (BASF, Bertelsmann, BMW, Celon, IBM, EnBW, Schering, ThyssenKrupp, Telekom, and others) during a meeting of the initiative 'Partner für Innovation'.

Finally, thanks to more than 1,000 scientists, who came to BESSY in 2004 in pursuit of their research programmes and who made our facility a lively and successful site for research and for cultural and scientific exchange.

Enjoy reading the Highlights 2004.

Prof. Dr. Dr. h.c. Wolfgang Eberhardt

Prof. Dr. Eberhard Jaeschke

Thomas Frederking

2

Champagne for BESSY I's last photon, 1999

Scientific Highlights

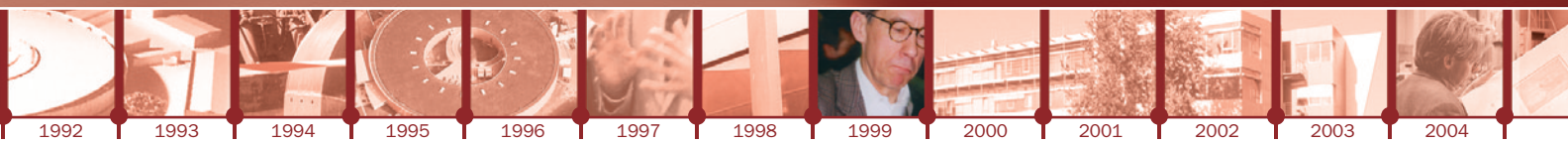

Scientific Highlights

Surface Sciences	*08*	
Solid State Physics	*14*	
Magnetism	*18*	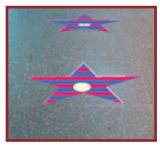
Nanosciences	*22*	
Atomic Physics	*26*	
Life Sciences	*28*	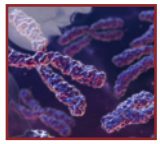
Archeometry	*32*	
Astronomy	*34*	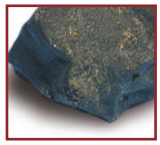
Micro Engineering	*36*	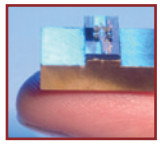

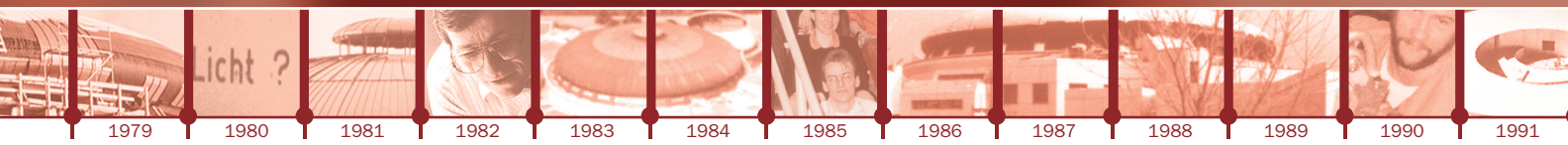

Demixing a melange: Transient interface sharpening in miscible alloys

Z. Erdélyi[1], M. Sladecek[2], L.-M. Stadler[2], I. Zizak[3], G. Langer[1], M. Kis-Varga[4], D. L. Beke[1], B. Sepiol[2]

1 University of Debrecen, Hungary

2 Universität Wien, Austria

3 Hahn-Meitner-Institut Berlin

4 Nuclear Research Institute of the Hungarian Academy of Sciences

Diffusion belongs to our everydays' life experience. When you carefully pour milk on your black coffee that you get a coffee and a milk layer and wait long enough, the two liquids will mix „automatically" by diffusion and you obtain a nice medium brown melange. It is now cold and to enjoy your melange you will probably have to heat it again. Diffusion processes always take place when two (or more) substances – even solids – share an interface. In solids these processes are not a major problem as long as the material layers are big and bulky but with continuously shrinking structures in microdevices such as microprocessors and read-write-heads atomic interdiffusion can cause serious problems, e.g. destruction of the device and reduced life-time.

Computer simulations have shown a new diffusion behaviour on nanoscale [1, 2]. For strongly composition-dependent diffusion coefficients, an initially diffuse A/B interface can sharpen even in ideal systems with complete mutual solubility. This sharpening is surprising at first sight because the direction of diffusion is always opposite to the direction of the composition gradient: $J = -D \operatorname{grad} c$, with J the atomic flux, D the diffusion coefficient and c the concentration – that is why you never get your black coffee back. Indeed, for constant D, the composition profile will gradually decay and a flattening of the (sharp or diffuse) interface is expected (Fig. 1a). On the other hand, when the diffusion coefficient strongly depends on the local composition, the flux distribution can lead to a sharpening of the interface (Fig. 1b, Fig. 2). The sharpening can be qualitatively predicted from the classical Fick I law although it is not able to provide correct kinetics on nanoscale [1, 4].

We studied Mo/V multilayers because they are completely miscible. Structures of 20 Mo/V bilayers with a modulation length ≈5-6 nm were produced by magnetron sputtering. The layers were separated by a roughly 1 nm thick diffuse interface with a constant composition gradient (Fig. 3). In order to follow the change of the composition profiles in situ during heat treatments we used X-ray diffraction measurements at the KMC2 beamline. The samples were placed on a heater inside a hemispherical Be window under high-vacuum conditions. Diffraction experiments were carried out at temperatures that gradually increased from 293 K up to about 973 K in 10 steps. At each temperature consecutive symmetrical scans between 53° and 66° of the scattering angle 2Θ were performed, measuring the scattering intensity around the (002) Bragg reflection of the Mo/V multilayer structure. The sample was kept at every temperature until no change in the diffraction pattern could be observed.

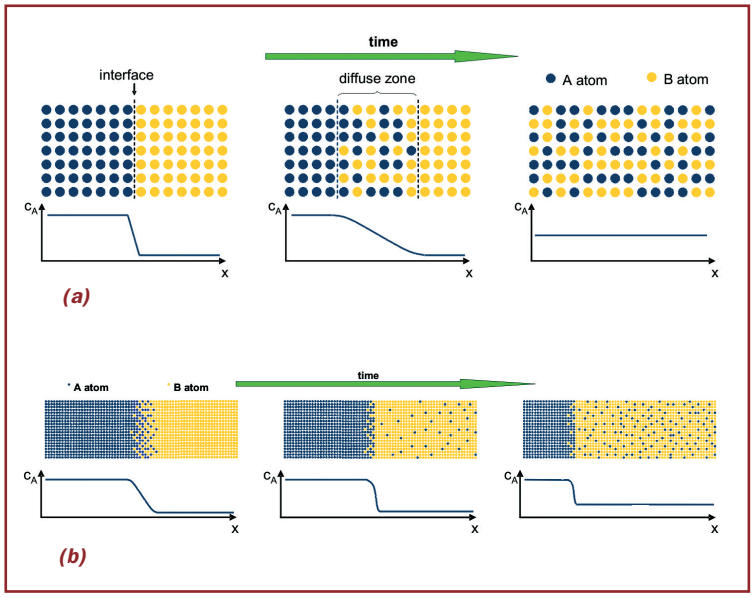

Fig. 1: Scheme of the intermixing in case of composition (a) independent and (b) dependent D.

References:

[1] Z. Erdélyi et al., Phys. Rev. Lett. ***89****, 165901 (2002)*

[2] Z. Erdélyi et al., Phys. Rev. B ***68****, 092102 (2003)*

[3] Z. Erdélyi et al., Science ***306****, 1913 (2004)*

[4] Z. Erdélyi et al., Surf. Sci. ***496****, 129 (2002)*

Acknowledgements:
The authors are indebted to Gero Vogl for helpful discussions. Supported by the Austrian Federal Ministry for Education, Science and Culture, by the OTKA Board of Hungary. Z. Erdélyi is a grantee of the 'Bolyai János' scholarship.

From the reconstruction of the diffraction patterns (Fig. 4) we found an interface sharpening during the heat treatment. This conclusion is also supported by the analysis of changes of the intensity ratios during heat treatment. A further proof of sharpening is due to the fact, that at a fixed temperature no more changes were observed after a certain time, i.e. a gradually increasing temperature was necessary. Since the interface is sharper, the Mo atoms are bound more strongly in the interface (the interface becomes more and more Mo-rich), consequently their diffusion into the V is slower (Fig. 2). Thus, in order to counterbalance this effect, we had to increase the temperature slightly (the diffusivity has exponential dependence on both the temperature and the composition).

The thickness of the Mo layers did not change apart from a tiny increase caused by thermal expansion. In contrast, the V-rich layers became much thicker, which cannot be explained solely by thermal expansion. The interface thicknesses decreased by about a factor of two (from 1.7 and 1.4 nm, respectively, to 0.78 nm), confirming the sharpening effect.

Our studies provide the first experimental evidence for the predicted interface sharpening. This behaviour is not only interesting to fundamental research. It could provide a useful tool for the improvement of interfaces and offer a way for fabrication of better X-ray or neutron mirrors, microelectronic devices or multilayers with giant magnetic resistance.

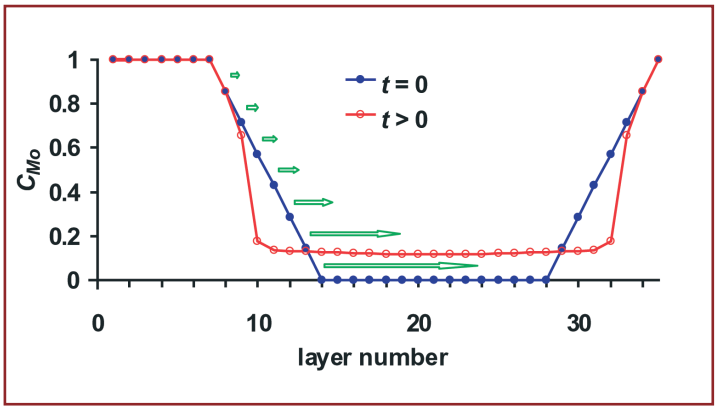

Fig. 2:
Composition distribution during intermixing in one period of a Mo/V multilayer calculated from an atomistic model, as in [1]. The arrows represent schematically the ‚flux distribution', i.e. their lengths are proportional to the absolute value of the atomic flux.

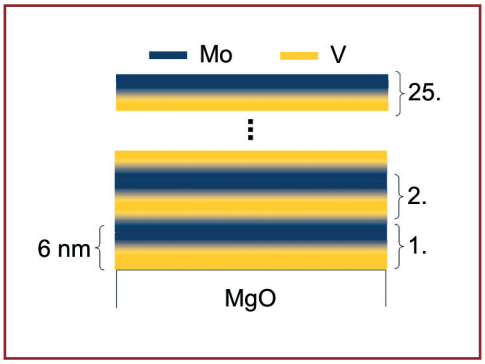

Fig. 3:
Scheme of the multilayer sample.

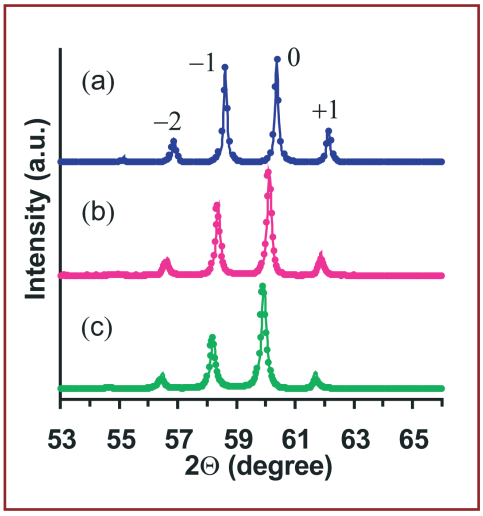

Fig. 4:
Diffraction patterns measured (circles) during the heat treatments and their reconstructions by the modified Stearns model (solid line): (a) room temperature, (b) 903 K, and (c) 953 K.

Contact:
Zoltan Erdélyi
zerdelyi@dragon.unideb.hu

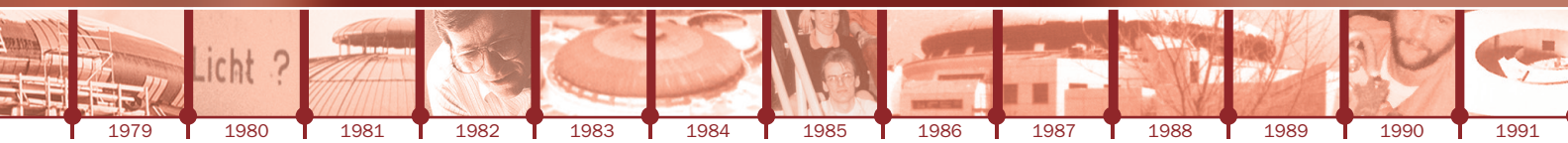

Fritz-Haber Institut der MPG
Department Inorganic Chemistry, Berlin

X-Rays sight active sites: Dynamics of catalytic surfaces under reaction conditions

M. Haevecker, A Knop-Gericke, R. Schlögl

The Japanese symbol for a catalyst means appropriately 'marriage broker', i.e. a catalyst offers an active site for a reaction to take place without being changed itself. In this way, a park bench can be regarded as a 'marriage broker' for twosomes. Without the catalyst the reaction would not or only slowly take place. 95% of the value produced in chemical industry is done with the help of catalysts, but their optimisation is normally done by a trial- and error approach.

Our group has built an instrument to follow the dynamics of catalytic surfaces under reaction conditions. The system is dedicated for the investigation of gas-surface reactions of single and polycrystalline solids. Such in-situ studies allow establishing structure-function correlations without having to make assumptions about the relevance of a specific species detected by surface analysis. X-ray photoelectron spectroscopy is here the key method as it can detect all elements besides hydrogen, exhibits pronounced chemical sensitivity and when used with synchrotron excitation can be used in highly specific modes of depth and energy resolution. Its greatest disadvantage as photon in – electron out technique is the required (ultra)-high vacuum operation to detect the photoelectrons.

Attempts to overcome this limitation use the concept of a small aperture and multiple differential pumping between sample and electron energy analyzer. It is only the incorporation of self-tuning electron optical elements that focus the electrons from the exit aperture into the hemispherical electron energy analyser that provides a useful count rate over a wide range of kinetic energy for electron spectroscopy ranging from about 100 to 1,000 eV.

Our realisation is outlined in Fig. 1. A sample chamber with a cooled thin silicon nitride window for the photon beam houses pellets of hetero-geneous catalysts that are placed on a sample stage ca. 1 mm in front of the aperture of 1 mm diameter of the first differential pumping stage. Depending on gas composition and the exact distance sample-aperture pressures of typically 5 mbar can be reached at the sample which can be heated with a ramp-controlled laser beam system between 300 K and 1,000 K. Reactive and corrosive gases including hot water vapour, oxygen and organic solvents can be used provided that the window is not attacked. A flowing gas atmosphere with on-line compositional gas detection can be used. Liquids, solutions and dispersions can be studied with a precision temperature regulation limiting the vapour pressure between ca. 0.1 mbar and 5.0 mbar. Additionally, gas phase analysis is possible with a conventional quadrupole mass analyzer and with a high sensitivity proton-transfer ion molecule reaction mass analyzer.

The spectral analysis of data is similar to that of conventional XPS with two prominent exceptions: in all relevant core level regions the spectra of the gas phase atoms occur besides those from the surface. The resulting complex spectral shapes can be analysed taking into account that the work function shifts the gas phase components relative to those of the solid and adsorbates. The emitted photoelectrons interact heavily with the surrounding gas phase giving rise to composition-specific strong alterations in the element specific photoelectron yields. The modifications reach up to an order of magnitude changes relative to the cross sections used for UHV surface analysis and need to be carefully calibrated for each system.

References:

H. Bluhm et al., J. Phys. Chem., B ***108****, 14340 (2004)*

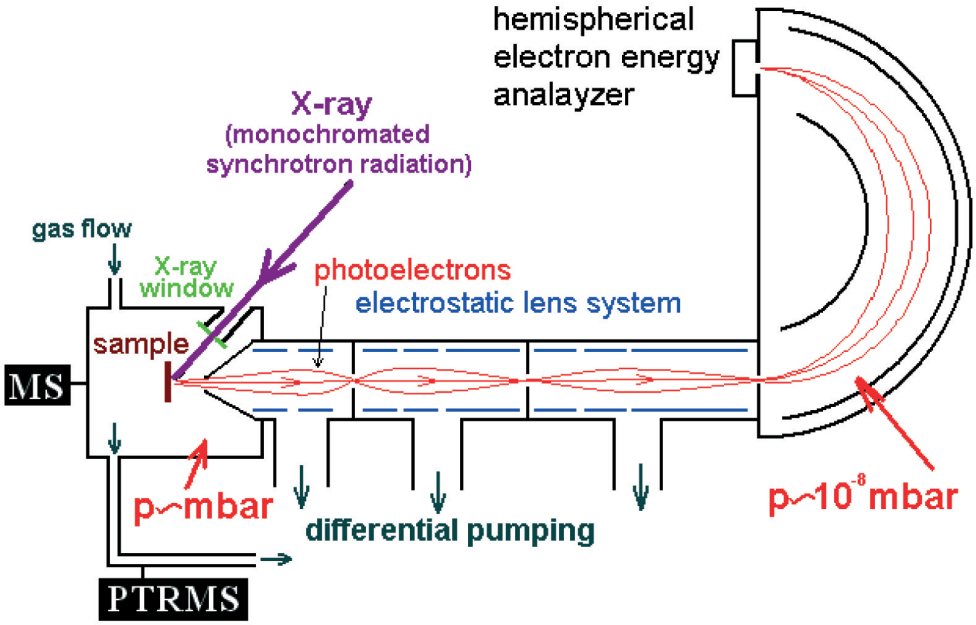

Fig. 1:
Schematic representation of the high pressure XPS instrument at BESSY.

An example is presented in Fig. 2 showing a polycrystalline silver surface active in the epoxidation of ethylene. This much studied reaction proceeds according to surface science via the formation of one species of atomic oxygen being present as electrophilic oxygen at the catalyst surface. The data in Fig. 2 reveal, however, that a mixture of species is present under steady state reaction conditions and that their relative abundance depends critically on the operation conditions. No peroxide or molecular species is present as often speculated in the literature. The difference spectra at 470 K reveal the presence of a smaller abundance of surface atomic oxygen (3 - 4) and a larger contribution from sub-surface species (4) which are catalytically inactive. This new finding and the fact that the unwanted nucleophilic oxygen species that burns ethylene to carbon dioxide is present as unavoidable companion of the desired oxygen species at high pressure explain the limited selectivity and why no other molecules than ethylene can be reacted to its epoxide over silver: all other molecules are C-H activated by nucleophilic oxygen and undergo thus additional reaction pathways leading to undesired products. The unambiguous detection of the desired and undesired oxygen species on the working catalysts surface gives now a unique handle to test for strategies to suppress the undesired species currently executed as an industrial cooperation between BESSY and a large epoxide producer.

The now smooth operation of the system permits the study of a wide variety of applications in material science. The possibilities range from charge neutralisation in polymer surface analysis by the addition of water vapour over the melting of ice and the effect of solutes on the kinetics of the solid liquid transition of this environmentally relevant system to surface analysis of biological systems in their native wet state and the study of electrochemical cells without the need for emersion.

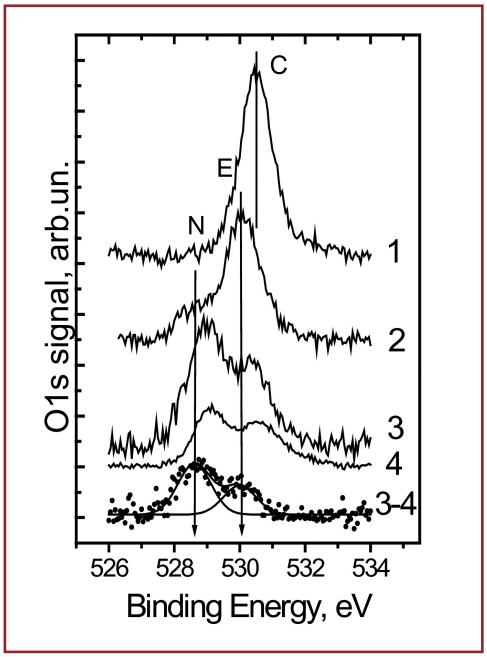

Fig. 2:
Oxygen 1s spectra during ethylene epoxidation at 0.5 mbar total pressure: (1) at 300 K, no reaction, (2) at 420 K, stable conversion, (3) at 470 K deactivating, (4) at 470 K without oxygen in the gas phase. The three oxygen species are carbonate (spectator, C), electrophilic (wanted, E) and nucleophilic (unwanted, N) atomic oxygen.

Contact:
Robert Schlögel
acsek@fhi-berlin.mpg.de

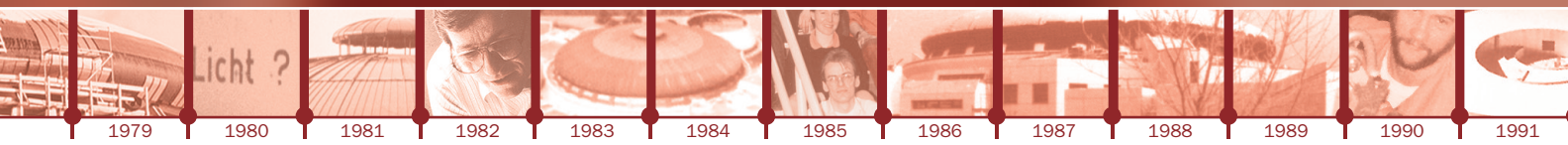

Does cooling protect for radiation damages?

P. Feulner[1], T. Niedermayer[1], K. Eberle[1], R. Schneider[1], D. Menzel[1], A. Baumer[2], E. Schmich[2], A. Shaporenko[3], Y. Tai[3], M. Zharnikov[3]

1 Technische Universität München

2 Walter Schottky Institut, Garching

3 Universität Heidelberg

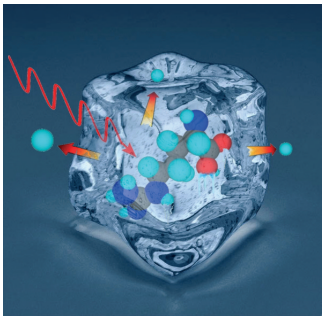

The effect of ionizing radiation on organic materials, biological macromolecules and cells is an important issue with wide practical significance both in science and everyday life, e.g medical diagnostics and radiation therapy. In particular, radiation-induced damage represents a severe constraint for the characterization of this kind of samples by advanced electron or x-ray spectroscopy and microscopy.
A possibility to reduce degradation is cooling of the samples down to cryogenic temperatures, i.e. about -230°C (43 K). This has been a standard method to reduce radiation damage, i.e. to extend the life time and therefore the quality of the data of biological samples [1]. Although the protecting effect of sample cooling is empirically well demonstrated, its exact microscopic mechanism is unknown until now. It is commonly assumed that while the basic irradiation-induced bond cleavage is unaffected by the temperature, the main effect is that the resulting fragments are frozen at their original position. Although disinte-gration at the molecular level takes place, simply the hindrance of mass transport in the sample allows the molecules to stay at their sites, so that the structure continues to be imaged as before [2].

As test systems, we have selected well-defined and highly ordered thin organic films - self-assembled monolayers (SAMs) of alkane-thiolates ($CH_3(CH_2)_{15}SH$: C16) on polycrystalline Au (111) and alkyls ($CH_3(CH_2)_{17}$: C18) on monocrystalline Si(111). Apart from the direct resemblance to lipid membranes, these films mimic highly organized biological macromolecules and are well suited for model experiments on organic and biological materials.

The experiments were performed at the U41-PGM and U49-II-PGM-I beamlines. X-ray and secondary electron induced damage was monitored by x-ray absorption spectroscopy (XAS), photoemission (PE), and desorption induced by electronic transitions (DIET) of ions and neutrals. XAS spectra were recorded either in a partial electron yield (PEY) detection mode or by monitoring DIET of ions. The exposure dependence of irradiation damage was obtained from consecutively recorded PE and XAS spectra. The irradiation was performed at photon energies between 250 and 315 eV. The dose varied from 3 x 10^{14} to 1.2 x 10^{17} photons/cm^2.

In Fig. 1, C K-edge XAS spectra of C16/Au are shown. The spectra for the pristine SAMs (bottom) exhibit overlapping Rydberg and C-H σ* resonances at 288.3 eV and two kinds of C-C σ* states at 294 eV and 300 eV [6]. Extended irradiation reduces the intensity of the original R* and σ* resonances [3,4] mostly caused by the SAM disordering and dehydrogenation, and gives rise to a new maximum at 285.1 eV assigned to a π* resonance due to double bonds created in the film after the dehydrogenation [3,4]. Most important, there is no significant difference in the reduction of the R*/σ* resonance intensity or in initial rate of formation of the π* resonance between 50 K and 300 K, which means that the processes responsible for these changes are mostly unaffected by the temperature.

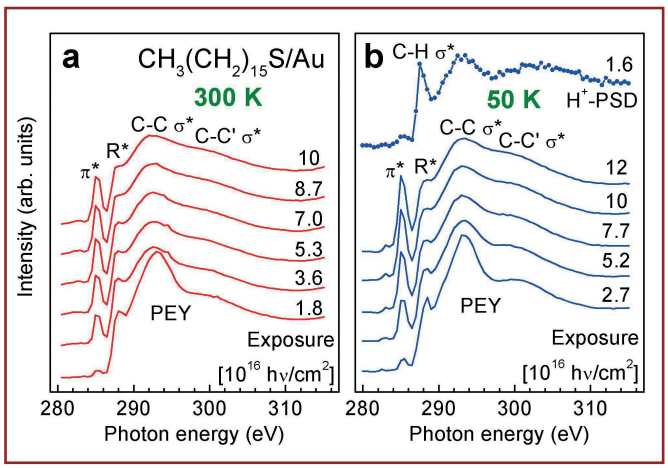

Fig. 1:
C K-edge PEY XAS spectra of C16/Au recorded after different photon exposures (hν = 270 eV) at 300 K (a) and 50 K (b) sample temperature. A H+-DIET spectrum at 50 K is also shown.

References:

*[1] G. Schneider, Ultramicroscopy **75**, 85 (1998); D. Weiß et al., Ultramicroscopy **84**, 185 (2000).*

*[2] V. E. Cosslett, J. Microscopy **113**, 113 (1978).*

*[3] M. Zharnikov and M. Grunze, J. Vac. Sci. Technol. B **20**, 1793 (2002), and references therein.*

*[4] M. Zharnikov et al., Langmuir **16**, 2697 (2000).*

*[5] K. Heister et al., Langmuir **17**, 8 (2001).*

*[6] D. A. Outka et al., J. Chem. Phys. **88**, 4076 (1988); K. Weiss, P. S. Bagus, and Ch. Wöll, J. Chem. Phys. **111**, 6834 (1999) .*

*[7] P. Feulner et al., Phys. Rev. Lett. **93**(17), 178302-1 (2004)*

Acknowledgements:
We thank M. Grunze for the support of this work. Support by BMBF, DFG and GIF.

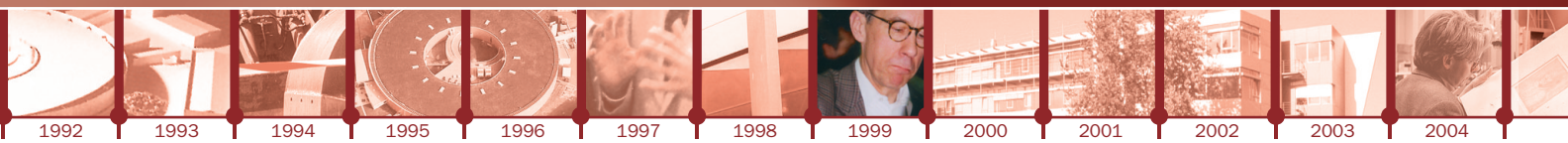

Next, we have investigated the temperature dependence of another prominent irradiation effect, namely the breaking of the Au-thiolate bond and the formation of dialkylsulfide species [3,5], which presumably requires the movement of the entire molecule. This process can be followed by S 2p PE. As a fingerprint of this reaction, an additional S $2p_{3/2,1/2}$ doublet appears in binding energy which is blue shifted by 1.3 eV relative to the Au-thiolate related doublet of the pristine layer; the latter doublet is the single feature in the spectrum of pristine C16/Au (bottom curves in Fig. 2) [5]. At 300 K, this dialkylsulfide doublet increases rapidly with irradiation (Fig. 2a). At 60 K, this feature is essentially absent (Fig. 3b), which implies a strong temperature effect.

Similar effects are observed in the DIET data (Fig. 3). At 300 K, there is a rapid material loss in C16/Au, indicated by a rapid increase in the Au4f PE signal, whereas this signal is practically constant at 50 K (Fig. 3a). This means that the overall DIET rate, which is mostly determined by large fragments, is much lower for the low temperature than for 300 K, i.e. such fragments stay together. Also in the mass spectra for another organic layer, C18/Si in Fig. 3b, we see DIET of large neutral fragments at 300 K, whereas these moieties are essentially absent and the desorption signal is much smaller at 50 K. Importantly, the quenching of reaction involving higher masses is not due to simply freezing the structure. In particular, heating C16/Au to 300 K after irradiation at 60 K had no significant effect on the PE spectra or Au4f PE intensity.

Thus, we obviously encounter two different scenarios for the formation of dialkylsulfide and large hydrocarbon fragments on one hand, and for the hydrogen abstraction and double bond formation on the other. The former reactions, which imply motion of the large species, proceed rapidly only at elevated temperatures, whereas the latter processes, involving small fragments, are merely independent of temperature (Fig. 4). Our results clearly show that the temperature directly governs the branching of the different channels of electronically stimulated reactions in organic materials, and not only the escape probability of products *after* the completion of the reaction. At the same time, we do not think that the primary electronically stimulated bond cleavage depends on temperature, but speculate that bonds can recombine if the fragments are forced to stay in place due to their reduced mobility at low temperatures [7]. We expect that the evaluation of data for intermediate temperatures which is under way will reveal details of this reaction kinetics. These results are important for all cryogenic approaches in advanced electron and x-ray microscopy and spectroscopy of biological macromolecules and cells.

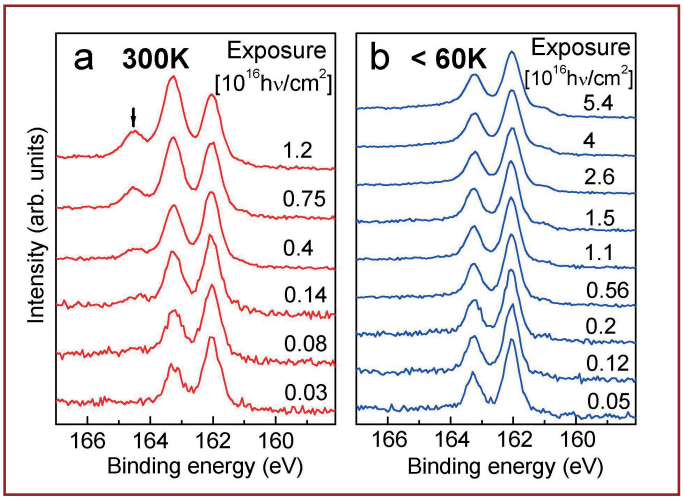

Fig. 2:
S 2p PE spectra of C16/Au recorded after different photon exposures (hν = 270 eV) at 300 K (a) and below 60 K (b); line in (a) marks the S $2p_{1/2}$ peak of the dialkylsulfide species.

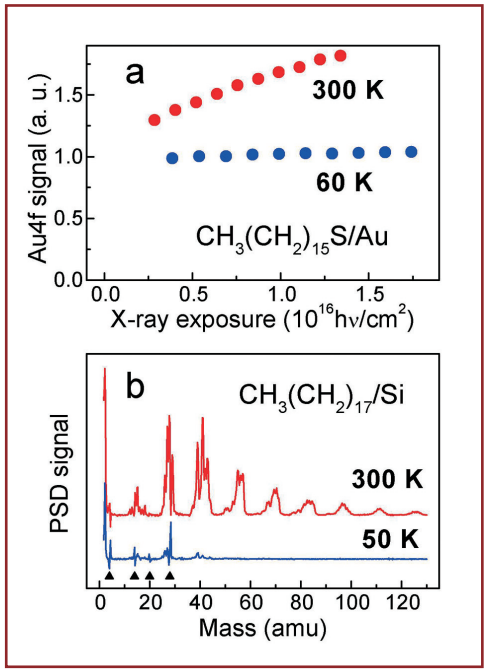

Fig. 3:
(a) Relative amplitudes of the Au 4f PE from C16/Au as a function of photon exposure (hν = 270 eV) for 60 K and 300 K sample temperature; (b) DIET of neutrals from C18/Si for 50 K and 300 K sample temperature (hν = 250 eV)

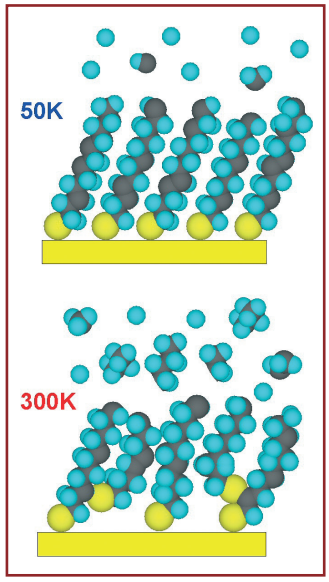

Fig. 4:
Different branching of electronically stimulated reactions in alkanethiol monolayers on Au at 300 K and 50 K sample temperature.

Contact:
Peter Feulner
feulner@tum.de

Michael Zharnikov
Michael.Zharnikov@urz.uni-heidelberg.de

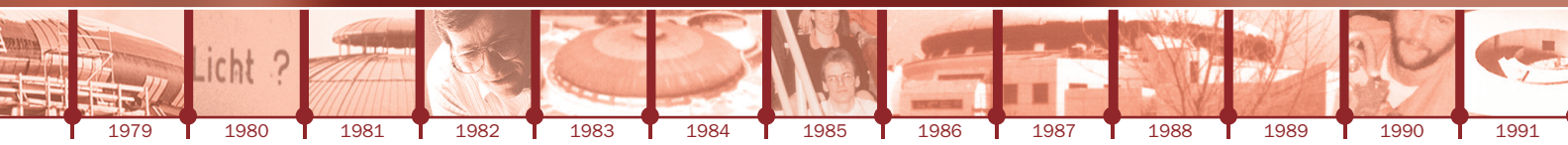

Towards finding out how an insulator turns metallic

C. F. Hague[1], M. Marsi[2], J.-M. Mariot[1], R. Delaunay[1], J.-P Rueff[1], Ph. Leininger[1], S. Eisebitt[3]

1 LCP-MR, Université Pierre et Marie Curie, Paris, France

2 Sincrotrone Trieste, Italy

3 BESSY, Berlin

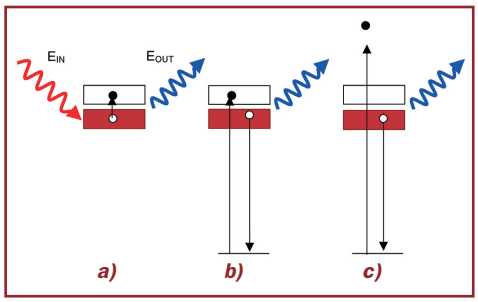

Fig. 1:
Schematic representations of: (a) an inelastic scattering process, (b) a resonant inelastic scattering process involving a core level, and (c) normal X-ray emission.

Most properties of complex materials depend on how their atoms bond together in crystal structures, some, more subtly, depend on the interactions of weakly bound electrons with one another. A change in temperature or pressure or a slight modification in composition may trigger dramatic changes in the electron-electron interactions provoking insulator↔metal↔ superconductor, and/or paramagnetic↔ ferromagnetic↔antiferromagnetic phase transitions. Trying to understand electron-electron interactions goes beyond mere academic curiosity. For example, they are central to the superconductivity of the copper perovskites [1]. Hi-tech superconducting wires made of copper perovskites are already used to fabricate electric motors for ship propulsion [2]. Tailoring materials to be superconducting at room temperature would revolutionise many aspects of everyday life.

The interplay between the relative energy levels of the outermost electrons, dependent on the crystal field and the interaction between the electrons, is particularly difficult to treat theoretically. Hence, there is need for detailed experimental studies. Here we present work on complex transition metal (TM) oxides where the energy required to make a 3*d* valence electron hop from one TM site to another is a key to the diversity of their electron transport properties. Resonant X-ray Raman spectroscopy (RXRS) is particularly well suited to such a study (Fig. 1). The goal is to determine the difference in energy between an incoming photon (E_{IN}) and an out going photon E_{OUT} as it looses part of its energy to excite a valence electron to a specific unoccupied state (Fig. 1a). The probability for this inelastic scattering process is, however, negligible. If we now choose E_{IN} equal to the energy needed to promote a core electron to the empty state via a dipole transition (2*p* to 3*d* in this case), the core level will be refilled simultaneously by a valence electron of same symmetry (3*d* to 2*p* transition) (Fig. 1b). This time the probability is relatively large: it is a resonant process. It has the final state we are looking for since it specifically picks out transitions involving electrons with the symmetry of interest. It is equivalent to measuring the energy required to remove an electron from one TM atom and adding it to a neighbouring TM atom.

This resonant inelastic X-ray scattering process is in competition with an elastic process (the excited electron and core-hole recombine) and other decay channels involving Auger electrons. Thus a very sensitive high-resolution soft X-ray spectrometer [3] in tandem with a state of the art undulator beamline such as U41-PGM is needed to separate the various effects.

In passing it will be noted that normal X-ray emission (Fig.1c) does not provide the information we require as the core electron is ejected and the emission process simply results from the unrelated filling of the core level by a valence electron.

Here we show how we have applied the technique to two widely different vanadium compounds: YVO_4 (single crystal) and V_2O_3 (epitaxial thin film [4]). The former is extensively used in laser techniques and the latter as a catalyst in industrial processes. Nominally an yttrium and a vanadium atom have eight valence electrons between them that can be transferred to the oxygen atoms. Each vanadium atom is tetrahedrally coordinated to four oxygen atoms and we expect a filled O 2*p* band and empty 3*d* states, so YVO_4 should fall into the band-insulator category (Fig. 2a). By contrast, V_2O_3 has a partially filled 3*d* band so normally it should be metallic (Fig. 2c).

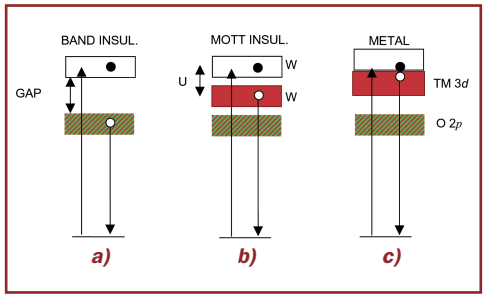

Fig. 2:
RXRS applied to: (a) a band insulator (b) a Mott-Hubbard insulator (c) a metal.

Refercences:

[1] J. G.. Bednorz and A. Müller were awarded the Nobel Prize in 1987 for this discovery.

[2] American Superconductor, Westborough, Mass.

*[3] C. F. Hague et al., Rev. Sci. Instrum. **76**, 23110 (2005)].*

*[4] B. Sass et al., J. Phys: Condens. Matter **16**, 77 (2004).*

*[5] J. H. Park et al., Phys. Rev. B **61** 11506 (2000).*

Acknowledgement:
We are indebted to A. Revcolevschi, G. Dhalenne, W. Felsch, and B. Sass for making available high quality samples.

In fact, it shows a transition from a Mott-Hubbard insulator to a metal without changing its crystal structure depending on pressure or stoichiometry (Fig. 3). To the right of the phase diagram, compression or doping with Ti brings V atoms closer together, so that the V 3*d* wave functions overlap more effectively. To the left of the phase diagram the 3*d* valence electrons are more localized, their wave functions overlap to a lesser extent, so that the Coulomb repulsion between electrons dominates and more energy is required to make an electron hop to a neighbouring site. As suggested by Mott the *d* band is then split into an upper (empty) and lower (occupied) Hubbard band of width W separated by the *d*-*d*-electron Coulomb interaction U (the band gap is approximately U-W) (Fig. 2b). There is a further phase transition to an insulating antiferromagnetic state below 100 K but this is related to a change in crystal structure.

RXRS data are presented in Fig. 4. First, we should point out that a structure in the emission spectrum that remains at constant energy when E_{IN} is increased across an absorption edge indicates normal X-ray emission disconnected from the excitation process (Fig. 2c). On the contrary, a constant difference between E_{IN} and E_{OUT} implies that E_{OUT} shifts (it is called a Raman shift). Thus if the structure disperses it can unequivocally be attributed to an excitation process.

The bonding O 2*p*-related states in YVO_4 disperse as the excitation energy increases (Fig.4a). In this case the constant energy difference between the O 2*p* bonding states and the elastic peak (green ticks) corresponds to the energy required to transfer an electron from the hybridized bonding states to the empty *d* states. The transfer energy, in this case, is ≈ 6.5 eV. The dispersion becomes weaker as the excitation moves into the second X-ray absorption peak. For excitation energies starting at 517 eV, there are also signs of a very weak but probably sharper feature (red arrows) which disperses strongly. It suggests the existence of a purely *d*-*d* excitation of significantly lower energy (≈ 4.2 eV).

For V_2O_3, taken at 80 K, there are three non-dispersing features situated at 507 eV and 510 - 512 eV (dashed lines in Fig. 4b) which are also present in the X-ray fluorescence spectrum. The 507 eV feature corresponds to a hybridised O 2*p* band lying below the lower Hubbard *d*-band (Fig. 2b). The 510 - 512 eV features related to V-3*d* normal X-ray emission appear as the excitation moves beyond the first weak shoulder in the absorption spectrum attributed to a_{1g} states [5].

The other salient features of the V_2O_3 data are a pronounced elastic peak whose relative intensity depends strongly on the excitation energy (green ticks) and an energy loss peak (red arrows), which disperses along with the elastic peak with an energy loss of ≈ 2.2 eV. This corresponds to a *d*-*d* excitation and indicates the presence of well-localized states. We find that the intensities of the elastic peak and the energy loss peak are slightly reduced compared to the metallic phase above 100 K. It suggests that in the low temperature phase the gap opens up as a result of charge transfer towards the O 2*p* band rather than directly as a result of a stronger localisation of the 3*d* valence electrons. The next step will be to apply the technique across the metal-insulator transition at room temperature. This requires comparing samples with different stoichiometries. Over the past decades theory has made considerable progress in explaining electron interactions in TM oxides. As instrumentation improves, we expect high resolution RXRS to provide the parameters to challenge the theoretical models for today's and future materials.

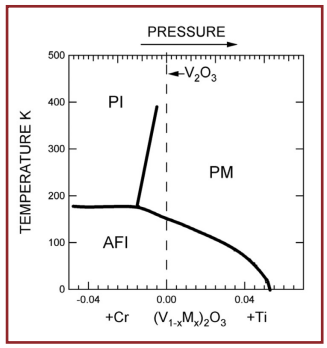

Fig. 3:
Phase diagram for V_2O_3 (PI and PM, indicate paramagnetic insulator and metal phases; AFI means antiferromagnetic insulator).

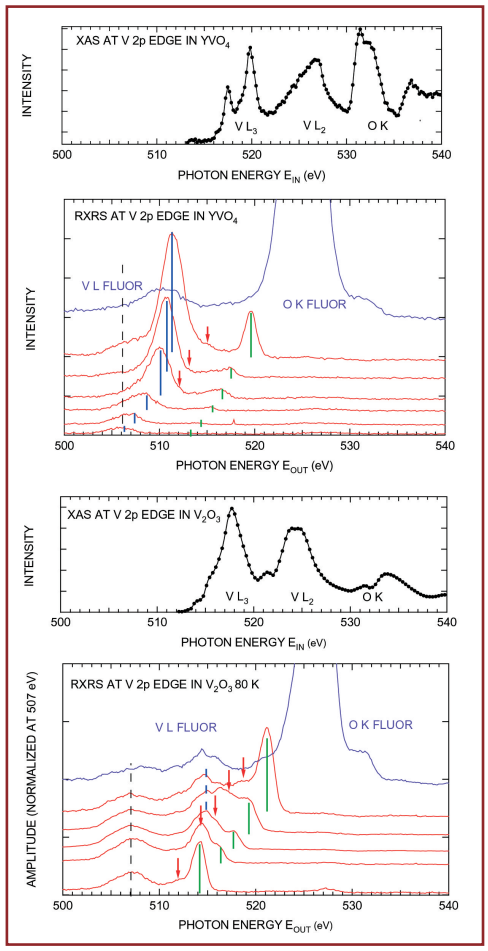

Fig. 4:
RXRS data for: (a) the band-insulator YVO_4 and (b) V_2O_3 in the antiferromagnetic insulating phase. Also shown are the absorption spectra covering the V L edges and O K edge energy region. The purple curves are normal X-ray emission spectra (fluorescence) taken at the O K edge.

Contact:
Coryn Hague
hague@ccr.jussieu.fr

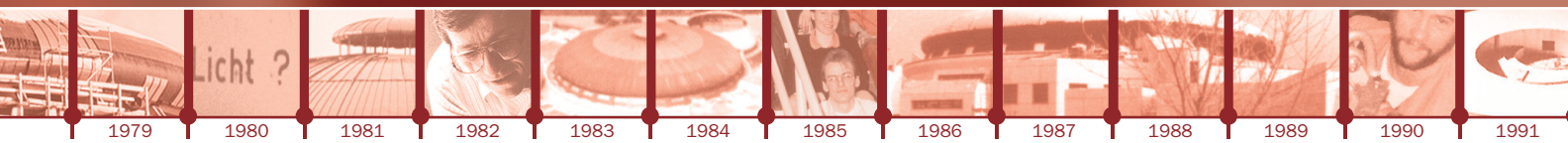

Finally a clue of the glue in high temperature superconductors

A. Koitzsch[1], S. V. Borisenko[1], A. A. Kordyuk[1,2], T. K. Kim[1], J. Fink[1], M. Knupfer[1], B. Büchner[1], H. Berger[3], C.T. Lin[4], B. Keimer[4]

1 Leibniz Institut für Festkörper- und Werkstoffforschung, Dresden

2 Institute for Metal Physics, Kiew, Ukraine

3 Institute of Physics of Complex Matter, Lausanne, Schweiz

4 MPI für Festkörperforschung, Stuttgart

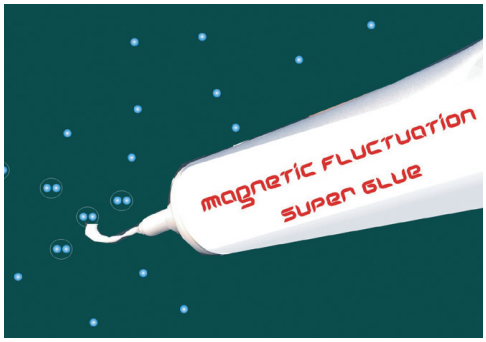

At low temperature some solids enter a bizarre state of matter, they become superconducting. They loose suddenly their electrical resistance and expel magnetic fields from their interior. It is easy to imagine technical applications for such behaviour: superconducting cables which transport high current without dissipation or superconducting magnets which produce high magnetic fields. In fact both of these are indeed used for quite some time now but its widespread utilisation is hampered by the fact that every superconducting device has to be cooled to very low temperatures. Aluminium for instance becomes superconducting only below 1.2 K.
In 1986 a new class of superconductors was discovered which showed transitions to the superconducting state at much higher temperatures than any 'classical' superconductor. Therefore they are called 'high-temperature' superconductors, although the highest achieved transition temperature is 160 K (or -113°C) which is still far below room temperature. Since then, these materials have been investigated with an enormous effort. But still the microscopic mechanism which is responsible for the appearance of superconductivity in these materials could not be unravelled. As the mechanism of classical superconductors was clarified half a century ago this represents one of the major open questions of solid state physics.

For both, classical and high-temperature superconductors (HTSC), it is known that in the superconducting state the conduction electrons are bound together into the so-called Cooper pairs. These Cooper pairs are essential for superconductivity. They act as the superconducting charge carriers. In classical superconductors the Cooper pairs are glued together by the interaction of the electrons with the crystal lattice, or in other words by the electron-phonon coupling. The decisive question is: what glues the electrons together in the high-temperature superconductors? To answer this question it is inevitable to know, to which degrees of freedom of the solid the electrons in these materials couple at all. Do they couple to phonons as in the classical case, or to magnetic fluctuations as neutron scattering experiments suggest [1, 2]?

To investigate this question we employed angle resolved photoemission spectroscopy (ARPES), which is based on the photoelectric effect explained by Einstein, exactly hundred years ago [3]. The U125/1 PGM beamline offers high energy resolution in connection with a small spot size and variable beam energy, which are preconditions for modern photoemission experiments. ARPES allows the determina-tion of the electronic states of the solid, i.e. of the band structure. Fig. 1a shows an ARPES measurement of the Fermi surface of $(Bi,Pb)_2Sr_2CaCu_2O_{8+\delta}$ (Bi-2212), a member of the Bi-based HTSC family. Bright yellow stands for high photoelectron intensity at a given k-space position *at the Fermi energy*, and therefore for the bands crossing the Fermi energy. The „barrel“ shaped structures are typical for this material.

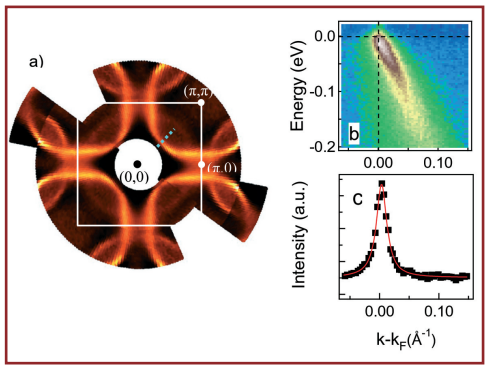

Fig. 1:
(a) Fermi surface of Bi-2212, (b) energy dependence along the diagonal direction of (a), (c) a cut along the horizontal direction of (b)

References:

*[1] H. F. Fong et al., Phys. Rev. B **61**, 14 773 (2000)*

*[2] M. Eschrig et al., Phys. Rev. B **67**, 144503 (2003)*

*[3] A. Einstein, Ann. d. Physik **17**, 132 (1905)*

Acknowledgement:
Supported by the DFG.

If the electrons couple to phonons or magnetic fluctuations - or whatever member of the solid state excitation zoo - fingerprints of this behaviour are found in the electronic structure, typically as a peculiarity of the electronic dispersion at the energy of the excitation the electron couples to. Therefore, we recorded the *energy dependence* of the photo intensity along the blue dashed line in Fig. 1a, shown in Fig. 1b, in a different colour scale. Making horizontal cuts through these data lorentzian shaped peaks as shown in Fig. 1c are obtained. From the position of the peak maxima we derive the dispersion curves and the width of the peak is related to the lifetime of the excitation. Fig. 2 shows dispersion relation for differently hole-doped samples. We do not find a straight line but instead a 'kink' around 70 meV - a hallmark of the presumed coupling. Indeed, any coupling of the electrons slows down their motion, therefore the Fermi velocity (the slope of the dispersion) is reduced.

As the coupling of the electrons to phonons or magnetic fluctuations follows different doping and temperature dependencies it is crucial to investigate both if one wants to discriminate between the two alternatives for the coupling. Fig. 3a shows the peak width as full width half maximum (FWHM) vs. energy for an optimally doped crystal, where 'optimally' refers to the fact that the superconducting transition temperature T_c is maximal for this doping. At temperatures above T_c we find a parabola. However below T_c an additional contribution develops around 100 meV. The upper inset shows the parabolic dependence for an overdoped sample. Based on this data we assume the existence of two contributions to the lifetime: first a normal electron-electron decay, which leads to the parabola and second - an additional channel due to the coupling. Subtracting out the parabola, one obtains the contribution due to the coupling alone (Fig. 3b), which appears to be highly temperature dependent. Fig. 4 shows a similar separation procedure for two differently doped crystals at fixed temperature. The result shown at the lower part is that the coupling contribution becomes stronger for underdoping.

The observed temperature and doping dependence matches the characteristics of magnetic fluctuations present in this material. Phonons on the other hand show weak temperature and doping dependence. We conclude therefore, that conduction electrons in high-temperature superconductors couple primarily to magnetic fluctuations. This does not answer the question whether or not magnetic interactions are ultimately responsible for the coupling of electrons into Cooper pairs, but it makes them to be the prime suspect for the glue of superconductivity in the HTSC.

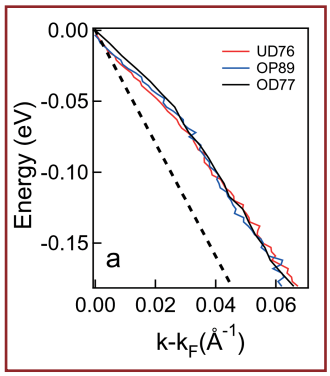

Fig. 2:
Electronic dispersion of Bi-2212 for underdoped (UD), optimally doped (OP) and overdoped (OD) samples.

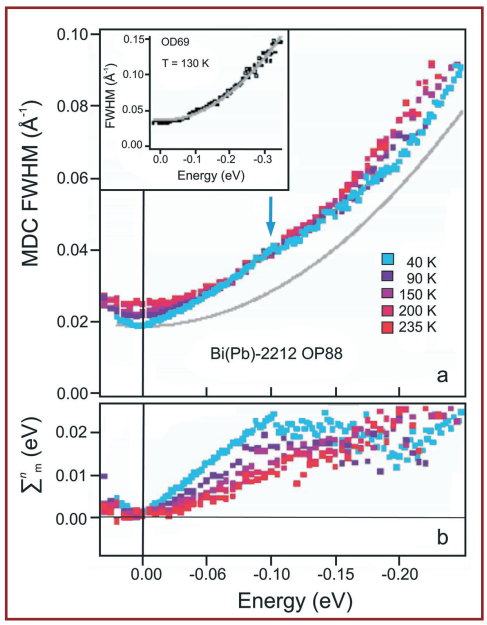

Fig. 3:
(a) Peak width vs. energy for various temperatures,
(b) Contribution to the peak width due to the coupling

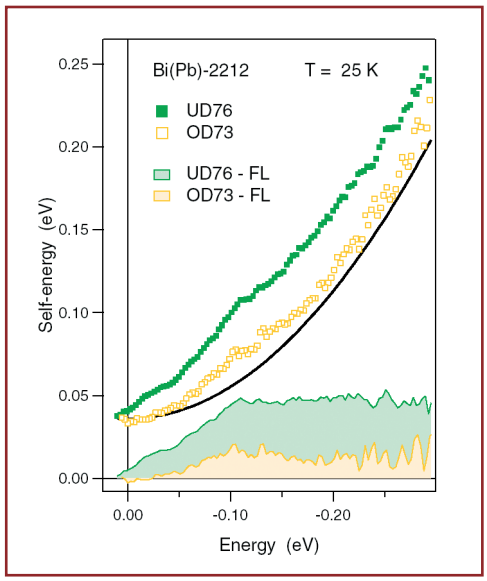

Fig. 4:
Upper part:
Peak width vs. energy for different doping levels.
Lower part:
Contribution to the peak width due to the coupling

Contact:
Andreas Koitzsch
a.koitzsch@ifw-dresden.de

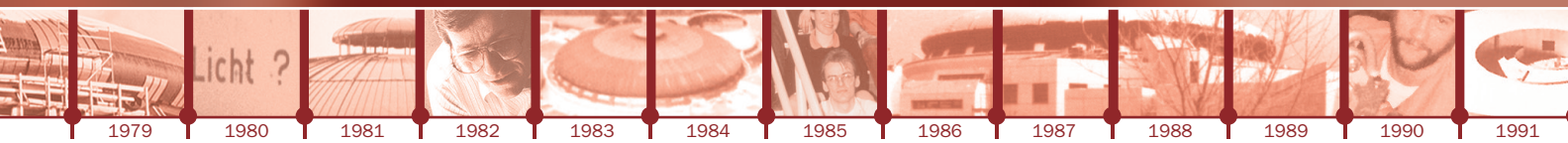

Stripes are stars! Pt helps Fe to stay magnetised

K. Kuhnke[1], T. Y. Lee[1], A. Enders[1], J. Honolka[1], M. Heßler[3], K. Fauth[2,3], G. Schütz[2], K. Kern[1]

1 Max-Planck-Institut für Festkörperforschung, Stuttgart
2 Max-Planck-Institut für Metallforschung, Stuttgart
3 Universität Würzburg

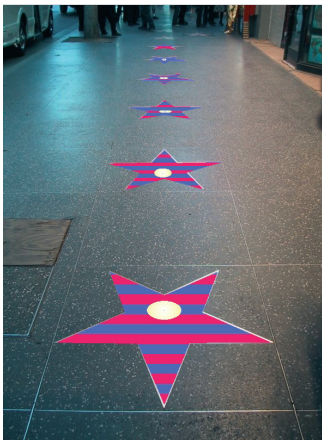

During the last decades we witnessed the miniaturisation of electronic circuits. From pocket calculators with a memory just large enough to store a few floating point values we saw a development towards palmtops with full programming capability and storage capacity for music and images. The fact that the miniaturisation still continues stimulates our interest to study the physics which will be required for their realization in many years from now. An extremely compact computer can still use miniaturised classical magnetic disks, and in addition there will be MRAMs which consist of transistors, whose logic state is controlled by a tiny ferromagnet. Magnets allow a cut of power consumption to zero stopping operations but not erasing data, a property which has since the beginning made magnetic memories very successful and remains attractive for data storage.

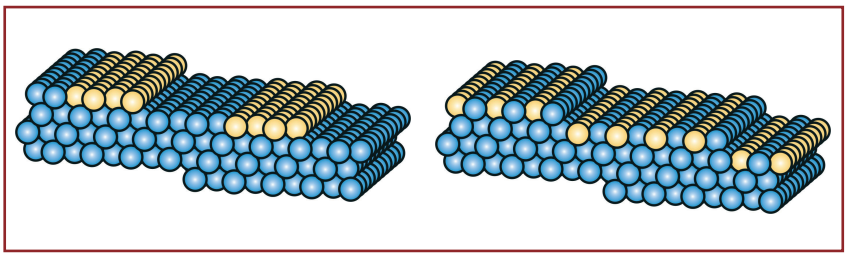

***Fig. 1:** The sphere models illustrate the different arrangement of Fe (yellow) and Pt (blue) atoms on the two samples.*

Since a few years physics has set off to study at which state of miniaturisation the limits of magnetic storage will be reached and how far new materials and structures may eventually lead. We thus become curious what the magnetic properties of clusters with a countable number of atoms would be. Much effort is put into this research and exciting results are emerging. Tiny metal particles are produced in different ways and tested for their magnetic properties. Adsorbate structures are made thinner and smaller. Preparing aggregates from single atoms [1] and using experimental methods which are still sensitive enough to measure their magnetism takes us to the limits. Smallness is, however, not the only goal. Equally important is the stability of the magnetization with respect to heat and other external factors that may lead to erasure of magnetically stored information.

One group of materials studied by industry and applied physics research groups are alloys containing two elements, one ferromagnetic, like Co and Fe and the other non-magnetic, like Pt. In fact, such alloys have favourable properties: In contrast to what one might expect, the non-magnetic Pt stabilises the magnetism of Fe or Co instead of reducing it!

We studied a PtFe alloy close to the described size limit: Depositing small amounts of Fe on a Pt surface we made an alloy layer of about equal amounts of Fe and Pt. Our earlier studies showed that we can easily produce different Fe patterns if we start with a surface in the shape of a staircase in which the height of each step is the height of one atom [2]. Depositing Fe near room temperature allows studying the magnetism of a one atom thick Fe stripe and repeating the preparation at a slightly higher temperature provides a FePt alloy which is as thin as a single atom. Fig. 1 sketches the atomic arrangements in the two cases. We employed X-ray magnetic circular dichroism (XMCD) at the beamline PM-3 to investigate the magnetic moments on the Fe atoms. The difference between Fe absorption spectra taken with reversed magnetic field (blue and black traces in Fig. 2) provides the XMCD spectra displayed at the bottom of Fig. 2.

Measuring Fe spectra for the same amount of Fe in the stripe (left) and in the alloy (right) we find that the observed magnetisation increases significantly (by a factor of 4.5) for the alloy. In the hysteresis curves (red trace in Fig. 3) we find that also the coercive field, i.e. the field required to destroy the stored magnetic information, rises to 0.6 T which is a surprisingly high value. Moreover, the magnetic moments are oriented perpendicularly to the sample surface leading to a large stray field which would facilitate 'reading' its orientation by an external magnetic head. Of course, this sample is not yet a memory for use in our computers. Our data were obtained at a temperature of 10 K and in a vacuum chamber at a pressure below 10^{-10} mbar, which is required to prevent sample contamination.

References:

*[1] P.Gambardella et al. Science **300** (2003) 1130*

[2] TY. Lee et al. in preparation.

*[3] J.A.Christodoulides et al. Phys.Rev.B **68** (2003) 054428;*

*[4] T.Shishidou et al. Phys.Rev.B **55** (1997) 3749*

Acknowledgements: Supported by the BMBF.

However, the results are exciting since comparable properties are obtained for PtFe alloy particles only at diameters larger than 5 nm [3], which are 'huge' structures with respect to the 0.2 nm thick alloy film.

Although we do not yet understand the detailed mechanism which improves the magnetic properties through the alloying of Fe with Pt, we were able to address the question how the Pt behaves in the alloy. We made use of the element specificity of XMCD and tuned at the PM-3 beamline from the magnetism in Fe to the magnetism in Pt. And, indeed, the Pt carries a magnetic moment proportional to the one on Fe. Comparing our XMCD spectra to published data from a CoPt bulk alloy [4] we find that the observed moments on Pt are aligned with the moments on Fe. Unfortunately, we cannot distinguish between different Pt sites and thus can only speculate that a major contribution may arise from Pt in the alloy layer and an additional part from Pt in the underlying material – probably from little more than the adjacent atomic layer. Earlier theoretical investigations of a Fe layer on Pt support such a picture but details have to wait for calculations of the exact alloy geometry.

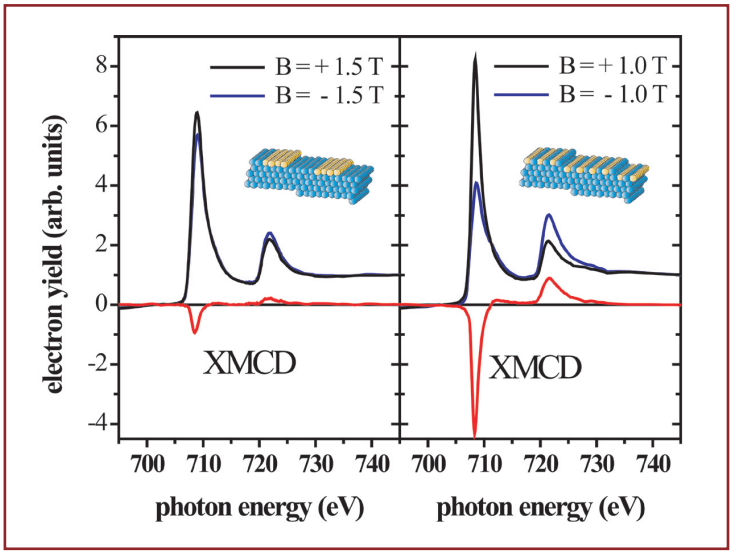

Fig. 2:
X-ray absorption spectra (top) and X-ray magnetic circular dichroic spectra (bottom) for Fe stripes (left) and for a surface alloy (right) with the same amount of Fe.

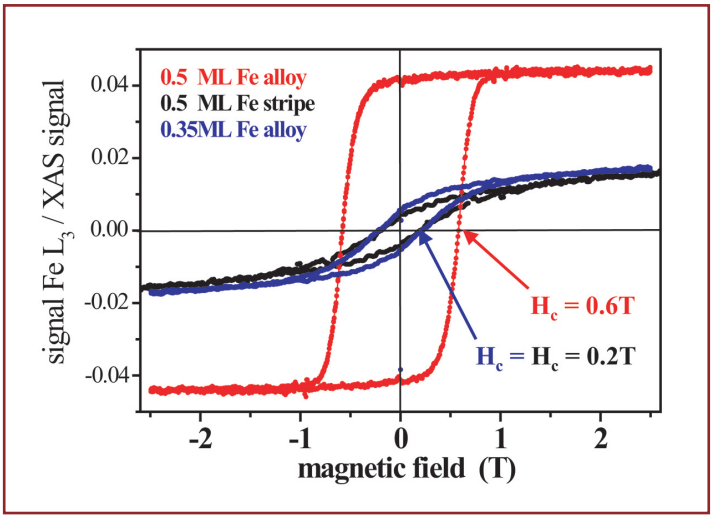

Fig. 3:
Hysteresis curves measured by XMCD on the Fe L_3 absorption edge. The red trace is measured for the alloy, the black curve for a Fe stripe at the same Fe coverage, and the blue trace for an alloy formed with a smaller amount of Fe.

Contact:
Klaus Kuhnke
k.kuhnke@fkf.mpg.de

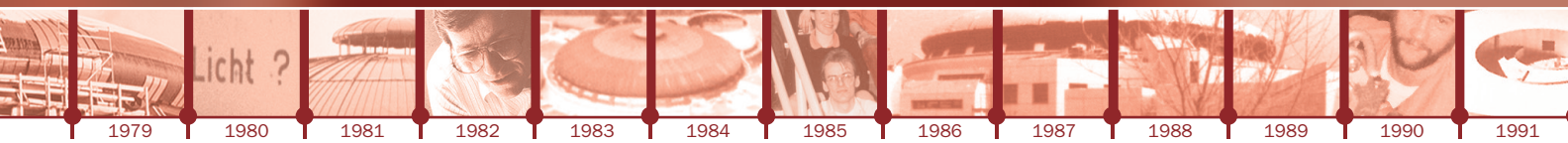

Spin-orbit interaction in a plane with electric and magnetic fields

O. Krupin [1], J.E. Prieto [1], S. Gorovikov [2], K. Döbrich [1], G. Bihlmayer [3], S. Blügel [3], G. Kaindl [1], K. Starke [1]

1 Freie Universität Berlin

2 MAX-Lab, Lund University, Sweden

3 Forschungszentrum Jülich

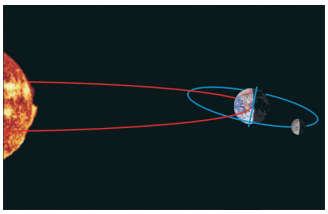

Our biological clock is tuned to the steady rhythm of day and night, thanks to the fact that the earth is spinning fast about itself while orbiting leisurely around the sun. Also the moon is spinning about itself, yet this motion is rigidly coupled to its orbital motion around the earth in a way, that the back side of the moon is never visible for us. Electrons in the atomic world behave quite similarly: they also spin around themselves while moving about a nucleus and, when left alone, they prefer to spin in the same rotational direction as they 'orbit around' the nucleus. So their spin and orbital motions are coupled as well. For 'orbiting' electrons, this phenomenon is well understood: every electron has a tiny compass (magnetic moment) associated with it's spinning motion; hereby it 'feels' the sense of its orbital rotation about the charged nucleus which creates a little magnetic field that orients the electron compass.

These days, the electron spin has become a 'rising star' in applied condensed-matter research that aims at building new electronic devices based on manipulating the electron spin in very small structures (spintronics) [1]. Usually, you just take a magnet to change the electron spin orientation ('spin flip') but that does not work in nanostruc-tures because sufficiently strong magnets are too big. One way out is to use the so-called Rashba effect [2], based on the fact that an electric field acts as a magnetic field in the rest frame of a moving electron. Electric fields of appropriate shape and strength for the effect to occur exist at surfaces and interfaces of solid crystals (where structural inversion symmetry is broken). So, the whole idea of studying the Rashba effect is to understand it better from an electronic structure point-of-view. Until now, research of the Rashba effect has been focused on semiconductor heterostructures [3] and nonmagnetic metals [4-6] – quite surprising when one considers that there are interfaces between ferromagnetic and nonmagnetic materials in all device schemes currently suggested [1,3]. Hence, we have started a joint experimental and theoretical project to investigate the Rashba effect at surfaces and interfaces of magnetic systems.

Here we sketch some first results we have obtained for magnetic lanthanide metal and metal-oxide systems.

Fig. 1 shows a set of angular-resolved photoemission spectra of Gd(0001), serving as a representative example of the valence band electronic structure of a (trivalent) lanthanide metal. In addition to the bulk 5d bands dispersing up towards the Fermi energy (on the left side), there is a surface state close to the Fermi level; electrons in this state can only propagate parallel to the surface but not perpendicular (owing to a partial bulk band gap). When emitted at some non-vanishing angle with respect to the surface normal, they have been 'caught in action': they have been photoemitted while propagating parallel to the surface. The larger the angle with respect to the surface normal, the faster they have been, and opposite angle means opposite propagation direction.

In terms of spin-orbit coupling, the straight electron motion in a plane is similar to the orbital motion of a bound electron around an atomic nucleus: in both cases it propagates perpendicular to an electric field. (The term Rashba effect is used for spin-orbit coupling in planar geometry.) In ferromagnetic Gd,

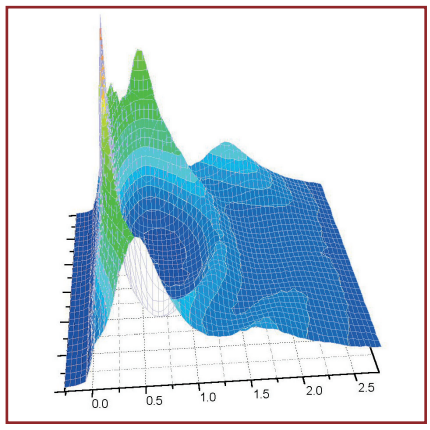

Fig. 1:
Angle-resolved energy-distribution curves of the Gd(0001) valence bands in a region of 16 Å around the center of the surface Brillouin zone. Recorded (at 80 K) with a fixed photon energy of 36 eV, the more strongly bound electrons appear on the right side.

References:

*[1] S.A. Wolf et al. Science **294**, 1488 (2001)*

*[2] E.I. Rashba, Sov. Phys. Sol. State **2**, 1109 (1960)*

*[3] I. Zutic et al., Rev. Mod. Phys., **76**, 323 (2004)*

*[4] S. LaShell et al., Phys. Rev. Lett. **77**, 3419 (1986)*

*[5] E. Rotenberg and S.D. Kevan, Phys. Rev. Lett. **80**, 3419 (1998)*

*[6] F. Reinert et al., Phys. Rev. B **63**, 115415 (2001)*

[7] O. Krupin et al., preprint (2004); arXiv:condmat/0403405

*[8] C. Schüssler-Langeheine et al., Phys. Rev. B **60**, 3449 (1999)*

*[9] P. Kurz et al., J. Phys. Cond. Matter **14**, 6353 (2002)*

electrons in this surface state have mostly spin 'up', while the same state for electrons with spin 'down' is not occupied. The question now is, what happens when we flip the spin orientation of the electrons in the surface state, but keep their propagation direction?

This is simply done by reversing the magnetisation of the sample. Fig. 2(a) shows that the surface-state energy changes upon flipping the spin – just a little, but significantly and reversibly. The energy shift upon spin flip is the Rashba shift; it is given as blue data points in Fig. 2(c). A much bigger Rashba shift is found after we have modified the system by adsorbing a small amount of oxygen on the surface in such a way that the O atoms form a two-dimensional lattice of GdO on top of the metal surface [8]. As is shown in Fig. 2(b), the electronegative O atoms strongly affect the entire surface electronic structure: now both the majority-spin state and the (exchange split) minority-spin state are occupied, both dispersing upwards towards the Fermi energy with increasing momentum. Again, their positions change between red and black upon magnetisation reversal; the associated differences are plotted in Fig. 2(c).

This is the first experimental investigation of two-dimensional electronic states in which magnetic exchange interaction and the Rashba effect coexist. To understand the present observations for Gd(0001) and p(1x1)O/Gd(0001) and, in particular, their strikingly different Rashba shifts in a quantitative way, we have performed ab-initio calculations using DFT in the LDA+U approximation [9]. The result for the surface-monoxide system is presented in Fig. 3. The calculated dispersion is in good agreement with the experimental data. The charge density distribution in Fig. 3(c) shows that the two-dimensional state is distributed over the whole region between the GdO layer and the sub-surface Gd layer; hence, the state is actually an interface state. The enhanced Rashba effect after oxide-layer formation is owing to the steep charge density gradients in the interface region, driven by the electronegative O atoms.

We suggest utilising the spin sensitivity of the Rashba effect in magnetic systems to study two-dimensional spin structures at surfaces and interfaces.

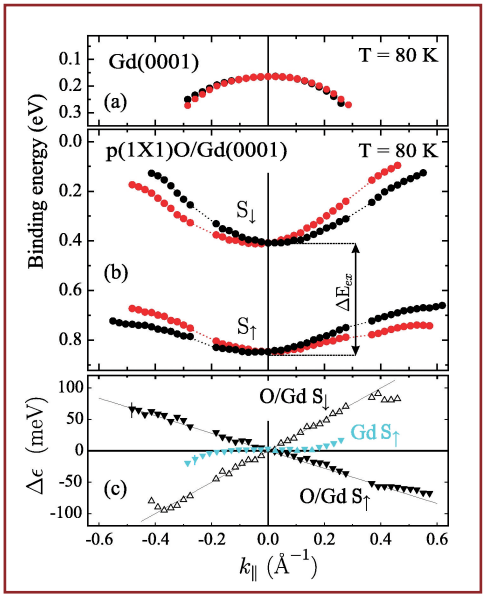

Fig. 2:
At ferromagnetic surfaces, the energy-momentum relation of two-dimensional states changes upon magnetisation reversal, owing to the Rashba effect. This effect is small (a) at the Gd(0001) metal surface and considerably larger (b) at the metal-oxide/metal interface. (c) Rashba shift of the states, described in the text; from [7]

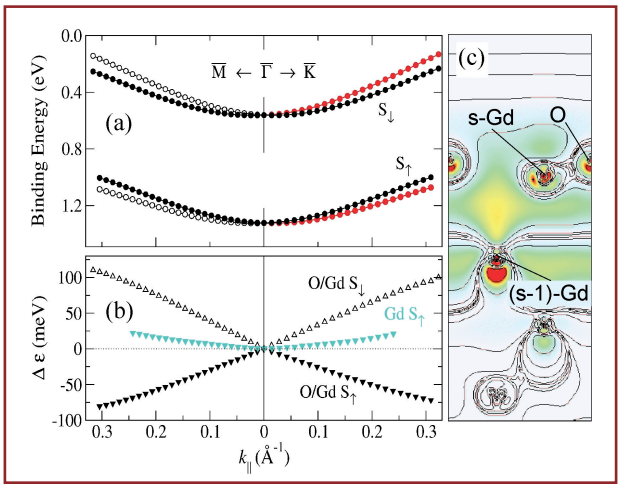

Fig. 3:
(a) Calculated dispersion and (b) Rashba shift of the surface state at p(1x1)O/Gd(0001). (c) Charge density distribution of the surface state in a plane perpendicular to the surface. The linear colour scale indicates high charge density (red), medium (yellow), low (green), very low (blue), and negligible (white); from [7].

The present findings can be of interest for future spintronic devices, especially at interfaces where Rashba and exchange interaction together control the electron spin. The Rashba effect at a metal/metal-oxide interface could in principle be used in a device that would become as thin as the interface itself, i.e. a few atomic layers. Yet, one has to solve several problems before: (1) make the conducting (metal) side of the interface so thin that conduction essentially goes via the interface state; (2) stabilise the whole interface between (chemically) inert layers.

Contact:
Oleg Krupin
krupin@bessy.de
Kai Starke
starke@physik.fu-berlin.de

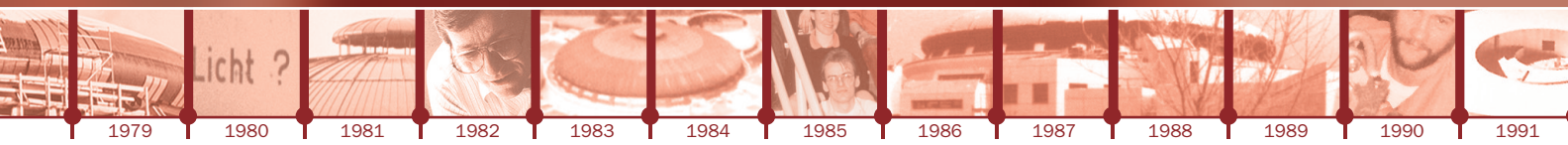

Strange birds in a cage: Controlled charging of trapped nanoparticles

B. Langer[1,2], M. Grimm[1,2], C. Graf[1], S. Dembski[1], R. Lewinski[1], S. Schlemmer[3], D. Gerlich[4], W. Widdra[5], U. Becker[6], E. Rühl[1]

1 Universität Würzburg

2 Max-Born-Institut Berlin

3 Universität zu Köln

4 Technische Universität Chemnitz

5 Universität Halle

6 Fritz-Haber-Institut der Max-Planck-Gesellschaft, Berlin

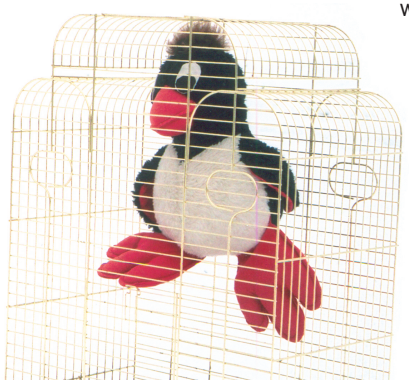

What happens to an isolated piece of matter, such as a single nanoparticle, when it is exposed to synchrotron radiation? Recent experiments give answers: (i) It charges up, where the smallest change in charge corresponds to one elementary charge. (ii) There is evidence for processes where no electrons are emitted after the impact of ionizing radiation. These fundamental experiments are also of interest to other fields of research: Nanoparticles and clusters bridge the gap between the gas phase and macroscopic condensed matter. The size dependence of the electronic and structural properties is sensitively studied by single, trapped particles which are exposed to synchrotron radiation.

The key component for experiments on isolated nanoparticles or microparticles is a quadrupole particle trap, as shown in Fig. 1. It consists of electrodes, where suitable AC- and DC-voltages are applied, stabilising the particle in the centre of the trap [1-3]. There is one requirement to the electrodynamically stored particle: It must carry electrical charges. Any change in mass or charge state leads to changes in trajectories or instabilities of the trapped particle. These are monitored by an optical detection system, which also serves to characterize the charge-to-mass ratio of the particle. This is accomplished by measuring scattered laser light from the particles, so that the secular motion frequencies of particle are probed. The trap is not only a sensitive monitor for any changes in charge state, it is also a sensitive mass balance which works in the picogram regime. This feature represents a distinct advantage compared to experiments on macroscopic samples of condensed matter, where both the mass and the charge state cannot be easily controlled in such an accurate way.

Once the particles are characterised, they are exposed to monochromatic synchrotron radiation. Photon impact by ionizing radiation changes the charge state of the stored particle. If the initial charge state is low and the photon flux is also kept low, one can observe step by step changes in charge state, as shown in Fig. 2. Note that this experiment took five hours, where just about 35 charging events are clearly resolved. The step heights correspond to multiples of the elementary charge e. The height distribution of these steps is a characteristic property of the material at the given photon energy. Fig. 3 shows a comparison of the distribution of emitted photoelectrons per absorbed photon for a single SiO_2-nanoparticle at 84 eV, 120 eV, and 500 eV photon energy. The largest step height is three at 84 eV, but mostly the charge state in increased by a single charge per absorbed photon. This behaviour changes with increasing photon energy, where up to seven electrons are emitted per absorbed photon at 500 eV. The experimental results are modelled by Poisson distributions (solid lines in Fig. 3), which suitably model the emission of secondary electrons. The distributions shown in Fig. 3 indicate that the amount of single ionization events is underestimated by the Poisson distributions [4]. Additional work has shown that this is due to the emission of primary photoelectrons, which is

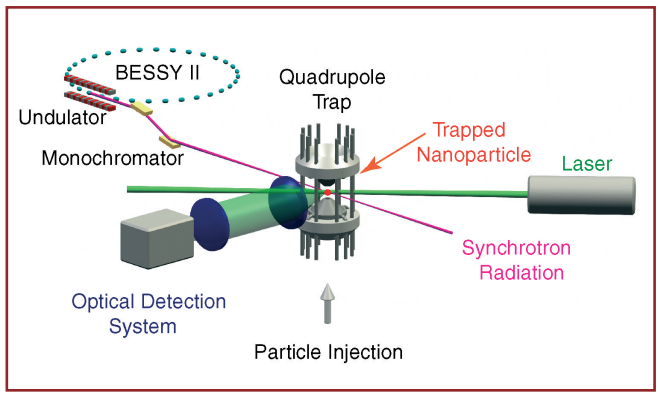

Fig. 1:
Schematic diagram of the experimental setup for investigating trapped nanoparticles.

References:

[1] M. Grimm et al., AIP Conf. Proc. ***705****, 1062-1065 (2004).*

[2] S. Schlemmer et al., J. Appl. Phys. ***90****, 5410-5418 (2001).*

[3] B. Steiner et al., Appl. Opt. ***38,*** *1523-1529 (1999).*

[4] M. Grimm et al., manuscript in preparation (2005).

[5] C. Graf et al., Langmuir ***19****, 6693-6700 (2003).*

[6] M. Hamza et al., Phys. Chem. Chem. Phys. ***6****, 3484-3489 (2004).*

Acknowledgements:
Supported by the BMBF and the DFG. We thank Andreas Hofmann and Melanie Grom for their work on nanoparticle synthesis.

superimposed to the distribution of secondary electrons [4]. The maximum of the Poisson distribution models the average number of emitted electrons per absorbed photon. This quantity increases slightly with photon energy, as shown in Fig. 3.
An interesting aspect is, that the Poisson distribution models a finite probability for absorbed photons that do not lead to any change in charge state, implying that the energy of a soft x-ray photon is absorbed and there is no emission of electrons, even though the photon energy is far above the ionization energy. The probability for this process increases, if the charge state of the particle is more and more increased. The explanation for this counterintuitive result is quite simple: The positive charges are distributed on the surface of the particle, leading to a strong electric field that retains the electrons at the particle. One may anticipate that a trapped nanoparticle may be charged until it reaches the limit for fission. Our experimental results indicate that this limit cannot be easily reached since the residual gas discharges efficiently the particles, even if the particle is stored in an ultrahigh vacuum surroundings. Previous experiments have reached charge states up to about 80,000 charges on trapped spherical SiO_2-particles of 250 nm radius [4]. This is almost an order of magnitude below the expected fission limit.

Going from nanoparticles with uniform chemical composition to structured nanoscopic matter of well-defined structure, such as core-shell particles, one finds a wide field of applications in materials science, catalysis, photonics, or medical science. Key to this research are chemical syntheses developed in colloidal science [5]. These serve to produce substantial quantities of structured nanoparticles, such as core-shell systems. Fig. 4 shows schematically, how nanoparticles can be selectively tailored according to the specific needs. The surface, buried interfaces, and bulk phases of single trapped particles are studied avoiding any contact to a substrate, which may modify the properties of interest. There are interesting perspectives: The trapped particles do not have to be solid [6]. Recent work has already shown that liquid particles can be stored and investigated by soft x-rays. Synchrotron radiation represents a sensitive probe for element- and site-selective excitation along with specific spectroscopic approaches. This will allow us to optimize the electronic structure, interaction with the surroundings, and optical properties of structured nanoparticles, so that they can be used as specific sensors, fast switches, or pigments absorbing in different wavelengths regimes.

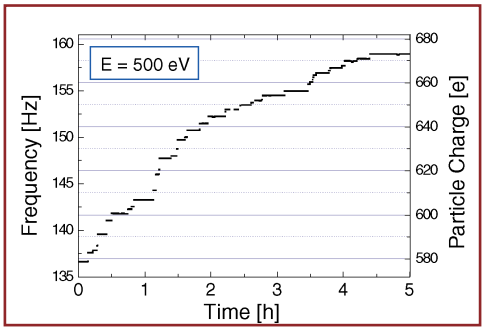

Fig. 2:
Typical charging curve of a single trapped SiO_2 nanoparticle (radius: 250 nm) as a function of time at 500 eV photon energy.
The vertical scale on the left hand side corresponds to the frequency of the particle in the trap. The absolute number of charges on the particle is shown on the vertical scale on the right hand side.

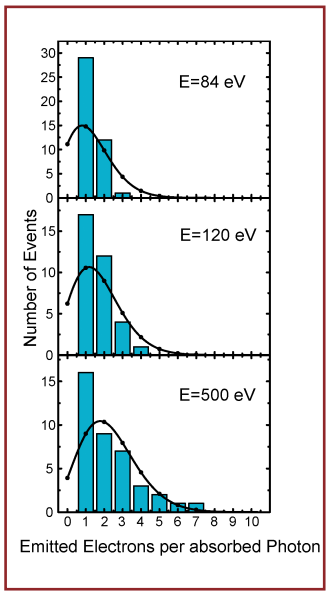

Fig. 3:
Probability for the emission of electrons per absorbed photon at various photon energies (blue bars). The full curves are obtained from Poisson distributions which model the emission of secondary electrons.

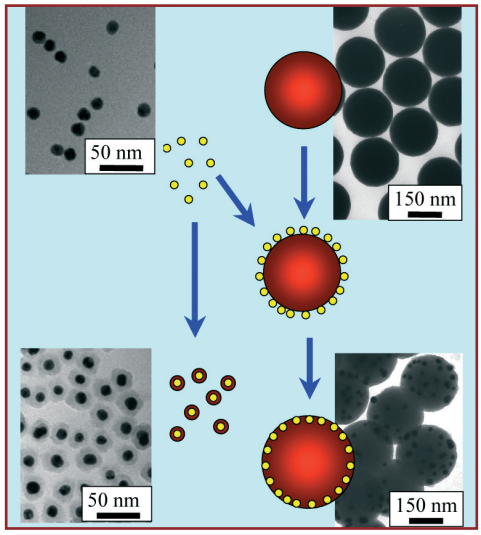

Fig. 4:
Nanoparticles with well-defined structures as developed by approaches of colloidal science are a promising perspective to study properties of trapped particles. Their chemical synthesis is sketched together with electron micrographs.

Contact:
Eckart Rühl
eruehl@phys-chemie.uni-wuerzburg.de

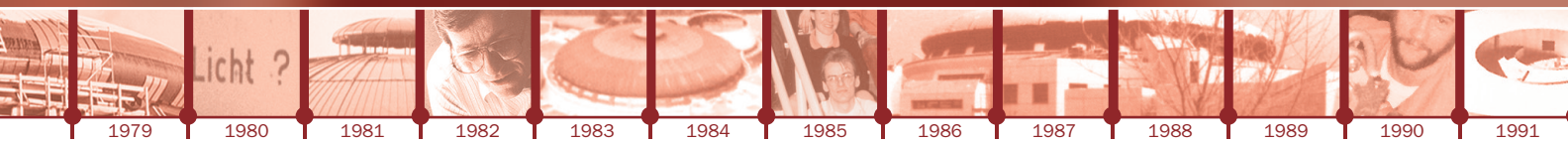

MoS_2 nanotubes: Old friends in new form

A. Zimina[1], S. Eisebitt[1], M. Freiwald [1], S. Cramm[2], W. Eberhardt[1], A. Mrzel [3], D. Mihailovic [3]

1
BESSY, Berlin

2
Forschungszentrum Jülich

3
Jozef Stefan Institut, Slovenia

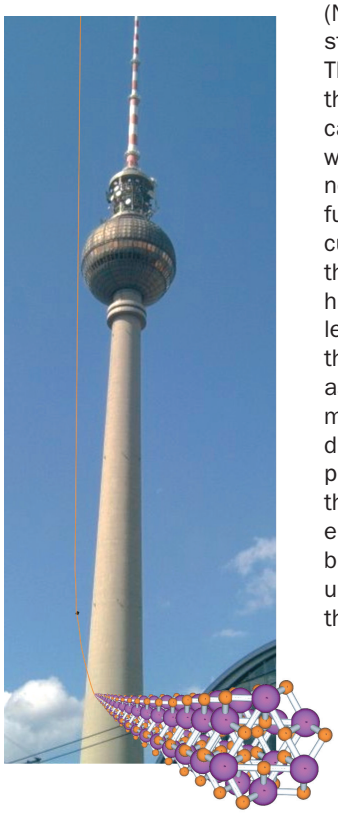

A few years ago the NASA was speculating on an escalator to a satellite orbiting the Earth. This science-fiction was stimulated by the astonishing properties of nanotubes (NT), which show an enormous mechanical strength compared to their size and weight. The first material which was found to exist in the form of fullerenes and nanotubes was carbon [1]. Now other, carbon-free materials, which posses layered structures in their normal modification, can be synthesized in fullerene- and nanotube-like forms [2]. If one cuts the fantasy down to earth-dimensions, the MoS_2 nanotubes studied here would have a diameter of only 3.7 mm if their length would be scaled up to the height of the Berlin TV tower (Fig. 1). Not only the aspect ratio of the NTs is astonishing. These materials can have a variety of applications due to their specific electronic and physical properties and their particular geometry in the nanometer range. Examples are field emission devices, electrodes in Li micro-batteries, conducting nanowires, sensors or ultra-low-friction lubricants. Prototypes of three terminal electronic devices such as transistors have been realized with carbon nanotubes.

For semiconducting nanotubes to be useful for nanoelectronics, well defined properties, stability and high purity is required. The properties of carbon NTs depend strongly on the chirality vector, which describes the exact geometry of a given nanotube. Very slight variation of the chirality vector can make the difference between metallic or semiconducting. Unfortunately, chirality-pure (or chirality-controlled) carbon nanotubes can not yet be synthesised. From this viewpoint, the situation seems more favourable for MoS_2 NTs, where perfect size control is not absolutely necessary, since changes in the length of the chirality vector do not cause large changes of the electronic structure and typically do not change the band gap character (i.e. direct vs. indirect).

Prospects for the application of NTs in electronics were improved with the reported synthesis of the sub-nanometer diameter single-wall MoS_2-I_x nanotubes with perfect diameter control [3]. The material grows in the form of bundles of individual tubes, with an outer tube diameter of only 9.6 Å. Bundles can be up to several hundreds micrometers long and consist of up to 10^6 individual nanotubes.

The general scientific question is why the electronic properties of the NTs are different from the bulk form, if the chemical composition remains unchanged. Turning from MoS_2 bulk material to the sub-nanometer diameter NTs, one would expect changes because (a) electronic states may be redistributed due to changes in the geometry of the interatomic bonds (b) extended electronic states may feel the effects of quantum confinement (c) inter-tube interaction within a bundle may differ from the interlayer interactions in bulk MoS_2. Theoretical calculations on large diameter MoS_2 tubes demonstrated that their electronic structure depends on the chirality and the band gap increases monotonously towards the bulk value with increasing tube diameter [4].

We studied the electronic structure of MoS_2-I_x nanotubes by atom-selective Soft X-ray Absorption (SXA) and Soft X-ray Fluorescence (SXF) spectroscopy [5]. The local partial density of the electronic states (LPDOS) in the valence band (VB) and conduction band (CB) is probed independently by SXF and SXA. With photon excitation using monochromatised synchrotron radiation the information obtained is related to the bulk of the material under investigation. 2H-MoS_2 bulk material and MoS_2-I_x NTs have been investigated at the UE56/1-SGM beamline.

In Fig. 1 the SXA and high energy excited SXF spectra of the 2H-MoS_2 and MoS_2-I_x NTs are presented. The spectra reflect the energy range in the vicinity of the top of the VB and bottom of the CB, where the electronic states are sensitive to the changes in the chemical bonding. The most notable changes in spectra of NTs compared to the bulk can be seen in the immediate vicinity of the band edges.

The peak at 162.5 eV in the absorption spectrum, which can be observed in the bulk material, disappears in the NTs. In SXF, spectral signal weight at high energies, corresponding to the states at the top of the

References

[1] M. S. Dresselhaus et al., 'Carbon Nanotubes', Berlin, Germany (2000)

*[2] R. Tenne et al., Nature (London) **360**, 444 (1992)*

*[3] M. Remskar et al., Science **292**, 479 (2001)*

*[4] G. Seifert et al., Phys. Rev. Lett. **85**, 146 (2000)*

*[5] A. Zimina et al., NanoLetters **4**(9), 1749 (2004)*

*[6] P. Raubaud et al., J. Phys: Condens. Matter **9**, 11107 (1997)*

[7] K. Hermann et al., StoBe Software (2002)

*[8] M. Verstraete and J.-C. Charlier, Phys. Rev. B **68**, 045423 (2003)*

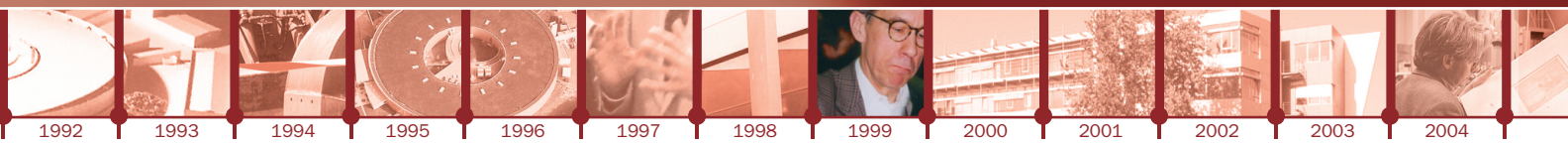

VB, is strongly increased in the NTs. The top of the VB and the bottom of the CB are dominated by Mo states. We observed those states in the experimental spectra via their overlap with the S site. Apparently, those states are affected most drastically when going from bulk material to the NTs. Interestingly, the band gap is reduced in the tubes as compared to the bulk. This is counter intuitive with respect to a simple quantum confinement model, which would not take bond angle distortion into account.

In order to understand the main changes in the electronic structure between bulk and MoS_2-I_x NTs, we performed electronic structure calculations of the simplest possible model structures. The most drastic change in the local geometric arrangement of the MoS_2-I_x NTs as compared to the bulk is the S-Mo-S bond angle. The simplest model structure containing this bond angle as a parameter is a three atom S-Mo-S cluster: the bulk material was modeled with a S-Mo-S angle of 82° and a S-Mo bond length equal 2.417 Å [6]; the MoS_2-I_x NTs were modelled with the smaller S-Mo-S angle of 63° suggested in Ref. 3, keeping the bond length constant. The simulation of the SXF and SXA spectra was made using the StoBe electronic structure package [7].

The calculated spectra follow the general trend of the experimental SXA and SXF spectra. This suggests that our simple model captures the essential effects in the changes of the local electronic structure between bulk MoS_2 and sub-nanometer MoS_2-I_x NTs. We conclude that the redistribution of electron density in the tubes compared to 2H-MoS_2 bulk material is mainly due to the S-Mo-S bond distortion. A charge distribution analysis in the ground state (Fig. 2) shows that electron density is redistributed from the S atoms towards the Mo atom due to the changes in bond angle.

From the combination of SXA and resonantly excited SXF spectra we determine a band gap of 0.4±0.2 eV for the MoS_2-I_x NTs in conjunction with the bulk 2H-MoS_2 band gap of 1.2 eV. This first experimental determination of the bandgap in sub-nanometer MoS_2-I_x nanotubes is in agreement with the general theoretical prediction of a smaller gap in the NTs as compared to the bulk material [4], but in contradiction to calculations for a variety of sub-nanometer diameter model systems, which were recently predicted to be metallic [8]. We hope that the insight in the local electronic structure can help facilitate future applications of our old friend MoS_2 in its fascinating new form.

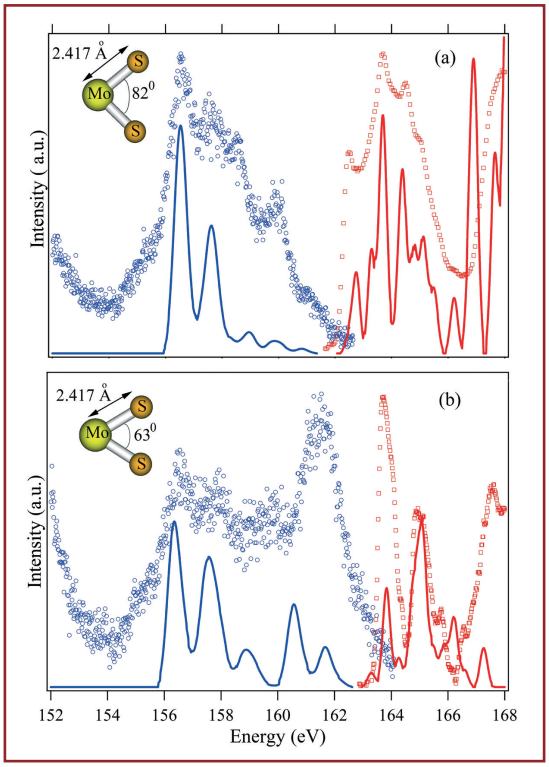

Fig. 1.:
SXA (red) and SXF (blue) spectra of (a) 2H-MoS_2 and (b) MoS_2-I_x nanotubes (Experiment: symbols; Calculation: solid lines).

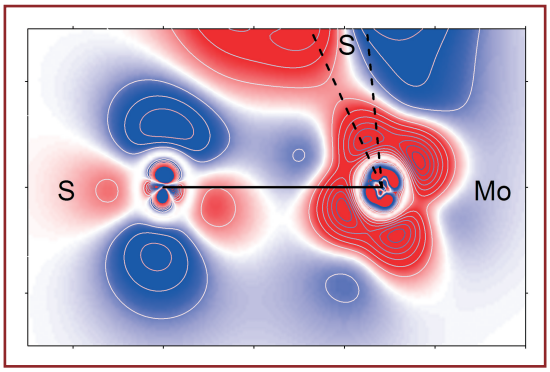

Fig. 2:
Map of the difference in electronic states in the valence band between nanotubes and bulk material.

Contact:
Anna Zimina
zimina@bessy.de

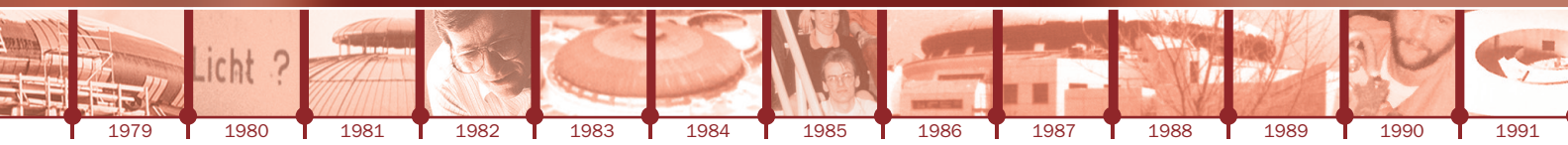

Johann Wolfgang Goethe-Unversität, Frankfurt am Main

Blown-up Helium atoms: „Guinea pigs“ for studying electron correlation

A. Czasch, M. Schöffler, M. Hattaß, S. Schößler, T. Jahnke, Th. Weber, O. Jagutzki, L. Schmidt, H. Schmidt-Böcking, R. Dörner

Most properties of matter such as colour, conductivity, magnetism, chemical behaviour etc. are based on the properties of the electron clouds - the glue between the atoms. We can measure many of these processes in great detail by studying the interaction of light with electrons. However, theoretical calculations are somewhat crude in comparison with the complex behaviour of electrons in atoms, molecules and solids. These calculations are based on quantum mechanics which should, in principle, enable us to determine the properties of electrons in a system. Unfortunately, the quantum mechanical equations cannot be solved exactly, as soon as more than one electron is involved. Already in a system with two electrons, like a Helium atom, the particles interact (correlate) in a complex manner so that in a simple ionisation experiment not only the leaving electron is involved but also the remaining electron becomes excited (Fig. 1).

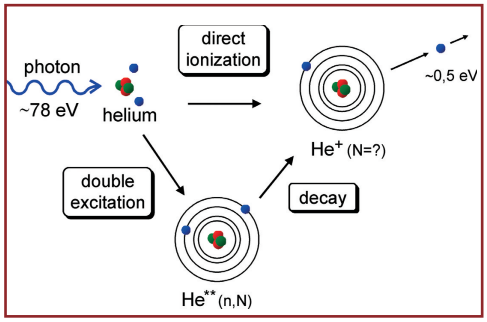

Fig. 1:
Two different pathways - direct ionisation or excitation and decay of a doubly excited state - leading to the same result. Interference effects between both channels were studied in this work.

The quantum mechanical correlations lead to perfectly entangled many-particle dynamics and the electrons seem to possess instantaneous knowledge of the motion of its companions and all particles including the nucleus act like one entity. In order to investigate these hidden correlations one has to study the dynamics of electron pairs.

We investigated the pair dynamics in Helium by exciting both electrons from the ground state to high lying levels close to the continuum threshold and by measuring the decay dynamics in the final state. Helium can be doubly excited via absorption of one photon. By choosing photon energies close to the double ionisation threshold at 79 eV the helium atoms become 'blown up' like a balloon shortly before bursting. Such a doubly excited atom can decay by electron or photon emission (Fig. 1). The remaining He^+-ions are left behind in hydrogen-like excited states with principal quantum numbers N. By measuring the kinetic energy E_{kin} of an emitted electron one can determine the final state N of the residual He^+-ion ($E_\gamma = E_{kin} + E[He^+N]$). The distribution of the momenta of the emitted electrons with respect to the photon polarisation and to the final He^+ state provides the information of the e-e correlation (as long as the decay of the excited state is fast enough to avoid e-e scattering in the excited or final state).

The fundamental questions we wanted to answer were: How does the ground state contribute to the correlated dynamics of the electrons in double excited states? Furthermore, it was speculated that as both electrons are raised up to higher excitation levels the system should resemble more and more a classical three body system. So, how does a quantum system behave when it approaches the border to the world of classical mechanics? The majority of classical three body systems exhibit chaotic behaviour. Is this also valid for doubly excited Helium? To answer the questions we had to perform so called complete measurements in which all momenta of the outgoing particles are recorded.

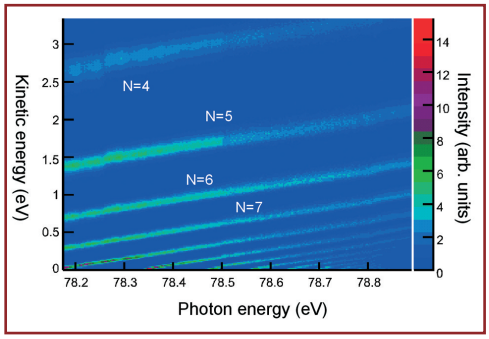

Fig. 2:
As the photon energy approaches the double ionisation threshold at 79 eV more and more final states of the Helium ions can be populated. Each line can be assigned to an excited state N of the residual He^+-ions. The intensities of these lines fluctuate. This behaviour is caused by the complex underlying physics.

References:

*[1] J. Ullrich et al., Rep. Prog. Phys., **66** 1463 (2003)*

*[2] A. Menzel et al, Phys. Rev. A, **54**(3) 2080 (1996)*

*[3] R. Püttner et al., Phys. Rev. Lett., **86**(17) 3747 (2001)*

*[4] Y. H. Jiang et al., Phys. Rev. A, **69** 042706 (2004)*

Acknowledgements:
Supported by the BMBF and the DFG. We thank J. M. Rost, E. Bray and A. Kheifest for providing R-matrix and CCC calculations.

Measurements of this kind have been proven extremely difficult due to insufficient detection efficiency and photon flux in the interesting energy regime close to the double ionisation threshold (between E_γ = 78 eV and E_γ = 79 eV). By combining a high flux undulator beamline (U125/PGM-1) with the COLTRIMS imaging system we were able to approach experimentally the double ionisation threshold.

The COLTRIMS imaging system features significantly higher detection efficiencies. The principle of this new imaging system is simple (Fig. 3): The photon beam from a synchrotron radiation source intersects a narrow supersonic helium jet. An electrostatic guiding field projects all emitted particles - electrons and He^+-ions - onto two position and time sensitive detectors. This method ensures the detection of all particles regardless of their initial direction of emission. Since the electric field and the dimensions of the spectrometer are known quantities it is an easy task to determine the initial momentum vector of each particle from its flight time and final position on the detector.

In our measurement we have covered a photon energy range between E_γ = 78.156 eV and 78.88 eV which is very close to the double ionisation threshold at E_γ = 79 eV. The data set consists of several independent measurements at different photon energies with a spacing of 3 meV and a photon energy resolution of 3.9 meV (FWHM). At any given photon energy the momenta of all emitted electrons were detected in coincidence with the recoiling He^+-ions. All these individually detected events can be combined in one two dimensional histogram (Fig. 2). Each line in this picture corresponds to a final state N of the residual He^+N-ions. As we move to higher photon energies we see that more and more lines emerge because higher final states He^+N can be populated. A closer look reveals that the intensities of these lines fluctuate. These fluctuations in the excitation function are clearly resolved. Since the statistical error bars are rather small, these fluctuations are real. We found structures in these excitation functions that are common to all observed decay channels.

In addition to that we found the lifetimes of the double excited states to be well below one nanosecond (10^{-9} seconds). These results raise some intriguing questions: If we imagine these highly excited state as two electrons orbiting the nucleus in a far distance we should expect very long lifetimes of these states in the regime of several microseconds. Yet the decay happens almost instantaneously. Therefore we believe that these doubly excited states never evolve into a pair of far orbiting electrons. Immediately after the excitation the electrons should be still in close vicinity to the nucleus as they were in the ground state - similar to Franck-Condon transitions.

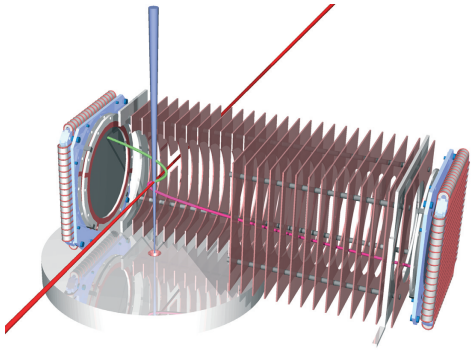

Fig. 3:
The COLTRIMS-spectrometer (cut open) with two time and position sensitive detectors. The synchrotron radiation beam (red) intersects a helium gas jet (blue). After absorbing one photon a Helium atom emits an electron (green trace) and thus becomes a positively charged He^+-ion (pink trace). An electrostatic guiding field which is applied via a chain of copper electrodes projects both particles onto the detectors. Since all emitted particles are detected, this setup provides a much higher detection efficiency compared to traditional techniques.

Two different theoretical methods (CCC and R-matrix) are applied to describe our data (Fig. 4). One should note that the results of these calculations are not satisfyingly consistent with each other. Apparently there is some discrepancy between the measured data and the results of the calculations. This is even more the case for the angular distributions (β-parameter) of the emitted electrons. It turned out that the results strongly depend on the accuracy of the modelled ground state. Therefore we believe that the experimental and theoretical study of highly doubly excited states of helium offers an interesting way to investigate correlations in bound multi electron systems.

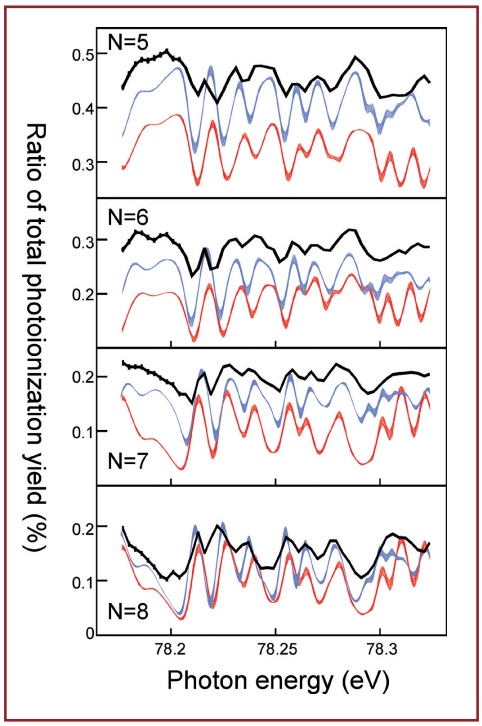

Fig. 4:
Ionisation rates for different final states of the He^+-ions. Our measurement (black), CCC-calculations (red), and R-matrix-calculations (blue). The minima and maxima follow a pattern which is common to all curves.

Contact:
Achim Czasch
czasch@atom.uni-frankfurt.de

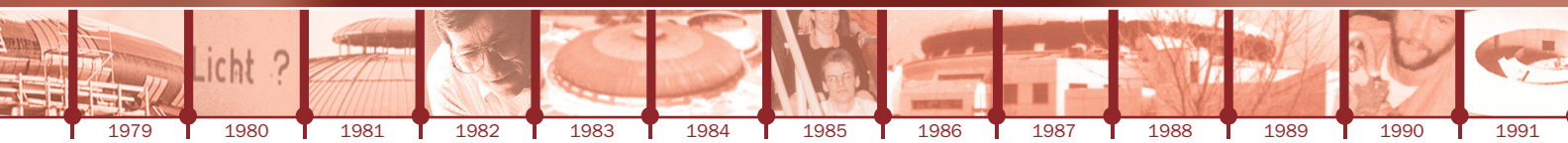

Physikalisch-Technische Bundesanstalt, Berlin

Towards monochromatic mammography? On the biological effectiveness of X-rays

M. Krumrey

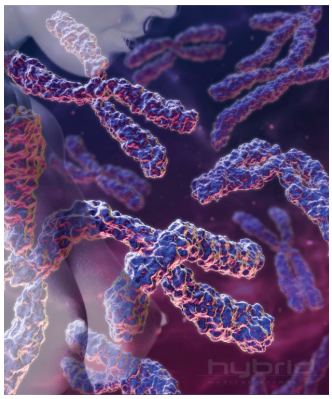

Breast cancer is the most common cancer among woman. In Germany, about 45,000 women are diagnosed with breast cancer every year, and some 18,000 die of it. It is consensus, that for fighting the disease successfully it is essential to detect the cancer at the earliest stage possible. Despite several other approaches under investigation mammography is still regarded to be the diagnostic method of choice. But there is an ongoing discussion concerning the benefits of mammography in relations to the risks. The main concern is that every mammography means exposure to radiation.

The biological effectiveness for ^{60}Co γ-radiation at about 1.25 MeV is used as reference (RBE = 1), because it is similar to the radiation to which the well-surveyed atomic bomb survivors in Hiroshima and Nagasaki were exposed.

The radiation risk assessments are based on the assumption that the relative biological effectiveness (RBE) of X-rays is 1, however, a few years ago an RBE of 8 had been reported for mammography X-rays [1]. As mammography is a soft tissue imaging technique, mainly X-ray tubes with Mo or Rh anodes are used and operated at relatively low voltages in the range from 25 kV to 35 kV. Even with the typical filtration by Mo or Rh foils, the spectrum extends from below 10 keV to the maximum energy (Fig. 1). Although a great part of the radiant energy is in the characteristic lines of the anode material contributions of other photon energies to the RBE have to be considered. In a joint project of the National Research Centre for Environment and Health (GSF) and the Physikalisch-Technische Bundesanstalt (PTB) we aimed to investigate the dependence of the RBE on the X-ray energy in order to provide recommendations on minimising risks due to radiation, i.e. in mammography.

We investigated the photon energy range from about 2 keV to 40 keV. As biological endpoint of radiation damage we chose the induction of chromosome aberrations in human blood cells. At high photon energies, blood from a healthy male donor was irradiated in disk-shaped chambers containing a 2-mm-thick blood layer. At low energies, however, the absorption within this layer would have been much too high. Therefore, we isolated lymphocytes and allowed them to attach as monolayer to a thin foil. At 17 keV, thick blood layers and monolayers have been irradiated to demonstrate the equivalence of the procedures. In both cases, a circular area with a diameter of 25 mm had to be uniformly irradiated.

The irradiations were performed at the PTB four-crystal monochromator (FCM) beamline and at the BAMline, a wavelength-shifter beamline jointly operated by the Bundesanstalt für Materialforschung und -prüfung (BAM) and the PTB. While at the BAMline a several cm-wide horizontal stripe of monochromatised synchrotron radiation is available for photon energies above 5 keV, the FCM beamline provides - like most SR beamlines - a focal spot with a size below 1 mm. Thus the blood samples had to be scanned through the beam: at the BAMline only vertically, at the FCM beamline line by line. Directly in front of the samples, the beam was shaped with rectangular apertures to match exactly the line-to-line distance. The dose rate behind the aperture was calculated from the photon flux which was measured using calibrated photodiodes or ion chambers. Their calibration is based on the PTB primary detector standards: the cryogenic electrical substitution radiometer and the free-air ionisation chamber [2]. The absorbed doses in blood, ranging between 0.25 Gy and 2 Gy, were obtained by adjusting the scan speed. Depending on the energy and the beam size, the deposition of 1 Gy took between 30 s and 3,000 s.

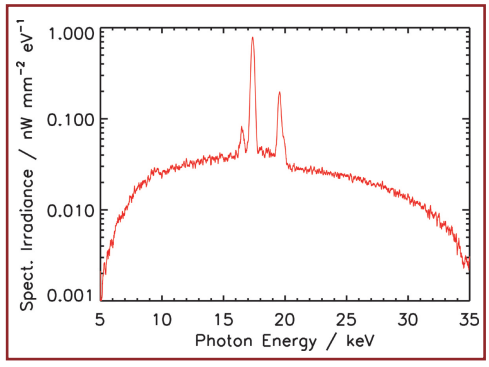

Fig. 1:
Spectrum of a mammography unit with Mo X-ray tube

References:

[1] D. Frankenberg et al., Radiat. Res. ***157****, 99 (2002)*

[2] M. Krumrey et al., Proc. SPIE ***5501****, 277 (2004)*

[3] E. Schmid et al., Radiat. Res. ***160****, 499 (2003)*

[4] M. Krumrey et al., Radiat. Environ. Biophys. ***43****, 1 (2004)*

[5] R. Thornagel et al., Metrologia ***38****, 385 (2001)*

[6] F. Diekmann et al., Eur. Radiol. ***14****, 1641 (2004)*

[7] R. Lawaczeck et al., Invest. Radiol. ***40****, 33 (2005)*

Acknowledgements:
The contributions of M. Hoffmann, G. Ulm (PTB), E. Schmid, D. Regulla (GSF), R. Lawaczeck, H. J. Weinmann (Schering AG), V. Arkadiev, N. Langhoff (IfG), and F. Diekmann (Charité) are gratefully acknowledged.

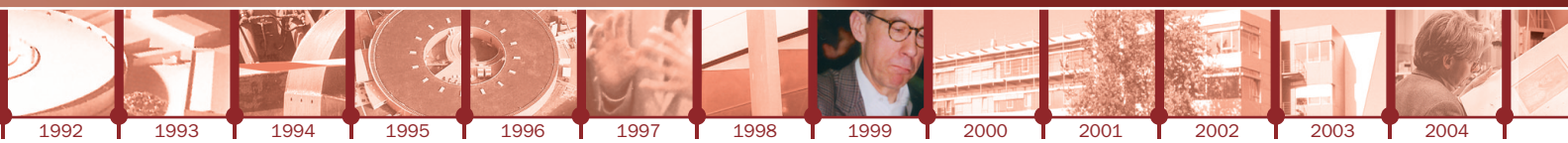

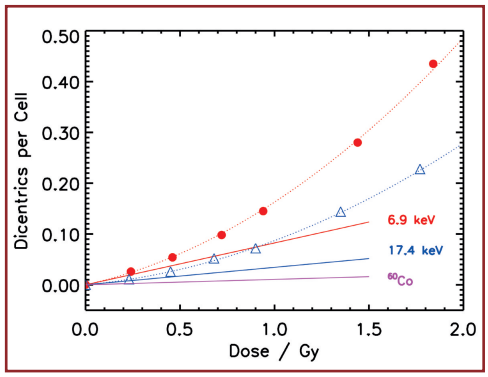

Fig. 2:
Dose response curves for the induction of dicentric chromosomes

Immediately after irradiation, cell cultures were established, and the chromosome analysis was performed in the Cytogenics Laboratory at GSF in the metaphase of the first cell cycle. In Fig. 2, the obtained number of induced dicentric chromosomes per cell is shown as function of the absorbed dose for two X-ray energies. The data can be described by a linear-quadratic model. By definition, the initial slope α determines the RBE: RBE = α/α_{ref}. Therefore, the initial slopes are shown for the ^{60}Co reference radiation (RBE=1) as well as for both X-ray energies, which are steeper, that means, the RBE is clearly higher than 1!

The results for all surveyed photon energies are shown in Fig. 3 [3,4]. There is a maximum RBE of about 8 at 7 keV. In the mammography-relevant photon energy range between 17 keV to 22 keV the RBE is below 4. Therefore suppressing low energy radiation in the mammography spectrum should significantly reduce the RBE. At the higher energies above the characteristic line, the scattering increases and thus reduces the image quality. It is therefore desirable to use only the radiation in the characteristic line. In the framework of a cooperation between industry (Schering AG and Institut für Gerätebau, IfG) and research institutes (PTB and Charité hospital), a monochromator module was developed and tested which can be added to a conventional mammography unit (Fig. 4). The monochromatisation is achieved by a curved, highly-oriented pyrolitic graphite (HOPG) crystal which has been chosen for its high integral reflectance. The spectra in Fig. 5 with and without monochromator module were measured with a Si(Li) detector system, calibrated against the primary source standard BESSY [2,5]. The absolute values of the spectral irradiance are required to calculate the dose. Studies with phantoms and biological objects resulted in considerably higher contrast for monochromatised radiation [6,7]. It should therefore be possible to obtain better images at identical doses or to reduce the dose with unaltered image quality.

Limitations of the monochromator module consist in the longer exposure time with the existing X-ray tubes, and the fact that only a stripe of monochromatised radiation is available, making a scan of the source detector unit necessary. This motion has already been implemented in some commercial systems. If more powerful X-ray tubes become available, monochromatic mammography with conventional instruments could be a real improvement.

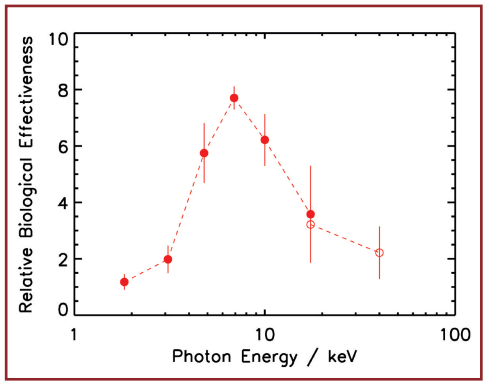

Fig. 3:
Relative biological effectiveness (RBE) determined with monochromatised synchrotron radiation

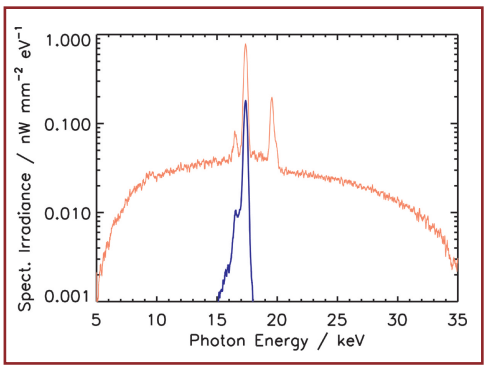

Fig. 5:
Spectrum of a mammography unit with and without monochromator module

Fig. 4:
Monochromator module with HOPG crystal attached to a conventional mammography unit

Contact:
Michael Krumrey
Michael.Krumrey@ptb.de

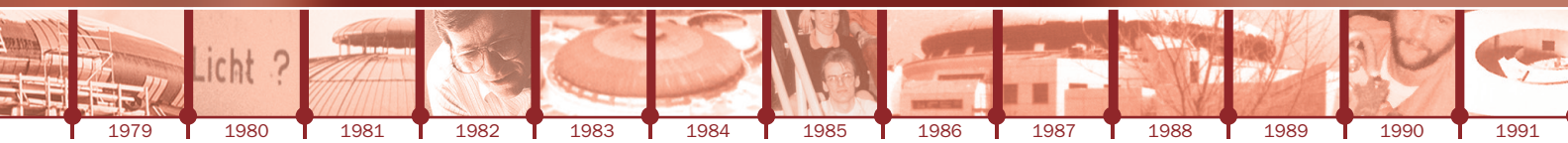

1
University of Aarhus, Denmark

2
Diamond Light Source Ltd., Chilton, UK

Relax! Molecular understanding of how the calcium pump works

T. L.-M. Sørensen[1,2], C.Olesen[1], R. C. Nielsen[1], J. V. Møller[1], P. Nissen[1]

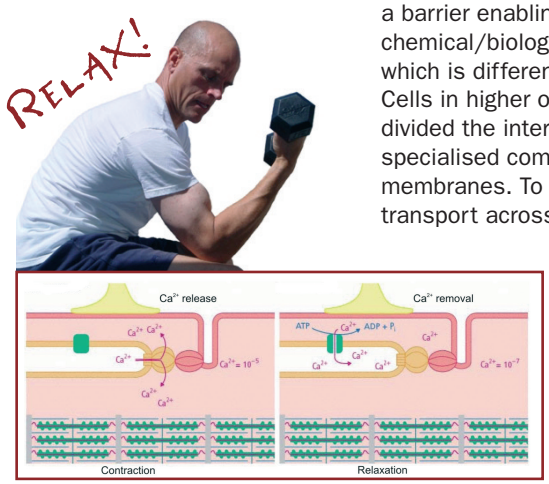

***Fig.1:** Muscle contraction and relaxation are influenced by the concentration of Ca^{2+} ions*

All living organisms are separated from the world around them by a membrane. This membrane is composed of lipids and acts as a barrier enabling the cell to maintain a chemical/biological environment inside which is different from that of the outside. Cells in higher organisms have furthermore divided the interior of the cell into specialised compartments separated by lipid membranes. To allow for signalling and transport across these membrane barriers, a large number of proteins are integrated into the membrane. These membrane proteins handle a variety of functions e.g. transport of ions, uptake of food, transmission of signals, and extrusion of toxic substances.

Ion pumps are integral membrane proteins responsible for establishing and maintaining electrochemical gradients for cations across biological membranes. These pumps are called P-type ATPases - P because they become phosphorylated during the enzyme cycle and ATPases because the transport of ions is driven by ATP hydrolysis. Prominent examples of cation pumps in higher organisms include the Na^+, K^+-ATPase, which maintains the membrane potential in animals and the ability to perform secondary transport, the H^+, K^+-ATPase which is the acid pump of the stomach, and the Ca^{2+}-ATPase, which maintains calcium levels as required for the use of this cation in signalling e.g. in muscles.

We study the Ca^{2+}-ATPase isolated from rabbit fast-twitch muscle which has a crucial role in muscle function. Upon receiving a nervous signal, muscle cells release Ca^{2+} Ions from the sarco(endo)plasmic reticulum (SR) of muscle cells into the cytoplasm, causing a contraction of the muscle by sliding actin and myosin filaments on top of each other. Before the next signal can trigger the muscle cell, the Ca^{2+} ions have to be removed from the cytoplasm. This is achieved by the activity of Ca^{2+}-ATPase, a 110 kDa protein located in the SR membrane which pumps Ca^{2+} from the cytoplasm and into the lumen, thereby terminating the activity of myosin-actin filaments causing muscle relaxation (Fig. 1).

The crystal structure of Ca^{2+}-ATPase shows that it is composed of three cytoplasmic domains: the A (actuator), P (phosphorylation), and N (nucleotide binding) domains, and 10 transmembrane segments, M1 through M10, which contain the two embedded Ca^{2+} binding sites [1]. This enzyme represents an attractive model system of the P-type ATPases and has been studied biochemically in great detail [2]. Our aim is to obtain crystal structures of defined functional states and thus to address the general question on how nature has devised a cation pump running on ATP.

At least two distinct phosphorylated intermediates exist. A high energy phosphorylated intermediate (denoted E1~P) which readily donates its phosphate back to ADP and a low energy intermediate (E2-P) which does not. The conversion between the two phosphorylated intermediates is coupled to the translocation of two Ca^{2+} ions across the membrane barrier, i.e. the transformation of the cytoplasmic oriented high-affinity Ca^{2+} sites to luminal oriented low-affinity sites.

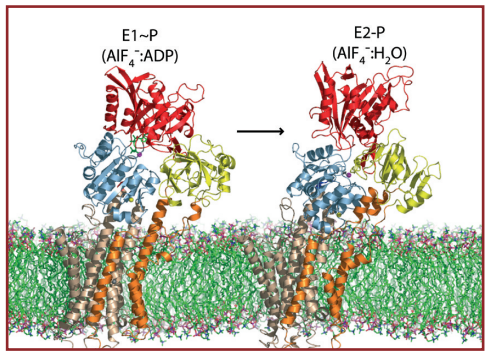

***Fig. 2:** Cartoon presentation of the structures of the E1~P:AlF_4^-:ADP and E2-P:AlF_4^- complexes of the Ca^{2+}-ATPase. Cytoplasmic domains: P (blue), A (yellow), and N (red). Transmembrane helices: M1-M3 (orange) and M4-M10 (wheat).*

References:

*[1] Toyoshima et al., Nature **405** 633-634 (2000)*

*[2] Møller et al., Biochim. Biophys. Acta 1286, **1** (1996)*

*[3] Sørensen et al., Science **304**, 1672-1675 (2004)*

*[4] Olesen et al., Science **306**, 2251-2255 (2004)*

We have solved two structures of the Ca^{2+}-bound Ca^{2+}-ATPase at 2.6 and 2.9 Å resolution in complex with i) a non-hydrolysable ATP analog (AMPPCP) and ii) ADP plus aluminium fluoride, which mimics the transition state of ATP hydrolysis [3], showing how it reacts with ATP by an associative mechanism mediated by two Mg^{2+} ions to form an aspartyl-phosphorylated intermediate state (Ca_2E1~P) (Fig. 2). The conformational changes that accompany the reaction with ATP pull the transmembrane helices 1 and 2 and close a cytosolic entrance for Ca^{2+}, thereby preventing backflow before Ca^{2+} is released on the other side of the membrane.

We have also solved the structure of the Ca^{2+}-free Ca^{2+}-ATPase at 3.0 Å resolution in complex with aluminium fluoride [4], which mimics the transition state of hydrolysis of the counterion-bound (protonated) phosphoenzyme (H_nE2-P) (Fig. 2). On the basis of structural analysis and biochemical data, we find this form to represent an occluded state of the proton counterions. Hydrolysis is catalysed by the conserved Thr-Gly-Glu-Ser (TGES) motif, and it exploits an associative nucleophilic reaction mechanism of the same type as phosphoryl transfer from ATP.

In the E1~P (Fig. 3) structure, we noted that the ADP moiety glues the N and P domain together. Release of the ADP leaving group upon phosphoryl transfer therefore facilitates a ~50° rotation of the N domain relative to the P domain, as is observed in the E2-P structure. This enables the A domain to initiate the 108°- rotation and 8 Å shift around the P domain as required for bringing the TGES motif of the A domain in apposition to the phosphorylation site. Because three polypeptide segments link the A domain to the membrane, these movements directly affect the orientation of M1 through M3.

On the basis of the crystal structures and functional data, we can extract a simple rationale for the operation of the SER Calcium pump in terms of two entrances (a cytoplasmic and a luminal one) controlling the active cation transport processes (Fig. 4): Phosphoryl transfer from ATP locks the cytoplasmic door on Ca^{2+}, whereas the subsequent release of the ADP leaving group opens the luminal door for Ca^{2+}/H^+ exchange. Hydrolysis of the phosphoenzyme locks the luminal door on H+, and subsequent release of the inorganic phosphate leaving group opens the cytoplasmic door for $H+/Ca^{2+}$ exchange. In this model, the strict conformational requirements of the associative reaction mechanisms of phosphoryl transfer and hydrolysis at the phosphorylation site provide the basis for coupling, a principle that should be generally applicable to P-type ATPases.

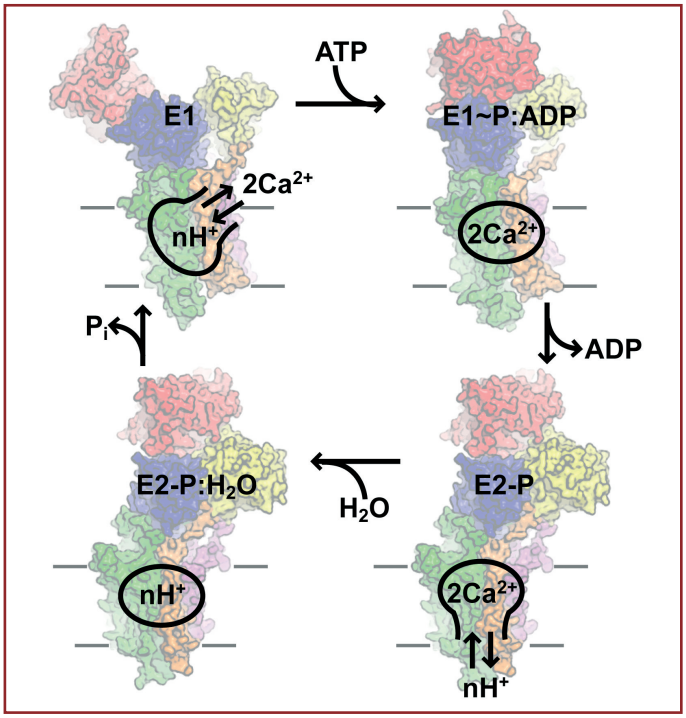

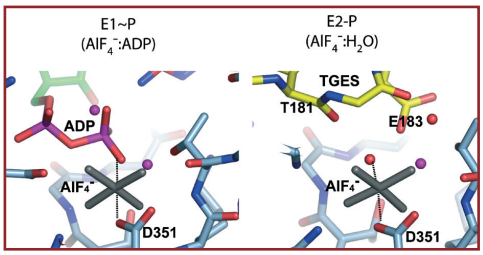

Fig. 3:
A view of the associative mechanism of nucleophilic attack at the phosphorylation site. Comparison of the phosphorylation site in the AlF_4^- analog between the transition state of γ-phosphoryl transfer (E1~P:ADP, left) and that of aspartyl-phosphate hydrolysis (E2-P:H_2O, right). Mg^{2+} is shown as a cyan sphere with liganding oxygens and water molecules in red. A water molecule is located for inline attack on the aluminum fluoride (grey) via interaction with the side chain of Glu183 and the main chain carbonyl group of Thr181. The ADP moiety and the TGES motif of the A domain occupy overlapping positions.

Fig. 4:
A schematic representation of the opening and closure of cytoplasmic and luminal entrances to the ion conducting pathway in the calcium pump. Ca^{2+} transport and H^+ countertransport are coupled to phosphorylation and dephosphorylation, respectively. For clarity, the scheme is reduced to four functional transitions. The unknown structure of the E2-P ground state is represented by the E2-P transition state.

Contact:
Thomas L.-M. Sorensen
Thomas.Sorensen@diamond.ac.uk
Poul Nissen
pn@mb.au.dk

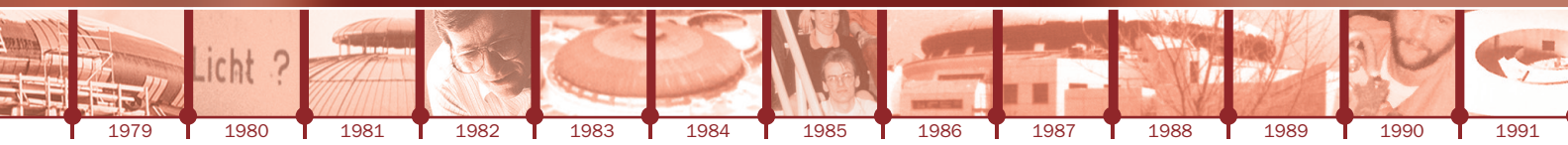

The Vikings in Berlin: SR-XRF analyses of the Hiddensee gold jewellery

B. Armbruster[1], H. Eilbracht[2], A. Grüger[3], M. Radtke[4], H. Riesemeier[4], I. Reiche[5]

1 Centre National de Recherche Scientifique, Toulouse, France

2 Humboldt-Universität zu Berlin

3 Kulturhistorisches Museum, Stralsund

4 Bundesanstalt für Materialforschung und -prüfung, Berlin

5 Centre National de Recherche Scientifique, Paris, France

Fig. 1: Cross-shaped pendant No. 12 of the Hiddensee gold jewellery.

Archaeological objects of gold count among the rarest pieces of jewellery from the Viking Age. This period of Scandinavian history, between 800 and 1050 AD, is actually characterised by silver as the dominating precious metal. Therefore, the discovery of a set of several golden jewels in the 1870s, on the western coast of the island of Hiddensee, was a scientific sensation (Fig. 1, 3).

But this scientific sensation still puzzles archaeologists and metallurgists. We know that the jewellery was produced around the year 1000 in a Viking workshop, most probably on Danish territory. But it is still unsolved how the objects came to the island of Hiddensee, west of the island of Rügen, since the find-spot was part of the Slavic area by that time (Fig. 2). It is further unclear who wore the golden jewels or for whom they were made, and why the pieces have been hidden on the island. Already the mysterious circumstances of the discovery have again and again aroused curiosity and arguments. The objects are said to have been washed ashore after two great storm tides in 1872 and 1874 and to have been saved by fishermen from Neuendorf. From there, they came to their present whereabouts, the Kulturhistorisches Museum Stralsund, under somewhat adventurous circumstances.

Sixteen objects with a total weight of some 600 g belong to the ensemble (Fig. 3): ten cross-shaped pendants, four small pendants, a disc-shaped brooch, and a neck ring. Except for the neck ring, all pieces consist of several components: a flat sheet forms the basis of a covering sheet in which the relief of the decoration was pressed. Both sheets are soldered, the space in between stays hollow. And finally, the decoration of wire and granules is soldered onto the covering sheet. These complex techniques, also called filigree and granulation, give evidence of the gold- and silversmiths' enormous metallurgical knowledge in those days [1, 2]. Its exclusive application underlines the value of the pieces of jewellery and thus their owners' social rank.

The scientific significance of the Hiddensee jewellery is based on three specialities: the large number of pieces, their unusual material, and the high level of workmanship they were produced with. These important

Fig. 2: The Viking world 800 - 1100 [after: A. Willemsen, Wikinger am Rhein (Ütrecht 2004) 78]

finds have not yet been sufficiently acknowledged so far. The only monographic publication dates from 1936 [3]! Thus, new interdisciplinary research was initiated, combining the work of archaeologists, goldsmiths, and scientists. The current archaeometric investigations aim for characterising the objects by metal-analysis, in order of finding out about the unity of the artefacts, of verifying their making at the same time, and of finding insights concerning the techniques of soldering.

Fig. 3: The golden objects 1-16 of the so-called Hiddensee treasure-trove.

References:

(1) H. Eilbracht, Filigran- und Granulationskunst im wikingischen Norden (Bonn 1999)

(2) B. Armbruster, in: K. Brandt et al., Haithabu und die frühe Stadtentwicklung in Nordeuropa 219-280 (Neumünster 2002)

(3) P. Paulsen, Der Goldschatz von Hiddensee (Leipzig 1936)

*(4) I. Reiche et al., NIMB **226** 83-91 (2004)*

(5) J. Wolters, in: U. Lindgren, Europäische Technik im Mittelalter 187-203 (Berlin 1996)

Synchrotron radiation induced XRF (SR-XRF) proved to be very well suited for the non-destructive analysis of ancient gold objects because it offers high spatial resolution and tunability of exciting photons. It also permits the analysis of many elements simultaneously. Furthermore, the experimental conditions at the BAMline allow the examination of microscopic points on the objects in air so that even small items (e. g. the soldered granules and pieces of wire or the soldering drops) can be characterised individually [4]. For this purpose major, minor, and trace element contents in the different golden objects were determined by using SR-XRF with 34 keV (Fig. 4). Each object was investigated at well chosen areas previously selected in the course of extensive microscopic studies.

First results show a great homogeneity of the gold alloy of all sixteen objects (Fig. 5), except for the brooch (No. 1), the neck ring (No. 2), and one of the cross-shaped pendants (No. 12). This finding is not surprising for the neck ring which was processed by help of a different technique (twisted wire instead of soldered sheet metal, wire, and granules), and not even for the brooch which is a unique piece among the filigree decorated objects. But there is no answer yet to the question why the cross-shaped pendant No. 12 has a significantly lower gold content than the other nine cross-shaped pendants. Perhaps it was produced separately and later added to the set?

Another important result is the composition of the solder. Remnants of metallic solder distributed on the sheets could clearly be seen under the microscope. For the solder, Gold had been alloyed with other kinds of metal so that the melting point was significantly lower than that of the gold alloy of sheets and decoration. Upon heating, sheets and decoration were connected by the solder without melting themselves. Normally the melting point of pure gold is 1084°C. By adding silver or copper to the gold the melting point can be reduced to a temperature between e. g. 850°C and 975°C, depending on the exact portions of the different metals [5]. Our investigations of pendant No. 13 for example confirm a high amount of copper in the solder (Fig. 6), and further calculations and data evaluation will show if additional metals were used and which temperatures were gained to process the jewellery.

In combination with archaeological, historic, and aspects of art history as well as with studies on the techniques of production, the scientific results will provide us with new insights into the goldsmiths' art at the time of the Vikings. Our results will serve as a database for investigations on other finds of precious metal from the Viking Age and we are planning to publish them in a voluminous monograph.

Even if it has been more than 1,000 years that the Vikings left their traces on Hiddensee, still today they are very much fascinating. One cannot withstand the beauty of the pieces of jewellery, their precious material, and their skilful technique.

Fig. 4:
Two cross-shaped pendants in the experimental set-up at the BAMline

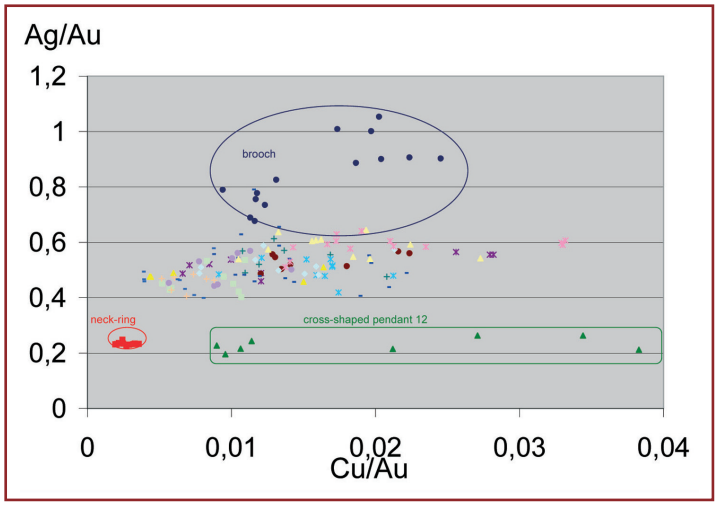

Fig. 5:
Scattered plot of all measured data on the 16 Hiddensee objects showing the homogeneity in the chemical composition except for the brooch, the neck ring and the pendant No. 12.

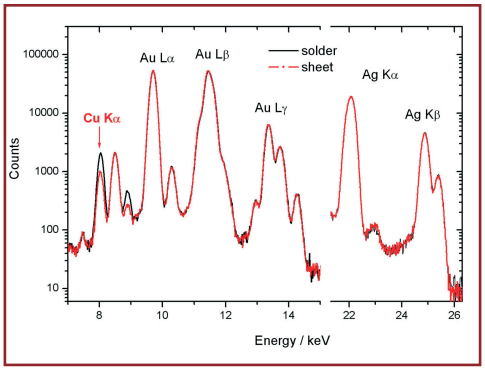

Fig. 6:
XRF-spectra of pendant No. 13 showing the raised Cu-content in the metallic solder compared with the sheet.

Contact:
Heidemarie Eilbracht
eilbrachth@geschichte.hu-berlin.de
Martin Radtke
martin.radtke@bam.de

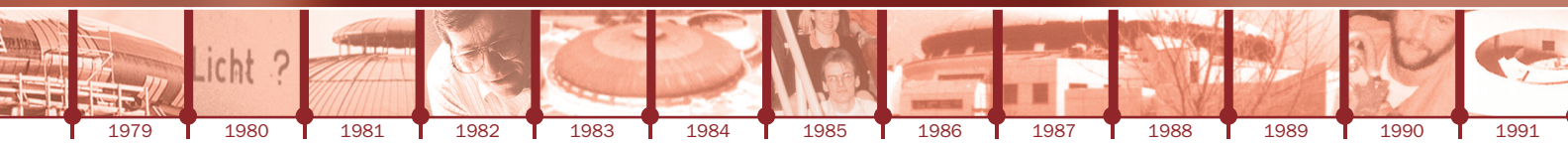

Reading messages from space - Nano-ESCA study of pre-solar meteorite dust

G. Schönhense[1] P. Bernhard[1], J. Maul[1], G. Huber[1], H.J. Elmers[1], N. Weber[2], M. Escher[2], D. Funnemann[3], Ch. Sudek[4], U. Ott[4]

1 Johannes Gutenberg-Universität, Mainz

2 FOCUS GmbH, Hünstetten

3 OMICRON Nanotechnology GmbH, Taunusstein

4 Max-Planck-Institut für Chemie, Mainz

Meteorites consist mostly of material that formed within our Solar System and therefore give us insights in the elementary composition of our 'cosmic home'. However, some meteorites contain small amounts of grains which are assumed to be of pre-solar origin, i.e. from a time before our Solar System had formed. Isotope-mapping studies using mass spectroscopic techniques [3] revealed that these grains deviate substantially in their isotope distribution from the 'normal' solar abundances [1, 2]; for $^{12}C/^{13}C$, e.g., by two orders of magnitude both ways). The grains contain include nano-diamond, silicon carbide (SiC) as well as graphite, refractory oxides, and silicon nitride [1, 2].
In addition, presolar silicates have recently been detected using isotopic mapping by NanoSIMS [3].

It is now accepted that most SiC grains originate from the stellar wind material expelled by carbon-rich asymptotic giant branch stars (the last major phase of life for stars less massive than about nine times the mass of the sun).

Besides the major structural elements, their silicon carbide grains contain a variety of diagnostic trace elements [2], which give not only important information about their nucleosynthetic origin (formation in a star), but potentially also about their incorporation into the meteorite and hence, possible modes of grain formation.

For studying meteorite grains, which are both small (sub-micron diameter) and rare, 'standard' mass spectrometric methods have a disadvantage - they are destructive. Therefore, it would be useful to have a non-destructive screening technique for choosing the most promising element(s) for isotope analysis in order to gain information on the element formation (s-process) and the incorporation. Nano-SIMS (Secondary Ion Mass Spectroscopy) can map elemental and isotopic abundances with a lateral resolution in the 100 nm range [4]. Of the two non-destructive methods, synchrotron X-ray fluorescence (SR-XRF) provides information on element distribution with a lateral resolution of about 0.6 µm [5].

At last, Nano-ESCA (Electron Spectroscopy for Chemical Analysis) bears additional important advantages, since it provides information both on the spatial distribution of elements within µm-sized grains and on the chemical environment of the elements of interest at a lateral resolution in the 100 nm range with an energy resolution of 0.1 eV.

The newly developed Nano-ESCA instrument [6] is derived from an electrostatic Photo Emission Electron Microscope (PEEM) column and a twin hemispherical analyzer in anti-symmetric configuration (aberration corrected) and runs in three operation modes (Fig. 1). In an exploratory study, we performed an analysis on an acid-resistant, SiC-rich residue from the Murchison meteorite (see box). Material was deposited on a Si wafer from an aqueous suspension and synchrotron radiation at beamline UE52-SGM was used for excitation.

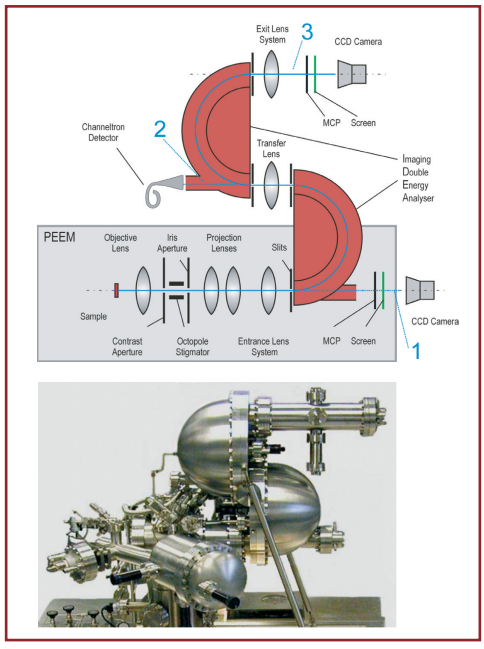

Fig. 1:
Electron-optical scheme and photograph of the Nano-ESCA instrument. Three operation modes are indicated: (1) direct non energy filtered PEEM-imaging, (2) selected area spectroscopy, and (3) energy filtered ESCA imaging for kinetic energies up to 1.6 keV.

References:

*[1] U. Ott, Nature **364**, 25-33 (1993).*

*[2] E. Zinner, Annu. Rev. Earth Planet. Sci. **26**, 147-188 (1998).*

*[3] A.N. Nguyen and E. Zinner, Science **303**, 1496-1499 (2004).*

*[4] P. Hoppe et al. New Ast. Rev. **48**, 171-176 (2004).*

[5] Y. Kashiv et al., LPS XXXII, #2192 (2001) and LPS XXXIII, #2056 (2002)

*[6] M. Escher et al., J.Phys.: Cond. Matt.. **17**, in print (2005).*

*[7] P. Hoppe et al., Astrophys. J. **430**, 870-890 (1994).*

*[8] S. Amari et al., Meteoritics **30**, 679-693 (1995).*

*[9] Ch. Ziethen et al., J. Electr. Spectrosc. Rel. Phenom. **107**, 261-271 (2000)*

Acknowledgements:
Thanks are due to M. Merkel (FOCUS GmbH) and B. Krömker (Omicron GmbH). Instrument development was partly funded by BMBF.

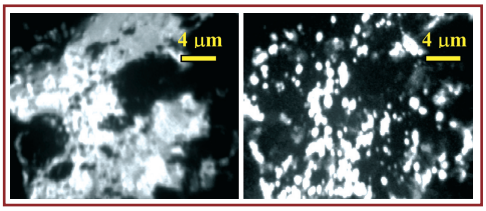

Fig. 2:
Energy filtered ESCA imaging at low kinetic energies. Left (5.8 eV): Si wafer (SiO_x substrate). Right (4.4 eV): SiC grains in the same field of view. Photon energy 140 eV.

Using energy-filtered ESCA imaging (operation mode 3) submicron SiC grains are easily recognized even on a Si wafer substrate, because of strong spectral differences between the oxidised Si wafer surface and the SiC grains at low energies (Fig. 2).

Fig. 3 shows images of the same field of view taken at selected XPS lines. Among the minor elements, Al plays an important role [2]. In (a) an area is shown imaged via the Al 2p electrons at a binding energy of 75.5 eV, which corresponds to Al bound to oxygen. The circled dot in all likelihood represents a corundum (Al_2O_3) grain (only weak Si 2p signal). In (b) the same area is shown imaged at 78.0 eV. The grain from (a) is not seen in (b), but there are other bright spots, which we believe to correspond to Al incorporated in SiC grains. This is substantiated in Fig. 4 (a) and (b), which are local spectra for the microareas indicated in Fig. 3; they were extracted from the same (x,y,E) data stack after acquisition of the image series. The Al 2p signal in spectrum (b) is clearly shifted relative to Al 2p in Al_2O_3, in accordance with the images. It has often been assumed that Al is contained within the SiC grains as AlN in subgrains or in solid solution in the SiC lattice structure [7]. With Nano-ESCA, we are now able to investigate the Al occurrence in detail.

Apart from major (Si, C) and minor (N, Mg, Al, Fe) elements, we find a variety of heavy trace elements such as Sr, Y, Zr, Nb, Mo, Ba and, interestingly the Rare Earth Element (REE) Er and possibly Dy and Tm. Ba and the REE had not been detected in with SR-XRF [5]. Among the REE, the only abundance data reported for single grains are for Ce and, in a few cases, Nd [8]. The fact that only certain grains show up at given energies indicates relative abundances to be highly non-uniform, in accordance with the variable Ce/Nd ratio observed in [8].

While there is still a need for quantification, Nano-ESCA is a valuable tool for non-destructive screening of pre-solar grains from meteorites for trace element contents. Owing to its sensitivity on the chemical environments in which various elements occur within these grains, it is superior to SR-XRF. Given tuneable soft X-rays the instrument is also capable of XANES-PEEM [9] providing additional information on the chemical structure. Application of Nano-ESCA needs not be restricted to pre-solar grains, but can be a valuable approach in studying other fine-grained extraterrestrial materials such as interplanetary dust particles (IDPs) and possibly cometary material caught by the NASA Stardust Mission.

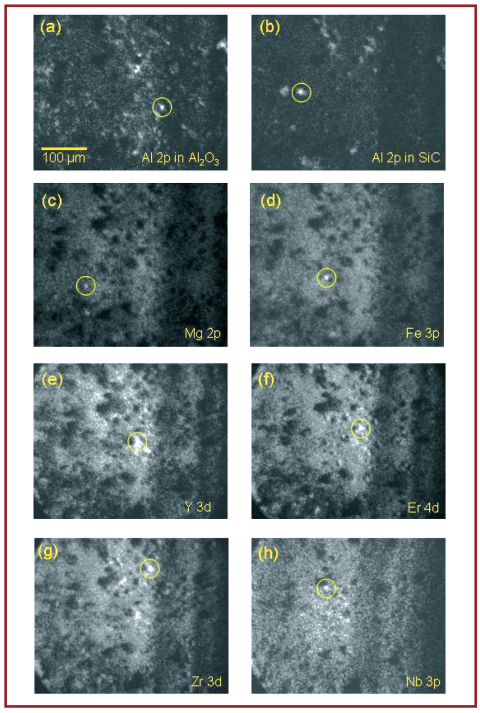

Fig. 3:
Energy-filtered images of the same field of view for various XPS lines.

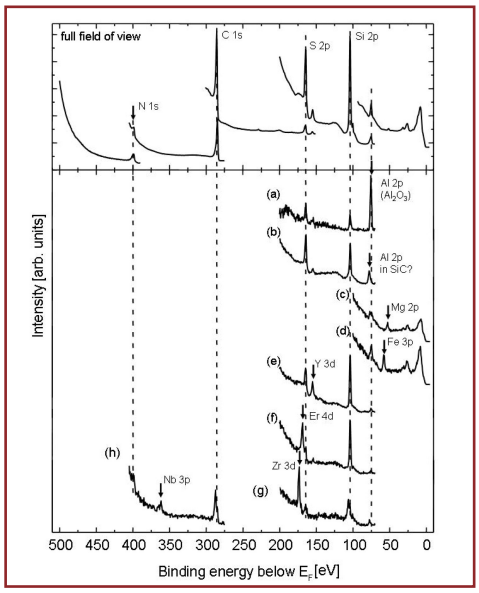

Fig. 4:
XPS-spectra of the full field of view (top) and extracted from the microareas indicated in Fig. 3 (a-h). Photon energies 250 eV (a,b,e-g), 150 eV (c,d) and 450 eV (h).

Murchison Meteorite

The Murchison meteorite is a rare type of stony (carbonaceous chondrite, type II) meteorite. It contains high temperature and low temperature minerals, water, as well as organic molecules such as amino acids. Approximately 100 kg of rock fell near Murchison, Australia, on September 28, 1969. The largest fragment collected weighed approximately 7kg.

Contact:
Gerd Schönhense
schoenhe@uni-mainz.de

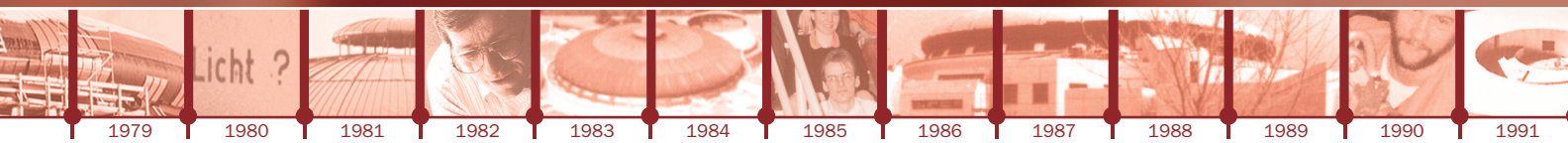

1
Ferdinand-Braun-Institut für Höchstfrequenztechnik, Berlin

2
BESSY, Berlin

Power on the fingertip: A tiny light source for various applications

Ch. Dzionk[1], G. Erbert[1], S. Schwertfeger[1], G. Tränkle[1], W. Eberhardt[2], B. Löchel[2]

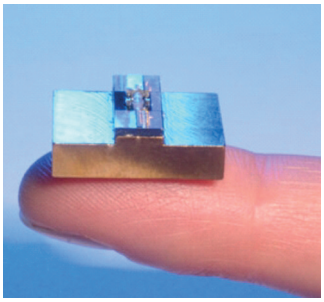

It is smaller than a finger nail, but has the potential to advantage display technology used in television, beamer systems, computers and notebooks. Two chips coupled by a lens and mounted on a small structured piece of silicon form a small but powerful entity: the MOPA (Fig. 1). This 'Master Oscillator Power Amplifier' (MOPA) laser system was developed in collaboration within the ZEMI (Centre for Microsystems Technology) network by the Ferdinand-Braun-Institut für Höchstfrequenztechnik (FBH) and the BESSY Anwenderzentrum Mikrotechnik (AZM). It delivers spectrally pure and highly focussed light with an output power 2,000 times stronger than that of a laser pointer – a combination not available up to now. The MOPA emits infra red light which can be converted into ultraviolet and visible light by frequency conversion [1]. One possible application for the powerful light source is in laser television. Laser TVs produce pin-sharp pictures since they provide a significantly increased brilliancy compared to today's equipment. Further applications are in the field of spectroscopy, as pump sources in fibre amplifiers in telecommunications, in medical technology, and optical printing techniques.

Realising high-brightness high-power diode lasers based on single emitter chips typically leads to compromises in some of the properties, such as efficiency, mode stability, or spectral behaviour. A very attractive configuration to avoid these disadvantages is the hybrid MOPA set-up.

In this laser system the output of a single-mode master oscillator (MO) with excellent beam properties but only limited power is coupled into a power amplifier (PA). This PA generates high output power maintaining the beam quality. The highest output power of 5 W using a hybrid arrangement has been achieved by O'Brien et al. [2]. However, when assembling such a hybrid system, the coupling of two chips generally requires a sophisticated mounting scheme. In contrast to our innovative small-sized MOPA system the standard breadboard has usually the size of a shoe carton.

FBH has developed and characterised several MOPAs before in the spectral range from 860 nm to 1064 nm. One of the major tasks within this project was to develop a simplified mounting scheme which has the perspective of a cost-effective production. The characteristic feature of this MOPA is the use of micro engineering, which allows that the three tiny optoelectronic components are aligned with high accuracy on a silicon micro-optical bench forming a very stable unit of only 13 x 5 mm² in size. The pre-patterned bench with its very small structures and special metal clips to hold the system components are produced by BESSY using the LIGA technique, i.e. lithography and galvanic deposition. The ideal material for such micro-optical benches is single crystalline silicon: It is cheap and techniques in chip production are well-approved.

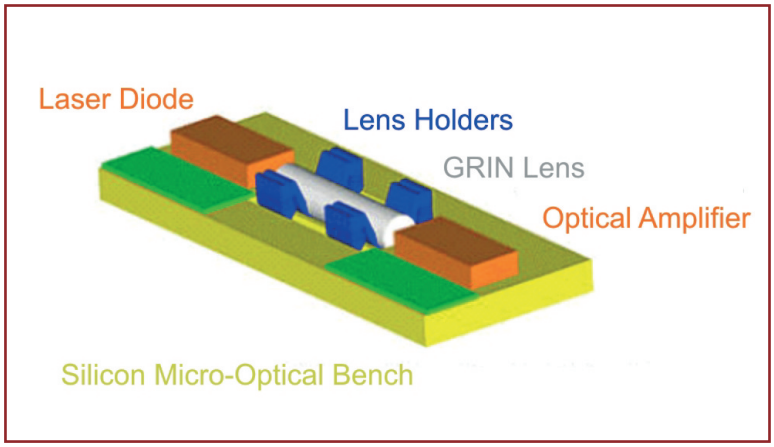

Fig. 1: Principle mounting scheme of the MOPA

References:

*[1] D. Woll, et al., Opt. Lett., **24**, 691–693 (1999)*

*[2] S. O'Brien, et al., IEEE Photon. Technol. Lett., **9,** 1217–1219 (9/1997)*

*[3] H. Seidel, et al., J. Electrochem. Soc., **137,** 11, 3612-3626 (1990)*

*[4] L. Hofmann, et al., Electron. Lett., **36,** 6, 534–535 (2000)*

[5] H. Guckel, et al. Proceedings of IEEE Micro Electro Mechanical Systems, 74-79 (1/1991)

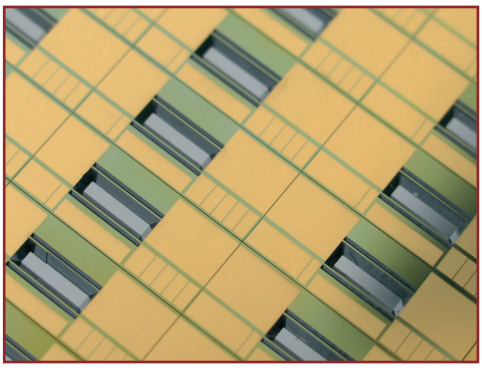

Fig. 2:
Micro-optical bench base plates

For generating the micro-optical bench a silicon (100) wafer has to be prepared by depositing protection, adhesion, and conductive layers using thin film processes. The deposited layers are patterned by standard semiconductor processes following UV lithographical steps (Fig. 2). Finally, the silicon bulk material is etched in a KOH bath [3] in order to generate a large groove for the lens and V grooves for exact positioning of the lens holders. After the wet etching the wafer is diced, yielding about one hundred benches per 4" wafer.

On the micro-optical bench a 2 mm long single-mode laser diode (MO) is mounted, as well as a glass lens and a tapered power-amplifier (PA) (Fig. 1). The MO consists of a distributed Bragg reflector laser (DBR) with an output power of about 60 mW ensuring longitudinal and lateral single-mode emission [4]. The emitted light of the MO is coupled into the 4 mm long tapered PA by a small GRIN rod lens with a diameter of 1 mm.

When soldering the laser chips to the micro-optical bench, a coarse alignment of the chips to the optical axis of the bench is achieved by using a special tool. This tool is manufactured by precise lithographical techniques and has alignment marks defining the optical axis. After soldering, the alignment tool is removed and the lens is assembled by using two specially constructed micro-lens holders which are deformable. These metallic lens holders are fabricated in a direct-LIGA process [5]. An extremely bulky resist layer of more than 1 mm thickness is patterned during a lithographic process by synchrotron light.

After developing, the patterning process ends in high-quality resist forms which then are filled with nickel in an electroplating step (Fig. 3). Finally, the lens holders are removed from the surface and cleaned. The lens is gripped by a vacuum tool and can be moved in three axis with very high precision, i.e. ±0.01 µm. The alignment process of the lens is carried out by operating the laser system while monitoring output power and beam properties (Fig. 4). To achieve a good coupling efficiency between MO and PA the mounting accuracy must be approximately 0.5 µm. If the correct position is reached, the lens is fixed using a UV-curable adhesive.

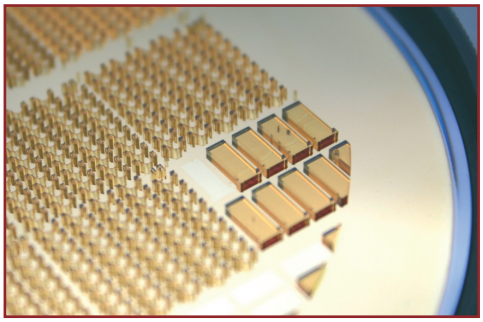

Fig. 3:
Wafer with lens-holders

With the first demonstrator a maximum continuous-wave optical output-power of more than 2 W was achieved. The emission spectrum was completely determined by the DBR laser. Single longitudinal mode operation at a wavelength of λ = 1061 nm was maintained over the whole power range. The results of this MOPA prototype are very promising and the technique already shows the great potential for large-scale production, one of the core requirements for applications in display technology.

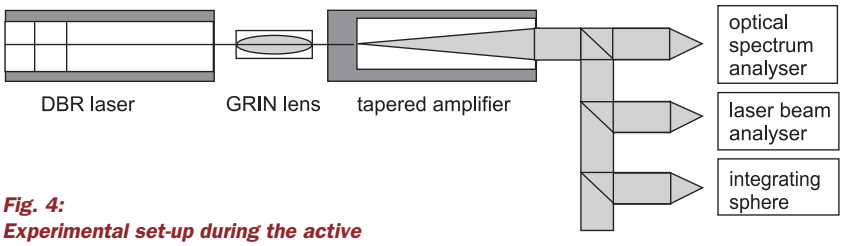

Fig. 4:
Experimental set-up during the active adjustment of the laser system

Contact:
Christian Dzionk
zemi@zemi-berlin.de

3

Pathfinders of BESSY, 1999

News & Events

News

Twice in 2004, we had the honour to present BESSY to the German Chancellor Gerhard Schröder. In September, he visited the new science faculties of the Humboldt Universität in Adlershof. On this occasion local networks between scientific institutions and companies were highlighted: BESSY had a presentation together with FMB, a company specialised on ultra-high vacuum systems and synchrotron radiation technology.

Again arranged by the Humboldt Universität, the Chancellor, the Federal Minister of Research and Education Edelgard Bulmahn as well as the Federal Minister for Economy Wolfgang Clement together with several prominent industrial partners held a meeting of the initiative 'Partner für Innovation' at BESSY. The group visited an exhibition of innovative results in the field of micro engineering, life sciences and optical technology as well as the experimental hall. This event was accompanied by a great press echo. Edelgard Bulmahn spent some extra time to have a look at the Viking gold jewellery which has been under investigation at the BAMline at this time.

On the way to our future facility, the Free Electron Laser (FEL), another major step was made. The technical design report (TDR) of the FEL was finalised and handed over to the Berlin State Secretary Hans-Gerhard Husung. Little later, the Standing Committee for Science and Technology of the Berlin Parliament had a meeting here and discussed the FEL project. Across all party boundaries the BESSY FEL project received the full support of the committee members. The TDR has been forwarded to the Wissenschaftsrat, the German Science Council, for evaluation, which is aimed in 2005.

Several high-ranking international and national groups were welcomed at BESSY, among them the Israelian Minister for Research and Technology, the Vice-President of the Mexican Council for Research and Technology, Jordanian Ministers, Korean economy delegation and Economy Councillors of several embassies as well as members of the CSU parliamentary party. BESSY still attracts visitors from all over the world. In 2004 about 2,300 people were guided through BESSY, more than one third were pupils and 360 students. During the Laser Optic Fair BESSY opened its doors for visitors and participants.

In spring, BESSY was evaluated by the Leibniz-Gemeinschaft. An external board of experts visited BESSY, talked to staff members and was informed in workshops. The results will be published by the mid of 2005 and are awaited with interest. The evaluation process of the Leibniz-Gemeinschaft sets new benchmarks also for other science institutions.

'Partner für Innovation' – an initiative of Chancellor Schröder with several partners from industry and politics meet at BESSY

The Berlin Standing Committee for Science and Technology votes for the FEL

Among the international visitors were the Israelian Minister for Science and Research Ilan Shalgi and the Jordanian Minister of Education Khalid Touqan

Among others aspects, the high level of scientific communication was noted not at last by the great number of invited speakers who gave insights into actual research topics.

The new members of the scientific advisory board (SAC) and the beamtime committee started their work in 2004. BESSY sincerely thanks the former members for their commitment and time they spent, especially the long-term chairman of the SAC Michael Grunze. We welcome the new members and are looking forward to a good cooperation.

Poster session during the evaluation

Events

2004 was the year of the 25th birthday of BESSY. It was celebrated - as appropriate for a girl in the twenties - with a party for all friends, staff members and their families. In his speech the Berlin State Secretary for Sciences Hans-Gerhard Husung emphasised the important role of BESSY in Berlin and especially in the science park Adlershof. The long-term companions Joachim Treusch, Hermann Schunck, and Alexander Bradshaw highlighted key moments from BESSY's past and expressed best wishes for the future. The second key note lecture by Joachim Stöhr clearly addressed BESSY's future and the amazing possibilities which will be opening up with the planned Free Electron Laser.

The festivities offered a further look in the future: The ground-breaking celebration for the Willy-Wien-Laboratory of PTB took place. This compact SR source, built in cooperation with BESSY, would create together with the FEL an unprecedented centre for synchrotron radiation – Europe's brightest triangle!

The celebration was found to be the right moment to publish a photo book called 'Strahlzeiten' showing once more that without the committed work of many the 25 years would have never brought such success. We are thankful that the photographer Bernhard Schurian was all 'eyes' to every days life at BESSY.

Already a tradition: BESSY opened its doors again at 'Lange Nacht der Wissenschaften' at June 12th, 2004. More than 5,300 people found their way to BESSY, in a growing number family with small children. Therefore, for the first time a children's lab offered experiments and actions for the little ones. Each year more children join a guided tour and enjoy together with numerous grown up the physics show. 'Splash' was performed by the 'Physikanten' showing fascinating experiments with water. At 21 stations staff members and users explained how BESSY works and what the light is used for. More and more hands on experiments are displayed.

During the summer holidays we offered the late Sunday morning lecture 'Physik zum Frühstück'. Together with a breakfast the physics all around light attracted many interested participants who use this chance to try out experiments by themselves or to ask long-time nourished questions. 'Lange Nacht' and 'Physik zum Frühstück' show that there is a great interest in public understanding of sciences, which encourages us to offer further events like these.

This years' exhibition of light objects by Annette Messig ended with an After-work party – a get-together for staff members and colleagues from other institutes of the campus. The display of light objects during the winter months is just one of the regular art exhibitions offering new views of the corridors.

Hands-on physics at 'Lange Nacht der Wissenschaften' and 'Physik zum Frühstück'

Opening of one of BESSY's regular art exhibitions

Users' Meeting 2004

Key note lecturer Robert Schögl explains how to study catalysts

The annual meeting took place at December, 2nd-3rd, 2004 and attracted more than 300 participants. This years' vendor exhibition was overbooked and highly frequented: 40 vendors showed their products and new developments. Gratefully acknowledged was the sponsoring of the traditional 'Berliner Buffet'.

The key note lecture was devoted to the chemical solutions to overcome the 'hurdles of life" by catalysts. Robert Schlögl (Fritz-Haber-Institut) presented insights into dynamic states during the catalytic process under reaction conditions. The work of Schlögl's group is one distinguishing research areas at BESSY which also attracts industrial partners. Talks presenting highlights of research areas such as surface science, solid state physics, magnetism, nanosciences, atomic physics, and astronomy illustrated the high expertise of BESSY users in their individual field. The still growing field of life sciences enriches the spectra of high ranking science taking place at BESSY. During the poster session in the experimental hall more than 120 posters were presented and led to a lively scientific discussion. The poster prize was awarded to Till Jahnke (Universität Frankfurt) and co-workers for their poster on interatomic coulombic decay in neon dimers, well known from last years Highlights.

Peter Kuske and William Peatman summarised new developments of the machine and the experiments, respectively. Alexandra Kastner gave an overview on the BESSY Online Access Tool which will be available by the mid of 2005 and will facilitate user affairs at BESSY. Uwe Hergenhahn, chairman of the Users' Committee, reported on the first year of their work. More information on the last two reports as well as on the results of the plenum discussion can be found in the 'User Pages' in this issue.

Vendor exhibition and relaxing party at the Users' Meeting

Innovation Award on Synchrotron Radiation

In densely packed electronic structures of modern electronics the fault diagnostics on single components is a growing problem. High lateral resolution and simultaneously information about the electronic properties of the sample are gained by a photoelectron emission microscope (PEEM). Ernst Bauer (University Tempe, Arizona), one of the pioneers of the PEEM development, has realised early that with this instrument the lateral resolution of electron microscopy can be combined with the surface sensitivity of photoemission spectroscopy. Andreas Oelsner and Gerd Schönhense (Universität Mainz) added a flight tube and a time-resolving detector. For this Picosecond-PEEM and their extraordinary contributions to the PEEM development as energy-, time and lateral resolving detection system Andreas Oelsner, Gerd Schönhense and Ernst Bauer were honoured with the Innovation Award on Synchrotron Radiation of the Society of Friends and Sponsors of BESSY. The improvement of the instrument was going along with an active marketing as all three laureates own their own companies.

Wolfgang Gudat with the Innovation Award laureates Gerd Schönhense and Andreas Oelsner and laudator Jürgen Kirschner (left to right).

Ernst-Eckhard-Koch-Prize

Even 18 years after the discovery of high temperature superconductors (HT_c) by Bednorz and Müller this phenomenon is still not well understood on microscopic basis, although HT_c are prototypes of highly correlated electron systems which play a central role in modern solid state research. One knows that conduction electrons are bound to electron pairs, the so-called Cooper pairs, but one does not know what the responsible interactions amongst the conduction electrons are. In his dissertation Andreas Koitzsch identified magnetic fluctuation as the 'glue' which holds the Cooper pairs together. For his dissertation which was graded 'summa cum laude' he received the Ernst-Eckhard-Koch prize.

The board of the Society of Friends and Sponsors of BESSY was extremely pleased that the response to this years' announcement was very high. A total of 12 dissertations from 10 universities have been nominated. The prize is awarded for an outstanding Ph.D. thesis in the field of research with synchrotron radiation.

On behalf of the 'Society of Friends and Sponsors', Wolfgang Gudat handed over the Ernst-Eckhard-Koch Prize to Andreas Koitzsch from IFW Dresden.

Workshops 2004

Course on Experimenting with Synchrotron Radiation	February, 16 - 27
Start-Up Meeting EU-project: Fs-Instrumentation	March, 26
European Strategy Forum on Research Infrastructures	May, 24 - 25
9th European Particle Accelerator Conference	July, 5 - 9
Workshop on Quantitative X-ray Microscopy	October, 26
Industrieforum 'Nanofabrikation – Neue Dimensionen der Mikrosystemtechnik'	November, 12
BESSY Users' Meeting	December, 2 - 3

4

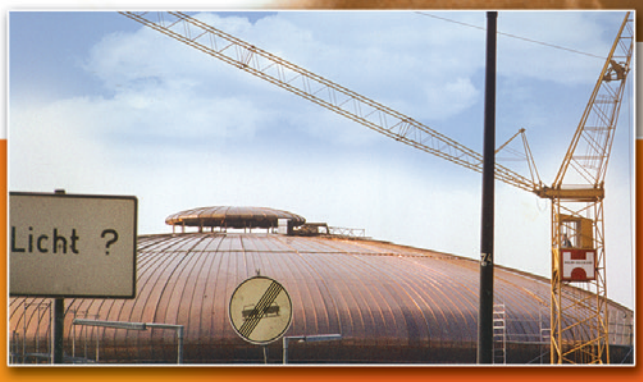

Just delivered: First visual mirror characterisation, 1982

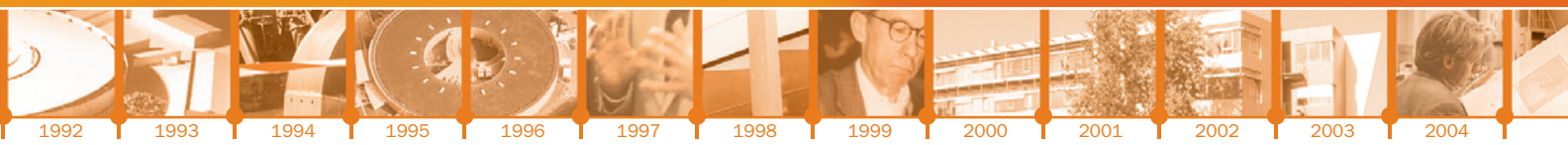

High precision optics: Mirrors, mounts and drives

The secret to providing brilliant synchrotron radiation for highly demanding experiments lies in having stable storage ring operation and optical components of nearly perfect characteristics to disperse the radiation and to guide the photons to the experiment. The synchrotron radiation must be transferred over a distance of 30-40 m from the radiation source point to the experiment, while the small focal spot with high brilliance and well defined photon energy is maintained.

The quality of a beamline also relies heavily on the optical design and on the precision mechanics to control and adjust the optical components. Thus, aside from the machine, the performance of a beamline lies in the domain of optics: metrology, manufacturing, mounting and moving the optical components.

Optimising Nano-Optical Components

The development of new and optimised optical systems is one of BESSY's strengths. Already during the construction of BESSY I it was recognised that no instruments were available to measure mirrors and gratings with the required accuracy. With typically three to five optical elements in a beamline, it was extremely difficult to pinpoint the cause or causes of poor performance. Neither money nor extremely long delivery times were a guarantee that the specification would be fulfilled. The manufacturers themselves were often unable to determine the figure accuracy for want of suitable measuring techniques. Traditionally, optical interferometry was used, by which a minimal shape error of in the order of a hundredth of the wavelength of the light could be determined, limiting the accuracy of slope errors to 0.1 arcsec rms. Over the years and with new verve after the funding of BESSY II we started to develop techniques to improve the characterisation of optical surfaces. Essential for the ultimate success achieved was a project called Nanometer Optical Components (NOK) bringing eleven partners from German industries and scientific institutes together to improve (1) the measuring and (2) the finishing processes. The test objects were optical components for synchrotron radiation: plane or curved substrates for gratings and mirrors of highest quality.

Fig. 1: The Nano-Optic Measuring Machine (NOM) in the optics laboratory

Under the coordination of BESSY the NOK metrology team developed a new approach based on deflectometry. The instrument resulting from these efforts, the Nano-Optic Measuring Machine, NOM, is unsurpassed in the world of optical metrology for accuracy and its ability to make three dimensional maps of complete optical surfaces (Fig. 1). This machine incorporates a hybrid principle of an autocollimator and a long trace profiler by which systematic errors can be minimised (Fig. 2). Special care was given to achieve temperature and vibration stability.

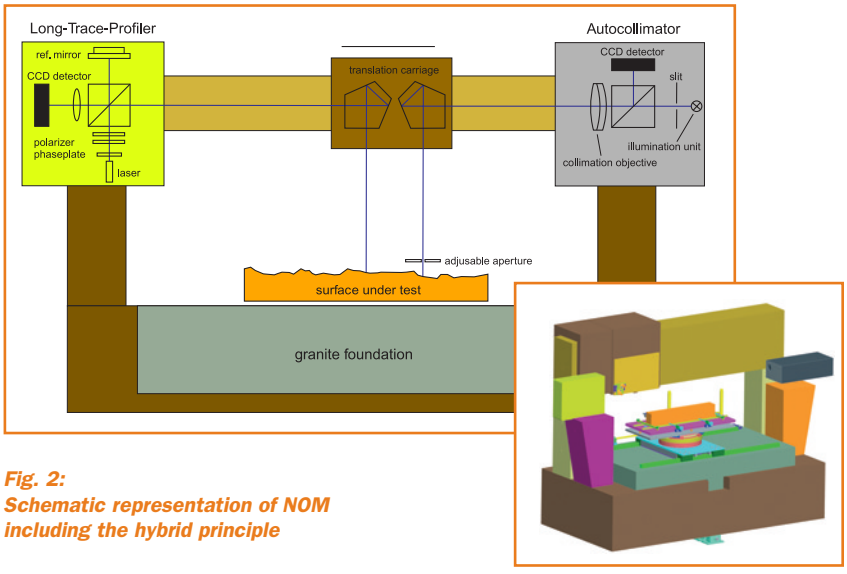

Fig. 2: Schematic representation of NOM including the hybrid principle

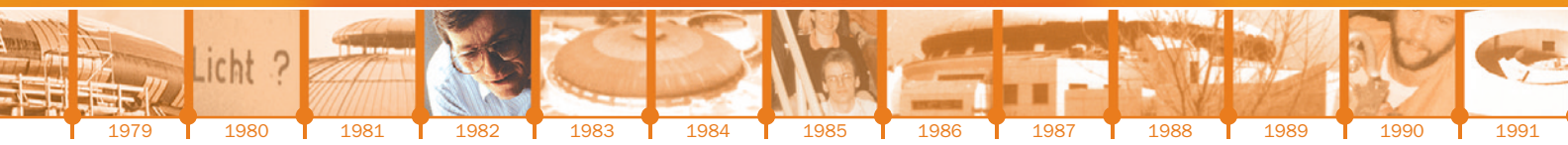

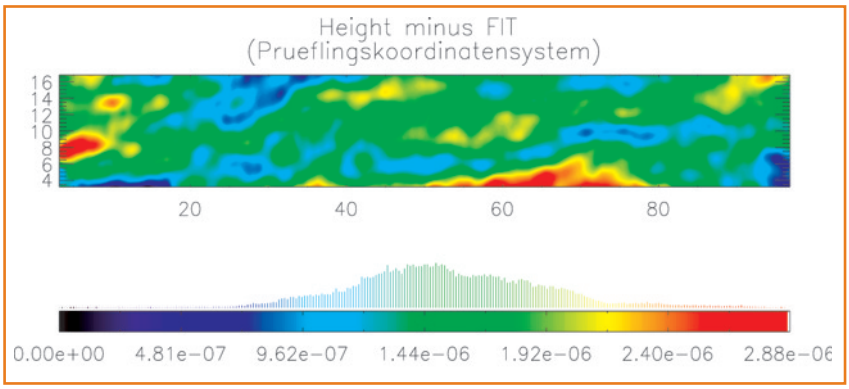

Fig 3:
3-D-mapping of a NOK demonstrator for a plane silicon grating substrate (100 x 20 mm and fit with radius 350 km): Deviation of the slope 0.02 arcsec rms and of the height 2.8 nm pv; 0.35 nm rms (λ/2000).

Deflectometry, in contrast to interferometry, needs no reference surface and measures directly the slope of the optical component. The sample is scanned stepwise. An optical diode above the test object emits light, which impinges nearly perpendicularly on the sample surface. The slope of the sample surface slightly off-sets the reflected ray. From the angle between the initial and the two and more reflected beams and the distance travelled, the slope of the surface can be determined. Integration of the slopes leads to the surface height. Surface maps are calculated from line scans along and across the sample and compared to scans along the diagonal in an auto-control procedure resulting in uncertainties below 1 nm (Fig. 3).

These developments have led to state-of-the-art measurements with an accuracy now in the range of 0.02 arcsec rms. In other words, it is now possible to measure deviations from ideal geometry with are comparable to height differences, from the highest to the lowest point (peak-to-valley – pv), of 2 mm over a base line of 1,000 km corresponding to the distance Berlin-London (Fig. 4)!

The manufacturing team of the NOK project set about improving the polishing and finishing techniques. With the help of the surface maps determined with the NOM the errors on the surfaces can be corrected by ion milling techniques (Fig. 5). Several beamlines at BESSY are now provided with nearly perfect mirrors and gratings manufactured in this way. Now the beam quality is limited by the mounting and moving the optical components.

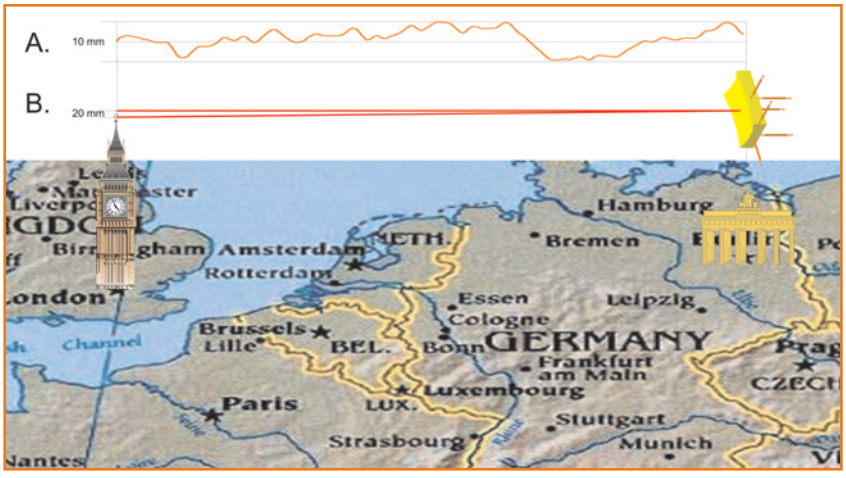

Fig. 4:
Achieved accuracies of mirror surfaces and positioning transformed to geographical scale. (A) A deviation of 1 nm peak-to-valley (pv) from ideal shape of a 100 mm grating blank corresponds to pv 10 mm for the distance of 1,000 km. (B) Positioning with a resolution of 10 nanorad corresponds to a shift of ~20 mm in the same distance.

Fig. 5:
Surface map before and after ion milling

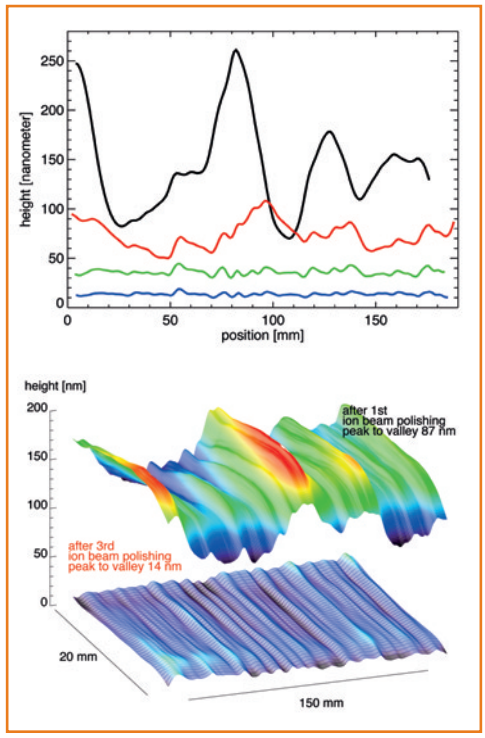

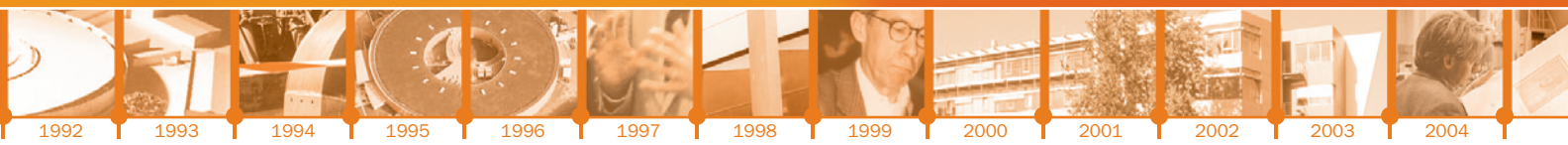

Cartesian Strut Arrangement

With the NOM it has also been possible to quantitatively determine the amount of distortion resulting from the mounting techniques used for the optical components in the respective monochromators or mirror chambers (Fig. 6). Up until the advent of storage rings of the third generation the mounting techniques employed, based on sound kinematic principles, were sufficiently accurate for most applications. This is no longer true. However, not only the mounting techniques need improvement. The entire suspension and adjusting elements have been a part of a re-design programe at BESSY. Optical components of several kilograms weight must be moved accurately and reproducibly with a resolution of 10 nanorad, 20 mm over a distance of 1,000 km (Fig. 4) and this, in some cases, several times per second!

Where only small movements are necessary, 20-50 mm for translations and up 2 degrees for rotations, kinematic bearing based on material elasticity have found increasing application, being inherently stiff and mechanically well defined. In this concept, well defined „weak points“ are systematically introduced into an otherwise rigid system. By this means desired torsions and deflections can be induced. Stiff lines of action are necessary for well defined movements. Push-pull struts are used which have flexural joints at both ends (Fig. 7). They are stiff in the longitudinal tension and compression direction but can flex for bending and twisting motions. The orientation of the struts determines which axes will be movable and which fixed.

At BESSY the Cartesian Strut Arrangement was developed and several derivatives haven been patented (Fig. 8). The arrangement consists of struts mounted parallel and perpendicularly to the desired motions and enables very precise movements in all six Cartesian coordinates to be made. It is a very special feature of this arrangement that the three orthogonal rotations occur with respect to the central point of the mirror surface, thus the mirror will not leave the incident light beam while being adjusted.

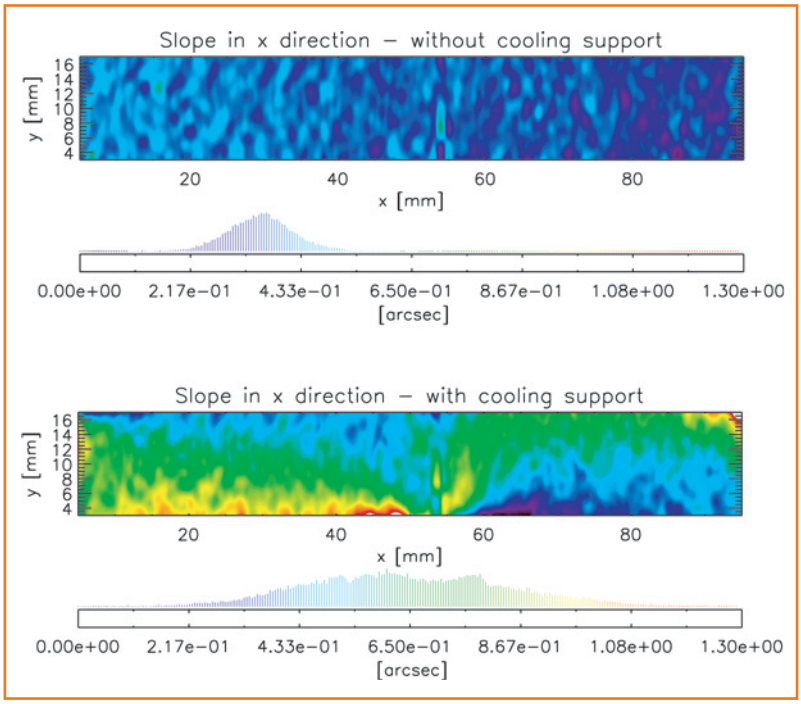

Fig. 6:
Mirror distortion upon mounting

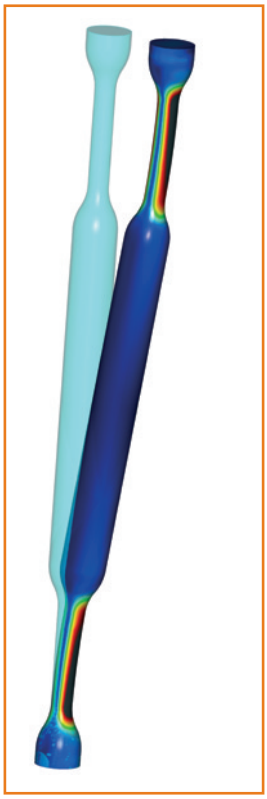

Fig. 7:
Push-Pull-Struts

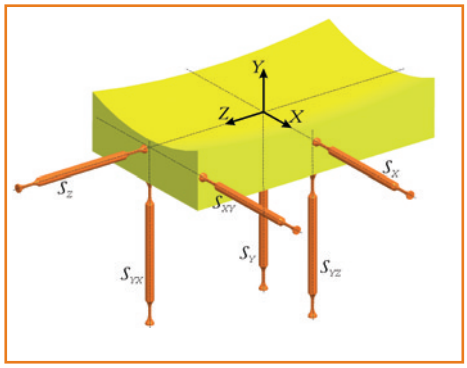

Fig. 8:
Cartesian Strut Arrangement

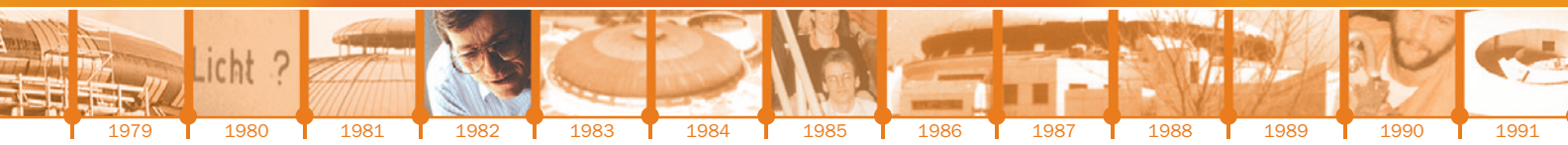

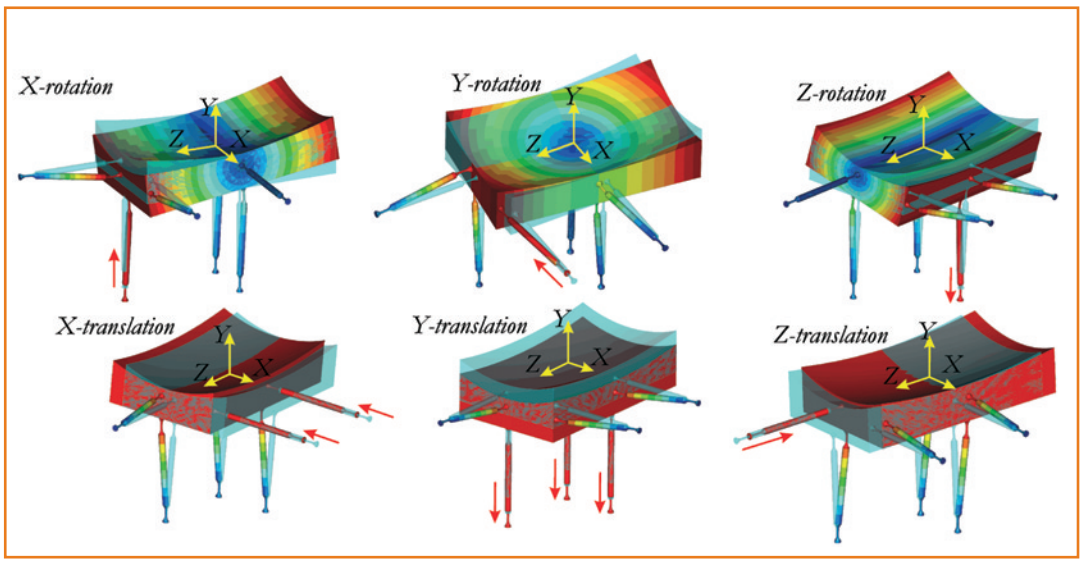

Fig. 9:
Movements of strut and resulting movements of the mirror

The movements are generated by modifying the length of a strut (linear drive) or by moving the base of a strut in its line of action (Fig. 9). The Cartesian strut system is statically determined, and every movement of a strut directly creates a movement of the mirror and can be driven by lead screws with stepper motors or piezo translators.

Several derivatives of the Cartesian strut system have been developed and implemented at BESSY. For the horizontally deflecting mirrors at dipole beamlines only the proportions have been changed due the mirror proportions of up to one meter in length with 60 to 100 mm width and depth (Fig. 10). Switching mirror units on ID beamlines contain a modified strut arrangement which is dedicated to the three orthogonal rotations around the mirror surface centre and also enables one vertical translation (Fig. 11). Two of these modules are placed in opposition to each other in a parallelogram which guides the lateral switch movement and acts as horizontal positioning stage at the same time (Fig. 12).

For the latest single switching mirror unit, this kinematic arrangement has been further modified to account for limited space at the front end of the beamline, minimizing the number of mechanical parts, and enabling

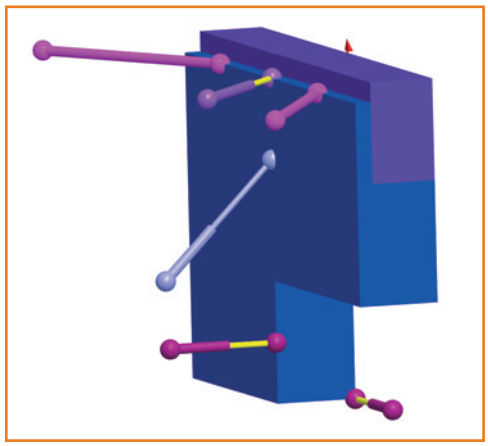

Fig. 11:
Switching mirror units on ID beamlines

fast movements of the angle of incidence (Fig. 13). The specially designed chassis accommodates the struts at the reflecting side of the mirror. The central strut moves the mirror in the beam path to deflect the light or removes the mirror for passing the beam straight through the chamber.

This mirror system has no separate mirror mount. The water cooling is connected rigidly to the mirror and provides an additional support. The mirror is driven by a lead screw drive augmented by a piezo stack translator in order to compensate for beam position variations. With this arrange-ment the refinement of the angular mirror position up to 20 times per second is possible. The Cartesian strut system has become the standard for new positioning mechanism at BESSY and is now applied in more than 30 devices. Some are working since 1998 without requiring maintenance.

Fig. 10:
Strut system for horizontally deflecting mirrors

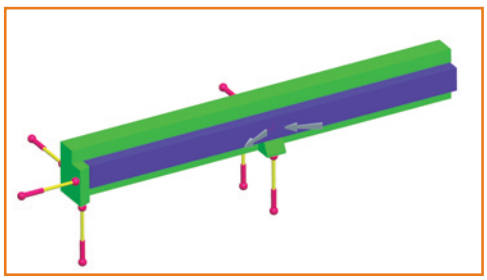

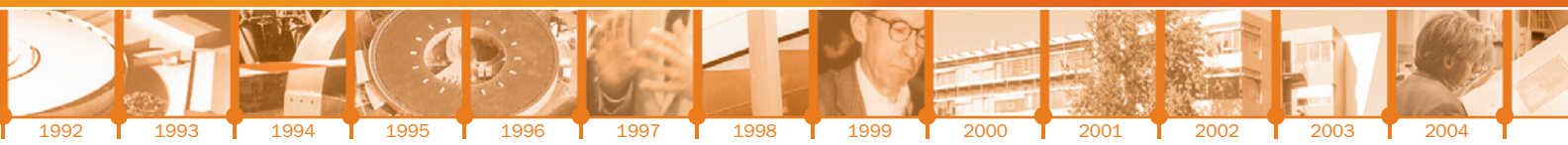

Outlook

For ambitious future projects such as the free electron laser (FEL) already proposed, new optimized beamlines are required to match the extraordinarily short pulses, the brilliance and the peak pulse power expected. In addition new beamlines to keep BESSY at the cutting edge of SR technology such as a proposed microfocus beamline for resonant scattering and a low energy (3 - 250 eV) PGM beamline (a collaborative project with FMB in Berlin-Adlershof) require further improvement of mirrors, mounts and drives.

Networks such as NOK or cooperation with companies from the optical industry have led to a massive development in high precision optics. These successful joint ventures are excellent examples of the synergic effects in a technology park like Adlershof and national network structures. These developments will also create new research as well as new career and employment opportunities.

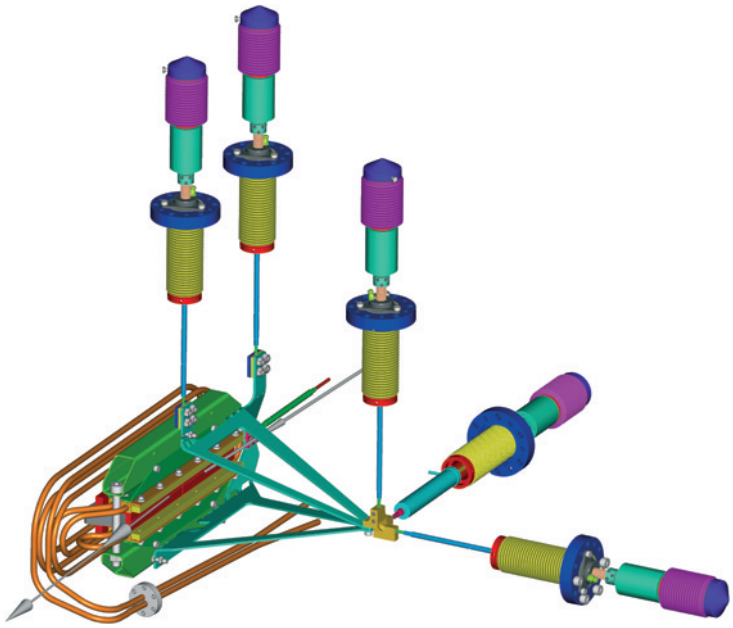

Fig. 13:
Kinematic arrangement

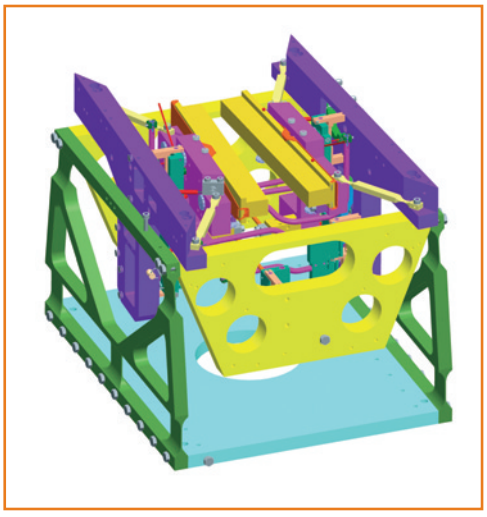

Fig. 12:
Lateral switch movement while horizontal positioning

The NOK cooperation:

A. Schindler, T. Hänsel, A. Nickel, G. Böhm (IOM Leipzig)

C. Schlewitt, B. Grubert, D. Kreitschik (Möller Wedel Optical GmbH)

O. Schnabel (Schnabel Elektrische Messtechnik Wedel)

I. Weingärtner, M. Schulz, R. Geckeler, J. Illemann (PTB, Braunschweig)

I. Rieck, C. Hellwig (Berliner Glas KG)

D. Bergner, U. Jungstand (Jenoptik Laser Optik Systeme GmbH)

K. Becker, G. Derst, A. Seifert (Carl Zeiss Laser Optics GmbH Oberkochen)

M. Berger, F. Hentschel (Optikkomponenten und Kristalle GmbH Berlin)

S. Rothe, U. Glaubitz, P. Hoffmann (Optik Elektronik & Gerätetechnnik OEG GmbH Frankfurt/Oder)

V. Herold (Friedrich Schiller Universität Jena, Technisches Institut)

BESSY Optics Team

H. Lammert, F. Siewert, T. Noll,
A. Erko, G. Reichardt, F. Schäfers,
O. Schwarzkopf, R. Follath, F. Senf,
C. Jung, Th. Zeschke

Supported by Bundesministerium für BMBF and VDI

Contact:
Heiner Lammert
heiner.lammert@bessy.de
Tino Noll
tino.noll@bessy.de

5

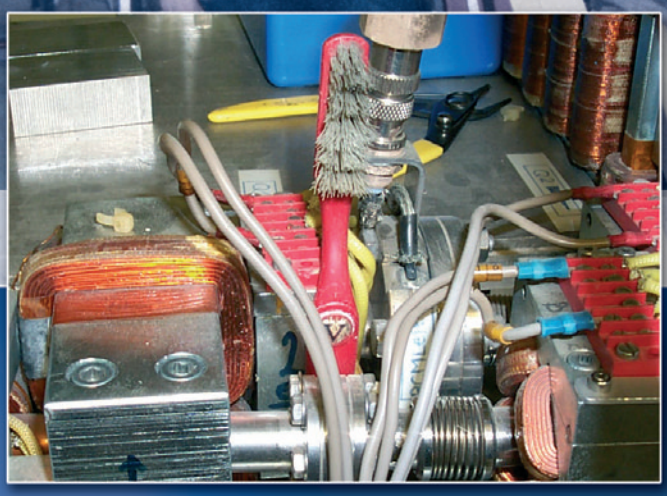

BESSY crew members and the 'famous toothbrush', 1987

Machine Status

In 2004 the BESSY II light source delivered 4,852 hours (36 weeks) beamtime. Standard operation mode was a multi bunch filling pattern. In the last quarter of the year hybrid mode was requested frequently, i.e. multi bunch with a single bunch of up to 5 mA stored in the gap left for ion clearing. Dedicated operation in single bunch mode (4 weeks totally) and 1 week in the low-alpha mode were also realised. Ten weeks were dedicated to commissioning work of machine, insertion devices and beamlines. Shut down activities summed up to 7 weeks, primarily related to the final implementation of the fs-slicing installation which became operational later in the year (Fig. 1).

Short Bunches

BESSY is the leading storage ring in achieving bunches shorter than 1 ps. These bunches are produced routinely after refinement of the optics for a small and negative momentum compaction factor.
The rms-bunch length of the sub-ps long bunches was determined from the emission characteristics of coherent synchrotron radiation (Fig. 2). The stability limit of short bunches is limited, however, for many experiments the bunch repetition rate of 500 MHz can compensate for that.

Operation of Insertion Devices

In addition to 12 conventional planar and APPLE-type undulators the BESSY storage ring is routinely operated with three superconducting wavelength shifters (WLS) and a superconducting wiggler. No other light source is operating that many strong insertion devices (ID).

Since the routine operation of the wiggler at 7 T starting in June some challenges had to be mastered: All superconducting IDs perturb the electrons vertical orbit due to mechanical vibrations generated by the He-recondensors, giving rise to a small beam motion at a frequency of around 1.6 Hz. During the last year these distortions could be significantly reduced by mechanical realignment of some of the recondensors, while the influence of the others were compensated by an active orbit feedback, or by simply switching off the most perturbing ones, sacrificing an increased liquid He consumption and tolerating more frequent refills which are enabled by the Linde TCF 50 cryo-plant. With the wiggler at 7 T, the lifetime is reduced due to the high gas desorption of the powerful photon beam, the increased ß-beat introduced by the strong focussing of the ID, and the decreased energy acceptance of the ring. The cold bore of the wiggler can release absorbed molecules if cooled not properly, resulting in a vacuum pressure increase and thus preventing user operation.

The APPLE-type undulators with their gap and shift depending focussing characteristics require a 2-dimensional tune feed-forward. This was implemented and successfully tested last year and is now in routine operation (Fig. 3). With this tune compensation in place the working point is sufficiently stable for operating in normal user mode. In the meantime, the compensation was refined in order to reduce the impact of these undulators in the short bunch operation mode since bunch length and the power of coherent synchrotron radiation are very sensitive to even very small horizontal tune changes.

Fig. 1:
Final implementation works of the fs-slicing installation (U139)

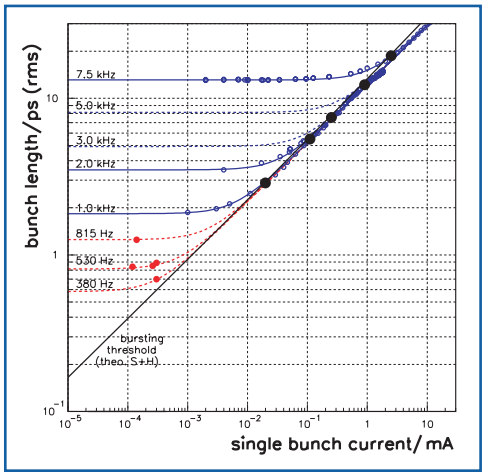

Fig. 2:
Bunch length as function of the bunch intensity. Data points in blue represent measurements employing a streak camera with a resolution limit of 2 ps.

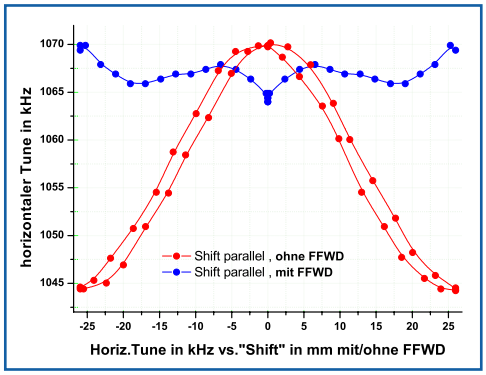

Fig. 3:
Feed-forward results for the UE52.

Beamline Developments

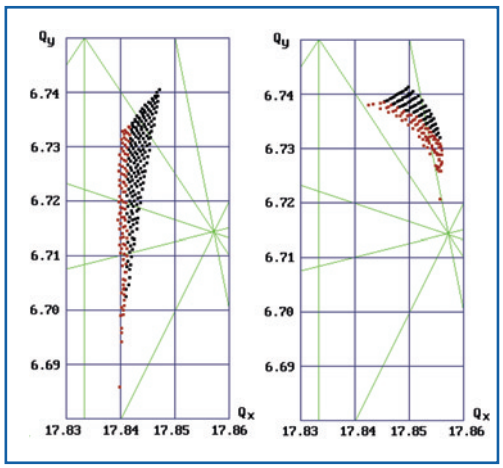

Fig. 4:
Measured frequency maps for all ID-gaps wide open (left) and one undulator (UE52) active (right). The undulator was set to a gap of 17 mm and shift parameters to generate vertical polarisation. Red dots represent measurements when more than 2% of the intensity was lost during the experiment.

Future Developments

Future activities are focussed on further improving beam intensity by investigating the possibilities for operating the storage ring in topping-up mode. This mode requires high injection efficiency at all possible operational conditions of IDs. At small gap settings all undulators have a noticeable impact on the horizontal dynamical aperture which is important for the efficiency of injecting beam into the storage ring (Fig. 4). Preliminary tests have shown that a fast global orbit stabilisation is feasible with the present hardware, only the corrector power supplies need to be replaced and equipped with fast interfaces. The available computing power then would determine the upper frequency limit of the feedback system.

With the installation of the new UE49 all straight sections are now occupied by IDs and additional space would only be available if existing undulators or some of the superconducting WLS in the straight sections could be replaced by superconducting dipoles ('superbends') instead of normal conducting dipole magnets. For improving simulations and optimising the reliability of the hardware, a prototype has been developed and built by the Budker Institute of Nuclear Physics in Novosibirsk awaiting further tests at BESSY (Fig. 5).

Fig. 5:
Superbend prototype with B_{max} = 9.3 T

The most extensive activity that was completed in 2004 was the installation of the fs-slicing hardware (U139, bending magnets, front ends) in the storage ring and the re-design and construction of the successive beamlines on the new optical axis. The initial results of these efforts were reached in April, when it could be verified that slicing had taken place and a portion of an electron bunch had been modulated in energy. The developmental work on the new diagnostics beamline designed for the very far infrared between 0.1 and 10 THz paid off here. On the basis of the terahertz signal just downstream of the slicing undulators the overlap between the exciting laser beam and the electron bunch could be observed using a fast InSb detector.

In July the first 'sliced' photons were detected at the end of the X-ray beamline (Fig. 6). In the second half of the year the main machine physics goal was to increase the extent of the energy modulation. This culminated in a signal to background ratio of 10:1 as theoretically predicted. Parallel to these efforts the beamline and the experimental set-up were being optimised.

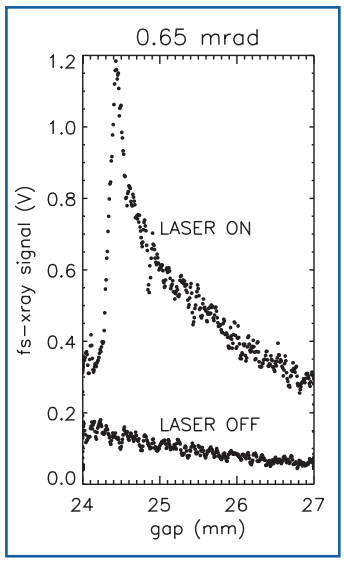

Fig. 6:
Third harmonics of UE56 measured with fs-X-rays

Contact:
Peter Kuske
peter.kuske @bessy.de

The progress of the slicing experiments benefits from the 'hybrid mode' of machine operation in which one electron bunch is injected into the middle of the ~100 ns gap in the filling pattern. This bunch is then available for fs-slicing experiments even during the normal operating schedule. The colleagues are pleased that their work is no longer relegated exclusively to night shifts.

The last available straight section of the storage ring, L08, is now occupied by a new undulator, UE49, installed during the long shutdown. This undulator is optimised for high brilliance photons from 95 to about 1,600 eV. The beamlines, still undergoing construction, will profit from the small horizontal betatron function in this section which leads to a very small source size in the horizontal plane to go along with the usual small dimension vertically.

The optics beamline on the L08 dipole has been successfully commissioned and put into routine use. It offers good resolution for energies 25 - 2,000 eV and a spot size of 300 x 100 µm^2. This beamline is primarily used in conjunction with the BESSY reflectometer and the SurICat apparatus (Fig. 7).

As a result of the developments in optical metrology it has been possible to obtain vastly improved mirrors and gratings for several monochromators (see 'Optic Special' in this issue). The U125-PGM1 and the 10m-NIM both offer a 10 fold brighter spot at the experiment and the U41-PGM improved brilliance and stability. After a sudden degradation of its performance, the UE56/2 -PGM2 (MPG) has been completely revamped and now performs again like the other world class plane grating monochromators on BESSY undulators. A resolution of >90,000 has been achieved.

The soft X-ray beamline KMC-1 with its new 'heart', a double crystal monochromator has been successfully commissioned. KMC-1 operates three in situ exchangeable pairs of crystals (InSb, Si (111) and Si (422)) for the energy range from 1.7 keV to more than 10 keV thus covering Si, P, and S K-edges. Extremely high resolutions within a flux of 10^{10} photons/sec have been achieved with the Si (422) in backscattering geometry.

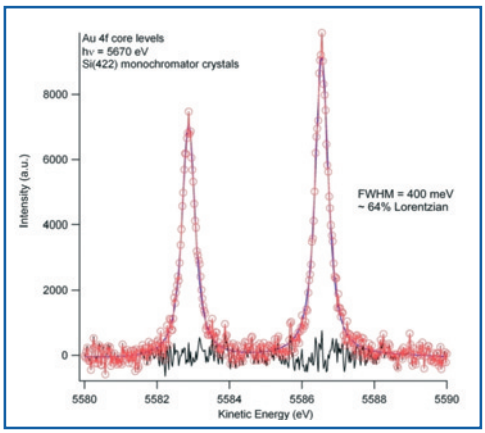

Fig. 8:
Au 4f $^5/_2$ and $^7/_2$ core levels at KMC-1 with Si (422) crystals in backscattering geometry

Using a SCIENTA 4000 photoelectron spectrometer an FWHM smaller than 400 meV at 5.67 keV at the Au 4f levels was measured (Fig. 8).

A new KMC beamline for microfocus experiments was delivered and installed in in autumn. It is located on the BAM-7T-WLS and will offer highly intense, focussed radiation with a spot size 1 - 30 µm diameter, over the energy range from 2.1 to 30 keV. Commissioning will take place in the early months of 2005. This is a joint project of the BAM, MPI-Golm and BESSY.

The two beamlines on the HMI 7T-multipole wiggler have been commissioned and are available to the BESSY user community. The one beamline (EDDI) offers a white beam with unfocused photons from 10 to 150 keV. With the help of slits, spot sizes down to 0.1 x 0.1 µm^2 are possible. An energy dispersive detector and a large goniometer can handle/probe weights of up to 50 kg. The second system (MAGS) consists of a double crystal monochromator for photon energies of 4 to 28 keV and a resolution of 20,000 (Si (111)). A Huber 6 circle goniometer and Displex cryostat (6 - 800 K) combined with an energy dispersive detector are available to potential users (Fig. 9).

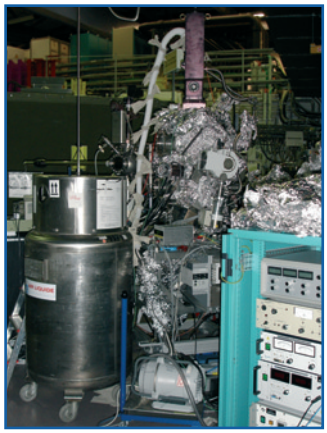

Fig. 7:
The SurICat apparatus at L08 dipole beamline. A multi-functional photoemission system equipped with a Scienta 100 analyser, liquid helium cooled manipulator, two preparation chambers and an Omicron standard sample system.

Fig. 9:
Six circle Huber goniometer at HMI 7T multipole wiggler beamline

Contact:
William Peatman
william.peatman@bessy.de

BESSY Soft X-ray FEL Project

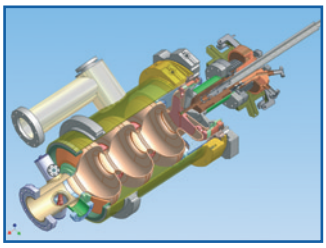

Fig. 10: Sketch of the superconducting RF photogun

A major milestone on the way to the BESSY Soft X-ray FEL was passed when the Technical Design Report (TDR) was completed in early 2004. The TDR demonstrates the feasibility of a VUV to soft X-ray laser using technologies available today and predicts the photon beam parameters that will make the BESSY FEL a veritable 'Second Generation' machine.

Superconducting RF-Gun

The need for a highly flexible high duty cycle photoinjector led to a collaboration by Forschungszentrum Rossendorf (FZR), Max-Born Institute (MBI), BESSY and DESY to push the development of CW injectors. Based on the superconducting gun development at FZR a dedicated injector is under construction which will be used for the ELBE accelerator. The injector will also generate 2 nC bunches at a frequency of up to 1 kHz important for studies for the BESSY-FEL. While the cryostat and the 3.5 cell cavity are under construction, MBI is developing a double channel laser system to cope with the different operation modes and BESSY is procuring the diagnostics.

High Duty Cycle Cavity for the PITZ-2 RF Gun

The room temperature low emittance gun now successfully in operation at the VUV-FEL at DESY Hamburg was developed within the PITZ collaboration by a consortium of DESY-MBI-BESSY and TU Darmstadt during the years 1999 - 2002. This RF photoinjector meets the parameters for the injector to the BESSY Soft X-ray FEL, except for the bunch repetition rate. Thus, a study was initiated within the PITZ-2 collaboration to optimise the heavily power loaded cavity for operation of macro-bunches consisting out of three single bunches at a repetition frequency of 1 kHz. At an acceleration field of 40 MV/m at the cathode surface the total power then dissipated in the gun-body is about 75 kW which requires efficient cooling. Using state-of-the-art FEM-codes for simulation of the electromagnetic fields the resulting power-losses in the cavity body were calculated to design details of the cooling geometry. Optimising the location, varying size and throughput of the cooling circuits, a solution was developed that will stand the high duty cycle operation of the cavity (Fig. 11).
At full power the resulting temperature rise does not exceed 40°C at any location of the gun-body. Typical operation temperatures thus will be in the range of 70°C at a peak input power of 3 MW, corresponding to a duty cycle of 2.5 %.

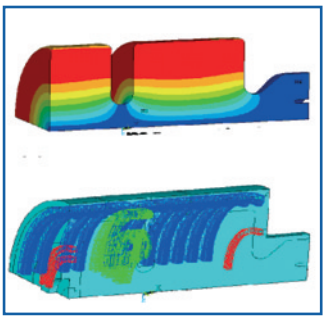

Fig. 11: Field distribution (upper graph) and resulting temperature profile of the cavity body (lower graph) in the PITZ-2 RF Gun

HoBiCaT Test Stand

To confirm the basis for a reliable CW operation of the TESLA acceleration modules a detailed qualification programme started at BESSY. Test of couplers and tuners, optimisation of cryogenic parameters such as bath temperature are performed at the HoBiCaT test stand. Successful commissioning of the Horizontal Bi-Cavity Test facility (HoBiCaT) took place in the third quarter 2004. LHe of 1.8 K is provided from the existing Linde TCF50 cryogenic plant connected to a pumping station. Two 9-cell cavities completely manufactured and processed by industry have been delivered and are available now for testing. Test with the TTF coupler at a power level of up to 8 kW CW have been successfully performed, demonstrating that only minor modification will be necessary to achieve safe operation in the BESSY superconducting CW linac.

Simulation on the FEL Continue

Work on the FEL process was continued since the TDR has been published. The simulations concentrated on detailed tolerance studies to quantify tolerance budgets for undulator field errors as well as other hardware. Further optimisation of electron bunch properties at the first HGHG stage was performed to relax the output power sensitivity to timing jitter of electron bunch and seed laser. Investigation of the FEL output characteristics on higher harmonics of the radiation emitted from the final amplifier has started. Though the harmonic power is much smaller than the one from the fundamental, peak powers in the order of some ten MW can be expected at the 3rd harmonic. Exploring the details of spectral performance and quantifying the harmonic power will be one topic for the future.

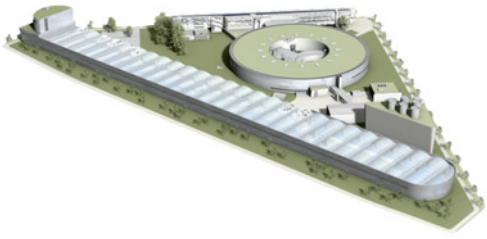

Contact:
Dieter Krämer
dieter.kraemer@bessy.de

Metrology Light Source of the PTB

Fig. 12:
Construction site of the Willy-Wien-Laboratory. The solid parts of the radiation shielding have been completed (right) The walls as well as the ceiling have a thickness of 1 m, the grey parts are constructed of normal concrete, the red parts are constructed of concrete with a ferric oxide additive for enhanced radiation shielding.

The PTB Metrology Light Source (MLS) project, i.e. the construction of a 600 MeV electron storage ring made considerable progress in 2004. The MLS will be built at the crossing of Magnusstraße and Max-Planck-Straße, just opposite to the BESSY II electron storage ring. The ground-breaking ceremony on September 24th, 2004 marked the official beginning of the construction work for the so-called Willy-Wien-Laboratory, i.e. the building that will house the MLS. Soon after, the fabrication of the 60-cm-thick ground plate along with the other ground work commenced, followed by the casting of the concrete shielding for the electron storage ring. The concrete housing for the storage ring has already been completed (Fig. 12).

On the technical side, the design of the storage ring optics and its vacuum system have been finalised by the BESSY MLS-Team (Fig. 13). The call for tender for major components of the storage ring has begun and first contracts have been awarded: the storage ring magnets, i.e., 8 bending magnets, 24 quadrupole magnets, 24 sextupole magnets and 4 octupole magnets, will be manufactured by the Budker Institute of Nuclear Physics SB RAS (BINP) in Novosibirsk, Russia and the 100 MeV injection microtron will be delivered by Danfysik A/S in Jyllinge, Denmark. Major parts for the radiation safety surveillance equipment have already been delivered.

The MLS will mainly be dedicated to metrology and technology development in the UV and VUV spectral range. Moreover, the MLS will be well suited for the production of IR and THz radiation. The option of operating the MLS in the so-called 'low alpha mode' that allows the production of coherent synchrotron radiation is also envisaged. To bring together future users, a first national workshop was held in May 2004. About one hundred participants from PTB, scientific institutions and representatives from some renowned German companies discussed the exploitation of the possibilities that will open up with the operation of the MLS in the broad spectral region from the THz up to the VUV, including the technologically important EUV spectral region.

Currently, the various activities are well in or ahead of time, so that all involved in the project are optimistic that user operation will start in 2008, as scheduled.

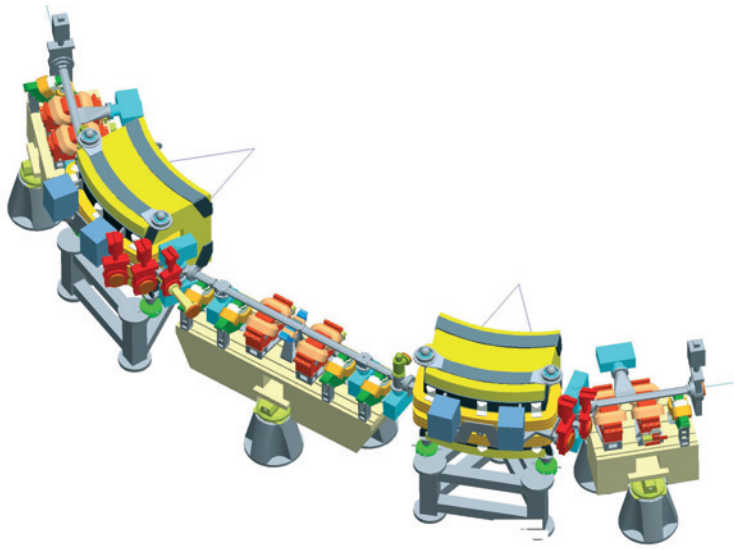

Fig. 13:
One quarter section of the MLS layout. The whole vacuum section for one segment will be assembled and baked off-site. For the installation of the vacuum system the bending magnets can be retracted and the other magnets - being grouped on girders – can be opened.

Contact:
Roman Klein
roman.klein@ptb.de

BESSY Projectteam-WWL
wwl@bessy.de

6

Consultations on how to install the first undulator for polarised light, 1990

Operation statistics

In 2004 the BESSY II storage ring was operated for 43 weeks. Among them were 36 weeks of dedicated user beamtime resulting in 4,852 beamtime hours, which is slightly less than 2003. This is a consequence of the postponement of the autumn shut down 2003 into spring 2004 which became necessary to allow enough time for the installation of the fs-slicing undulator system.

Operation is based on a schedule of 7 days per week, 24 hours per day (three 8 hour shifts). Special operation periods provided this year were 4 single bunch weeks and one week of low-α operation. In 7 MC-weeks some additional 800 h were used for studies to optimise the light source and user instrumentation and to advance accelerator technologies and physics.

The distribution of the allocated beamtime among the users of the different institutions and communities can be seen in the beamtime allocation graphics.

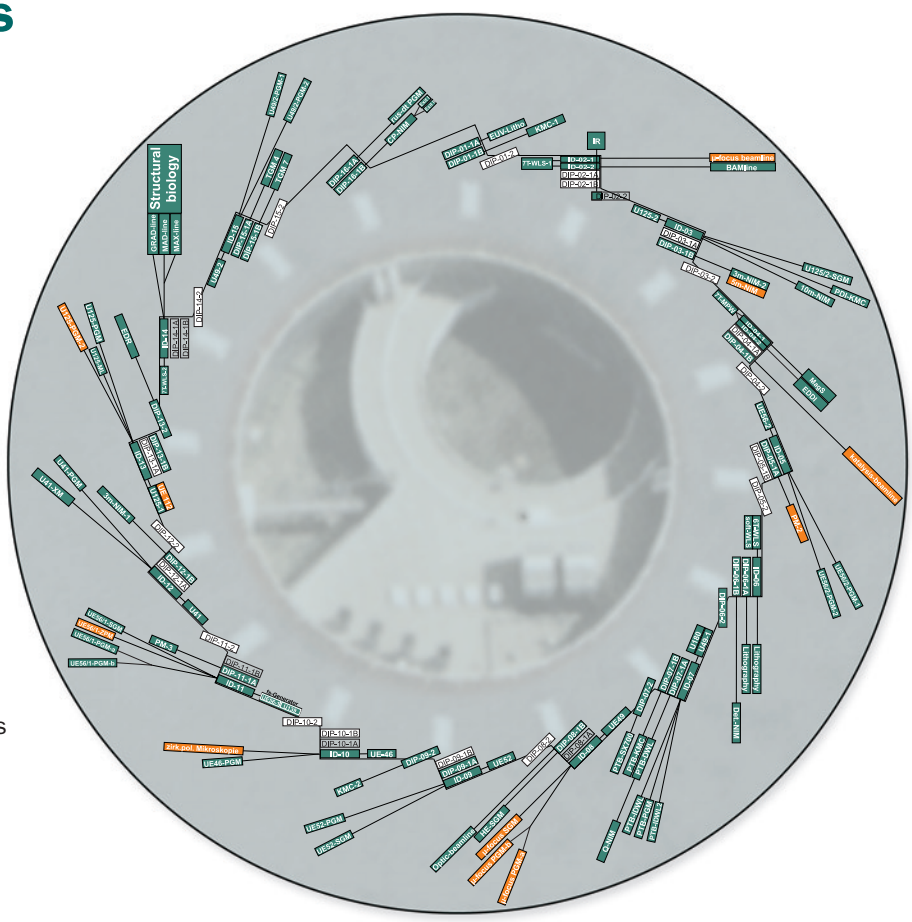

Beamtime at BESSY

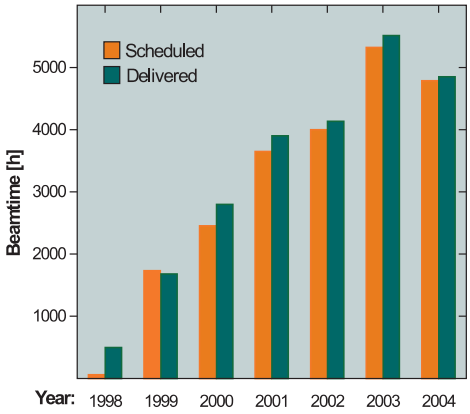

A remarkable change could be achieved for users from European countries. After the dry spell of the last two years, the new EU-I3 funding programme made it possible to increase their contingency to almost 10 %.

In 2004 more than 1,100 external scientists carried out more than 500 independent projects per year in basic research at BESSY. An exceptional increase of activities was registered in the protein crystallography beamlines.

in operation
under construction
planned

Beamtime allocation in 2004

Insertion Device Beamlines

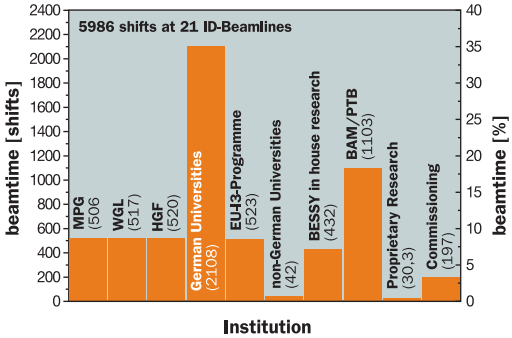

Bending Magnet Beamlines

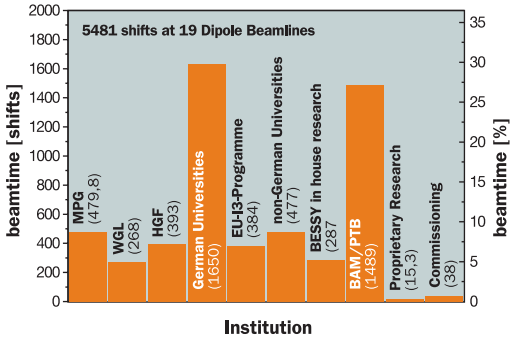

MPG = Max-Planck-Gesellschaft
WGL = Leibniz-Gemeinschaft
HGF = Helmholtz-Gemeinschaft

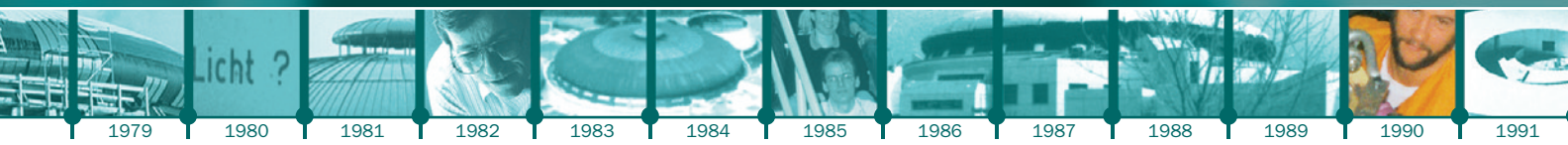

Improvements for users

In an effort to improve user operation several organisational changes have been implemented:

- the User Committee has taken up its charge,
- a new weekly user schedule inaugurated,
- parking zones in the experimental hall defined,
- and the introduction of experimental group supervisors.

The User Committee has already helped to achieve several further improvements. The new members of the User Committee have been elected during the Users' Meeting. Due to other pressing commitments W. Kuch did not run again for the UC. We would like to thank him for his engagement.

User Committee	
Uwe Hergenhahn	*MPI für Plasmaphysik, München*
Wolfgang Braun	*Paul-Drude-Institut, Berlin*
Christian-Herbert Fischer	*Hahn-Meitner-Institut, Berlin*
Ralf Püttner	*Freie Universität Berlin*

The new weekly schedule provides uninterrupted user measuring time from 7 AM Tuesday through to 10:30 PM Sunday (including the Sunday PTB Main User Shifts).

Service work in the storage ring tunnel takes place Mondays from 7 AM to 3 PM. Beamline commissioning is Mondays from 3 to 11 PM. Machine commissioning shifts can be held in the nights Sunday-Monday and Monday-Tuesday and are announced on the preceding Wednesday. The rotation of user groups can now take place on Monday using commissioning time for setting up.

Parking zones in the experimental hall have been created for preparation of user apparatuses for upcoming experiments with SR and for their use in between assigned beamtimes. Two BESSY containers, vacuum and electronics, were removed from the hall to make more space available. Requests for use of a parking space should be submitted to the user coordinator ("sicherheits-technische Anmeldung") at least three weeks in advance of the time that space is needed.

As in the accelerator group, where one of a small team of very experienced accelerator scientists is available per cellular phone essentially around the clock, seven days each week, a similar group of scientists from the experimental group has been defined who are also available 24-7 per cellular phone. In this way, the 'Hallendienstler' have, in addition to the service numbers from the six specialist groups (i.e. interlock, ID's, vacuum, beamlines, networks and data acquisition systems), backup for other problems that may arise. Questions of coordination can be dealt with quickly by the respective supervisors of the accelerator group and the experimental group. The supervisors also meet at the end of each 6 week measuring period in order to be certain that problems mentioned in the Beam Time Reports and Run Book have been dealt with and to discuss the needs for the subsequent user period.

In the course of 2005, we plan go online with a new user service, the BESSY Online Access Tool (BOAT). BOAT will provide all user related forms and information concerning beamtime, radiation protection and accommodation pooled in one application. Furthermore, BOAT will offer a comfortable way to overview and manage proposals, reports and users personal information and last but not least, it will be also a help for us to coordinate and accelerate the processing of the incoming applications.

We hope that these efforts will pay off in improved user operations at BESSY.

Shift	Mon	Tue	Wed	Thu	Fri	Sat	Sun
Early 7-15 h	Machine Servicing						Main User PTB except where denoted with an asteriks in the operation schedule
Late 15-23 h	ID/BL Commis-sioning						
Night 23-7 h	Machine Commis-sioning						Machine Commis-sioning

User operation	Parasitic use possible (in general, special beam conditions)	See TV Monitor for status	No User operation

User/Machine support: 24 hours/7days
(Sat/Sun, Sun/Mon nights: Dawn-special,
PTB-Sundays: no late shift)

Industrial users

Not at least the evaluation by the Leibniz-Gemeinschaft raised the question again on the industrial application of synchrotron radiation (SR). BESSY continuously intensifies the contact to industry by participation on several fairs, e.g. the 'HannoverMesse' jointly with Micro Resist Technologies, 'Systemintegration in der Mikroelektronik" (SMT) in Nürnberg and the 'Laser Optic Berlin' (LOB). During the latter, we welcomed fair visitors and showed on site available facilities and currently running projects.

In November, BESSY hosted the second 'Industrieforum', jointly organised by the three main German SR sources together with HASYLAB, Hamburg, and ANKA, Karlsruhe. The workshop was entitled "Nanofabrikation - Neue Dimension der Mikrosystemtechnik" and addressed mainly companies not yet involved in SR based micro engineering projects. It aimed to point out the possibilities SR sources can offer in solving problems in analysis and fabrication. We were proud that Hans-Olaf Henkel, president of the Leibniz-Gemeinschaft, found the time to welcome the participants and to encourage the use and research in high-tech fields. One of the key note speakers emphasised that the technique of SR based micro engineering is about to break through in industrial applications but would still need a 'blockbuster product' to make it a technology of the present and not of the future.

Besides the contact on fairs BESSY is always open for the interest of industrial partners. Two new experimental stations should be mentioned as representatives for many which are summarised in the list on page 66. By the end of the year BESSY has taken over the responsibility for one of the protein crystallography experiments. The beamline and the experimental station are automated to a great extend so that 'Mail-In Crystallography Services' are available, i.e. sending in cryogenic samples and getting data sets back shortly after data collection (www.psf.bessy.de). The second example is an experimental station which allows dynamical studies of catalysts under reaction conditions (see page 10). At this station projects with a great epoxide producer are currently under investigation.

Contact for industrial activites:
Walter Braun
industrialuser@bessy.de

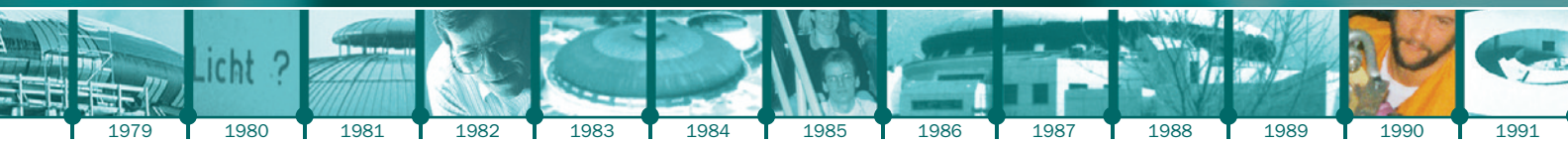

ID Beamlines at BESSY *(January 2005)*

For general information on beamlines see BESSY website under www.bessy.de/users_info/beamlines

BAM
Bundesanstalt für Materialforschung und -prüfung

BTUC
Brandenburgische Technische Universität Cottbus

FUB
Freie Universität Berlin

FZJ
Forschungszentrum Jülich

HMI
Hahn-Meitner-Institut

IRP
Institut für Röntgenphysik Universität Göttingen

MPG
Max-Planck-Gesellschaft

MPIKG
Max-Planck-Institut für Kolloid- und Grenzflächen-forschung

PDI
Paul-Drude-Institut

PTB
Physikalisch-Technische Bundesanstalt

Uni Bi
Universität Bielefeld

Uni Kl
Universität Kaiserslautern

Uni Wü
Universität Würzburg

Insertion device	*Monochromator*	*Energy Range (eV)*	*Contact Persons*	
7T-WLS-1	KMC	6 k - 50 k	H. Riesemeier (BAM) B. Müller (BAM)	A. Erko
	µSpot	2 k - 30 k	A. Erko H. Riesemeier (BAM)	O. Paris (MPIKG)
U125-2	SGM	20 - 500	R. Püttner (FUB)	G. Reichardt
	KMC	6 k - 12 k	W. Braun (PDI) P. Jenichen (PDI)	A. Erko
	10m-NIM	<10 - 35	G. Reichardt	I. Packe, P. Rotter
UE56-2	PGM 1	60 – 1,300	W. Mahler (MPG)	B. Zada (MPG)
	PGM 2	60 – 1,300	W. Mahler (MPG)	B. Zada (MPG)
6T-WLS 0.4T-LFD	Litho	>2,000	B. Löchel H.-U. Scheunemann	M. Bednarzik H. Köhrich
U49-1	13°		R. Klein, A. Gottwald (PTB)	
	PGM	20 – 1,900	B. Beckhoff (PTB)	
	-	Direct beam	R. Klein (PTB)	
UE49	PGM a/b*	85 – 1,600	F. Senf Ch. Jung	M. Mast J.-S. Schmidt
UE52	SGM	85 – 1,600	K. Godehusen F. Senf	T. Zeschke
	PGM	85 – 1,600	D. Batchelor (Uni Wü) Th. Schmidt (Uni Wü)	Ch. Jung
UE46	PGM	120 – 1,700	D. Schmitz (HMI) H. Rossner (HMI)	F. Senf
UE56-1	PGM a	60 – 1,300	T. Kachel J.-S. Schmidt	Ch. Stamm
	PGM b	60 - 1.300	T. Kachel J.-S. Schmidt	T. Zeschke
	ZP-mono	715 / 786 / 861	A. Erko	I. Packe
	SGM	60 – 1,300	S. Cramm (FZJ)	
U41	STXM	~250 - ~600	P. Guttmann (IRP)	G. Schneider
	TXM	~250 - ~600	P. Guttmann (IRP)	G. Schneider
	PGM	170 – 1,800	Ch. Jung	M. Mast
U125-1	PGM 2 a/b*	5 - 180	R. Follath	St. Dorausch
	Multilayer	80 - 700	U. Kleineberg (Uni Bi)	
	PGM 1	20 - 700	O. Schwarzkopf	F. Eggenstein
7T WLS-2	KMC 1	4.5 k – 17.5 k	U. Müller	
	KMC 2	4.5 k – 17.5 k	M. Fieber-Erdmann (FUB)	
U49-2	PGM 1	85 – 1,600	O. Schwarzkopf	J.-S. Schmidt
	PGM 2	85 – 1,600	P. Hoffmann (BTUC)	W. Braun

**** under construction***

ID02-2 7TWLS/1-KMC1	BAM/PTB
ID02-2 7TWLS/1-BAM/µSPOT	BAM/MPIKG
ID03-1 U125/2-SGM	BUS
ID03-2 U125/2-KMC	PDI/HUB
ID03-3 U125/2-NIM	Uni KI/BESSY
ID05-1 UE56/2-PGM1	MPG
ID05-2 UE56/2-PGM2	MPG
ID06-1a 6T-LITHO	BESSY
ID06-1b 0.4T-LITHO	BESSY
ID07-1 U49/U180 13°	PTB
ID07-2 U49/U180-PGM	PTB
ID07-3 U49/U180 direct beam	PTB
ID08 -1 U49 GM a/b	BESSY*
ID09-1 UE52-SGM	BESSY
ID09-2 UE52-PGM	UFF-CRG
ID10-1 UE46-PGM	HMI
ID11-1 UE56/1-PGM a/b	BESSY
ID11-2 UE56/1-SGM	FZ Jülich
ID12-1a U41-STXM	U-Gö/BESSY
ID12-1b U41-TXM	U-Gö/BESSY
ID12-2 U41-PGM	BESSY
ID13-1 U125/1-PGM1 a/b	BESSY*
ID13-2 U125/1-ML	Uni Bi
ID13-3 U125/1-PGM	BESSY
ID14-1 7TWLS/2-KMC1	BESSY
ID14-2 7TWLS/2-KMC2	FUB
ID15-1 U49/2-PGM1	BESSY
ID15-2 U49/2-PGM2	BTUC

** under construction*

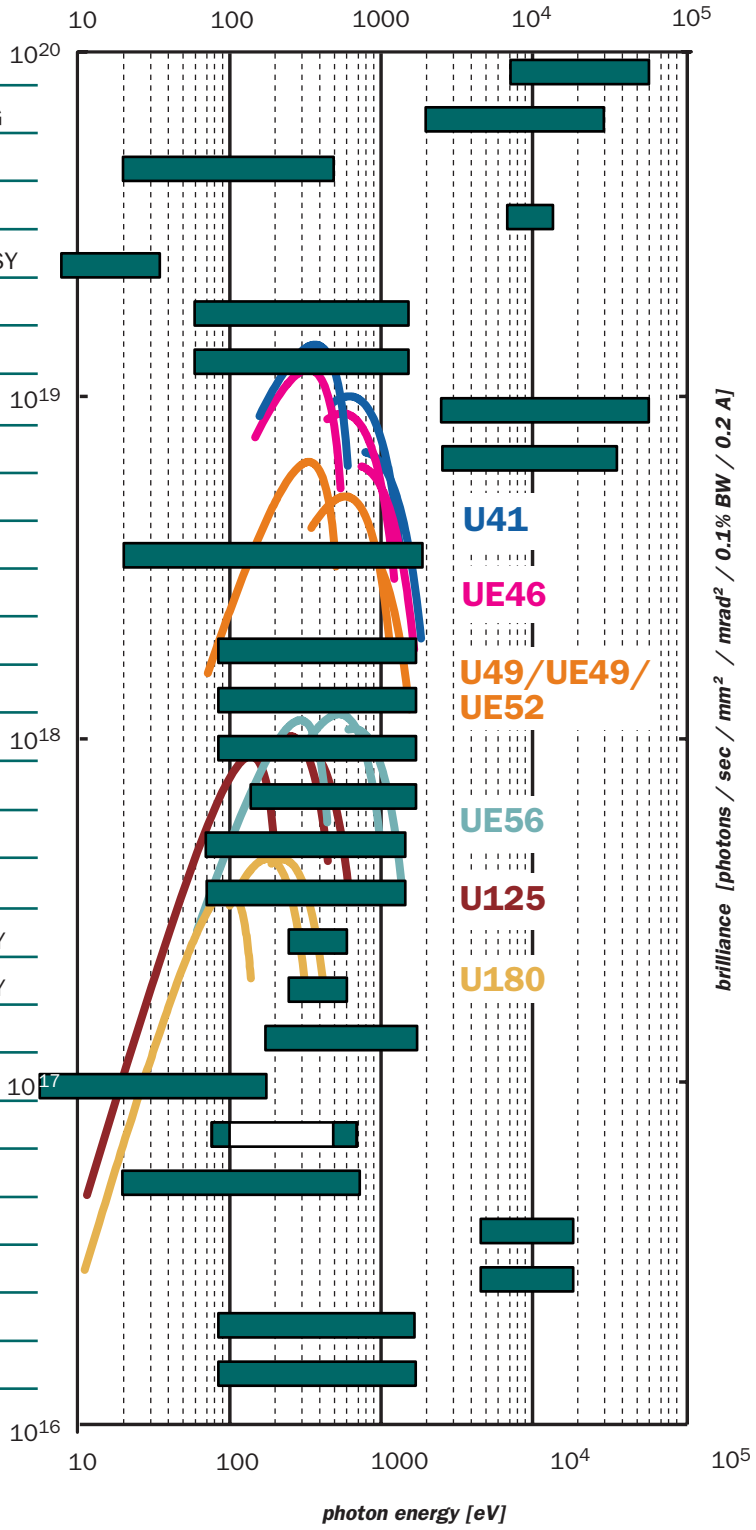

BESSY II,
1.7 GeV, 200 mA coupling 1%

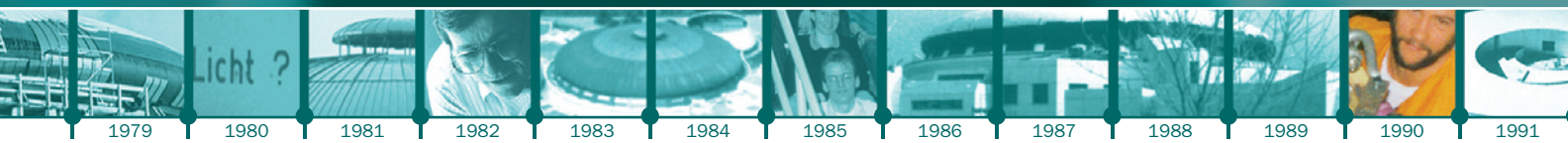

Dipole Beamlines at BESSY *(January 2005)*

For general information on beamlines see BESSY website under www.bessy.de/users_info/beamlines

PTB
Physikalisch-Technische Bundesanstalt

Uni P
Universität Potsdam

BAM
Bundesanstalt für Material-forschung und -prüfung

HMI
Hahn-Meitner-Institut

Uni D
Universität Dresden

Uni Pet
University St. Petersburg, Russia

Monochromator	*Energy Range (eV)*	*Contact Persons*	
Litho EUV	95	H.-U. Scheunemann	H. Köhrich
KMC 1	1.7 k - 10 k	F. Schäfers	M. Mertin
IR stations	THz – 0.5	U. Schade	
3m-NIM-2	4 - 35	I. Packe	G. Reichardt
Litho	direct beam	B. Löchel H.-U. Scheunemann	M. Bednarzik H. Köhrich
1m-NIM 1	3 - 35	M. Richter (PTB)	
1m-NIM 2	3 - 35	R. Thornagel (PTB)	
	white beam	R. Thornagel (PTB)	
KMC	1.7 k - 10 k	M. Krumrey (PTB)	
PGM	30 – 1,800	F. Scholze (PTB)	
HE-SGM	200 - 700	A. Lippitz (BAM)	O. Schwarzkopf
Optics-BL	20 – 2,000	F. Senf	
KMC 2	4.5 k - 15 k	A. Erko	I. Packe
PM 3	20 – 1,900	T. Kachel	F. Eggenstein
3m-NIM-1	4 - 35	I. Packe	G. Reichardt
EDR	2 k - 12 k	W. Leitenberger (Uni P) Y. Bodenthin (Uni P)	A. Erko
TGM 4	8 - 120	K. Godehusen	M. Mast
TGM 7	8 - 120	C. Pettenkofer (HMI) W. Bremsteller (HMI)	
PGM-RD-BL	30 – 1,500	Y. Dedkov (Uni D) S. Molodtsov (Uni D)	
CP-NIM	4 - 35	F. Schäfers	M. Mertin

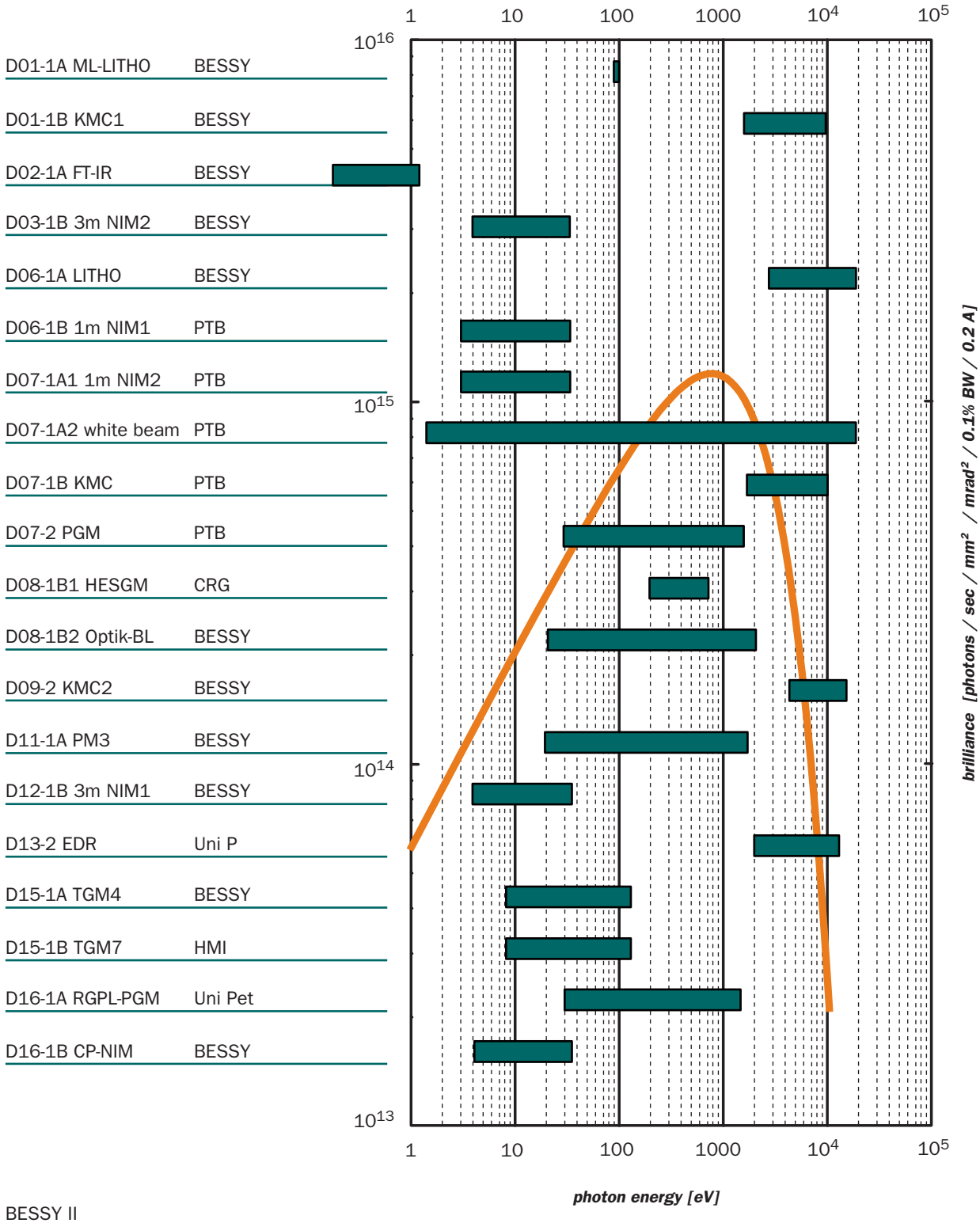

BESSY II
1.7 GeV, 200 mA coupling 1%

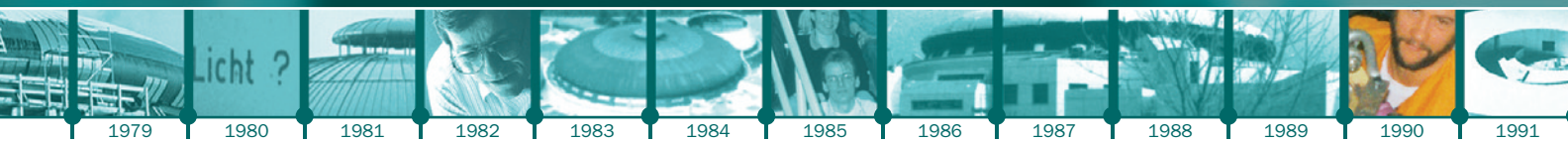

Experimental stations

For more information please look on the BESSY website (www.bessy.de) or contact W. Braun (braun@bessy.de) or Ch. Jung (jung@bessy.de).

Experiment	Contact	Location	
THz spectroscopy[BioSR, Ind]	holldack@bessy.de	IR	IR
IR-spectroscopy and -microscopy[BioSR, Ind]	schade@bessy.de	IR	
IR ellipsometry[Ind]	hinrichs@isas-berlin.de	IR	
HIRES - high resolution electron spectrometer	rader@bessy.de	variable	UV
UVIS - protein circular dichroism spectroscopy[BioSR]	baumgaer@rz.uni-potsdam.de	3m-NIM-1	
PHOENEXS - photoemission and near edge X-ray spectroscopy	bressler@bessy.de	variable	
MUSTANG - multi-user stage for angular resolved photoemission	giannina-nicoletta.gavrila@bessy.de mike.sperling@bessy.de	variable	
SAMIC - spectroscopy and microscopy integrating chamber[Ind]	patrick.hoffmann@tu-cottbus.de	U49/2-PGM/2	VUV
Two-Photon-Photoemission Experiment	weinelt@mbi-berlin.de	variable	
SURICAT - photoelectron and absorption spectroscopy[Ind]	antje.vollmer@bessy.de	optics beamline	
SPEEM - spin resolved photoemission microscopy[planned]	hermann.duerr@bessy.de	UE49-PGM a	
HIRE-PES - energy resolution photoemission	christoph.jannowitz@physik.hu-berlin.de	variable	
Stored Nano Particels	ruehl@phys-chemie.uni-wuerzburg.de	variable	
Ps-PEEM - time resolved photoemission microscope in the ps-regime[Ind]	schoenhe@mail.uni-mainz.de	variable	
High resolution spinpolarisation photoelectron spectroscopy	c.m.schneider@fz-jülich.de	variable	XUV
So-Li-AS - solid-liquid-analysis system	mayerth@surface.tu-darmstadt.de	variable	
VUV/XUV ellipsometry[Ind]	esser@isas-berlin.de	variable	
Scattering experiments in the VUV/XUV-range	eugen.weschke@physik.fu-berlin.de	variable	
MPG high-pressure XPS[Ind]	knop@fhi-berlin.mpg.de	variable	
EUV-lithography[Ind]	scheunemann@bessy.de	variable	
X-ray lithography[Ind]	loechel@bessy.de	variable	
Fluorescence spectroscopy[Ind]	ruediger.mitdank@physik.hu-berlin.de	variable	
Soft X-ray emission spectrometer	eisebitt@bessy.de	variable	
CISSY - CIS- diagnostic using Synchrotron radiation	fischer@hmi.de	variable	X-ray
ROSA - rotateable spectrometer apparatus	szargan@rz.uni-leipzig.de	variable	
SMART - spectro-microscope	thomas.schmidt@physik.uni-wuerzburg.de	UE52-PGM	
XM - X-ray Microscopy[BioSR, Ind]	guttmann@bessy.de	U41-XM	
Reflectometry[Ind]	schaefers@bessy.de	optics beamline	
Polarimetry	schaefers@bessy.de	variable	
Diffraction, XANES, EXAFS	erko@bessy.de	KMC-2	
micro-XANES, -EXAFS, -fluorescence[BioSR]	erko@bessy.de	7T-WLS-1	
X-ray diffraction during MBE	braun@pdi-berlin.de	U125/2-KMC	
Protein crystallography[BioSR, Ind]	umue@bessy.de	7T-WLS-2	
BAMline - nondestructive testing in analytical chemistry[Ind]	heinrich.riesemeier@bam.de	7T-WLS-1	
EDDI - energy dispersive diffraction	genzel@hmi.de	7T-MPW	
MagS - resonant magnetic scattering	feyerherm@hmi.de	7T-MPW	

[planned] under construction *[BioSR] suitable for biological samples* *[Ind] suitable for industrial users*

The multipurpose infrared beamline

was built for biological and materials science investigations. The beamline utilises infrared synchrotron radiation from a bending magnet. Due to the large angle acceptance the beamline provides useful intensities from the near to the far infrared over the energy range from about 10,000 down to 2 cm^{-1}.

The IR beamline can be used for spectroscopic and microscopic investigations of biological systems and for investigations on the structural and functional interactions of proteins. Additionally, the beamline is available to study vibrational, structural, and electronic properties of bulk materials, surfaces and thin layer systems.

The beamline is equipped with several experimental stations comprising of two Fourier transform infrared spectrometers (Nicolet, Bruker), an mid infrared microscope (Nicolet), a mid-infrared ellipsometer (ISAS) and a near-field microscope dedicated to the THz range (BESSY). To investigate samples at different temperatures suitable cryostats working between 4 K and room temperature are available.

A dedicated THz beamline on a bending magnet was built for diagnostics at the “femtoslicing” source. The beamline is designed for the very far infrared between 0.1 and 10 THz and has been successfully used for the femtosecond-laser electron bunch overlap diagnostics using a fast InSb detector. The beamline will be open for external users in 2006.

The MUSTANG (Multi User STage for ANGular resolved photoemission)

is a two chamber system with preparation and analysis chamber to perform a variety of experiments such as UPS, LEIS, XPS, SSXPS (Small Spot XPS), AES, SAM, ISS, and NEXAFS. The load lock and transfer system from Omicron allows to store up to 4 samples under UHV conditions and additional 6 samples under HV conditions.

To maintain a wide range of sample preparation techniques the setup includes a SPECS scanable sputter gun, two TECTRA electron beam evaporators, a quartz microbalance, a quadrupol mass spectrometer, and a gas inlet system. Three kind of sample heaters (resistant heater, direct current heater through the sample surface and electron beam heater), the possibility to cool the sample down to -160°C, and the option to combine heating, cooling, sputtering and evaporation at the same time allows a wide range of sample creation and preparation.

Multiple detectors are available, i.e. an hemispherical energy analyzer PHOIBOS 150 and an ERLEED. The 9 channeltron detector will be replaced soon by a channelplate detector allowing angular resolved scans with an angular acceptance of up to ± 8° and an angular resolution down to 0,1°.

MUSTANG went into operation in January 2003 under the direction of A. Goldmann (Universität Kassel) and is now supervised D. Zahn (Universität Chemnitz).

The CISSY end station

is dedicated to the material characterisation of components of '**CIS**' ($CuInS_2$) thin film solar cells, to push a knowledge-based development of solar modules of the next generation.

CISSY combines soft X-ray emission (XES) and photoelectron (PES) spectroscopy with in-situ preparation in a single ultra-high vacuum apparatus, allowing the deposition of materials layer by layer to be interrupted for the contamination-free analysis of (buried) interfaces, surfaces, and bulk materials. XES and PES have been shown to give valuable complementary information about the elemental and chemical composition from different depths (PES ~1 nm, XES ~100 nm) as well as laterally resolved composition maps of the cells.

CISSY consists of a central analytical chamber equipped with an XES 300 spectrometer (Gammadata Scienta) as well as a CLAM 4 electron analyser (VG Vacuum Systems) for PES. The adjacent preparative chamber includes an ion gun for surface cleaning, a sputter deposition unit and a glove box for wet chemical layer deposition or surface treatments. Samples can also be introduced through a load lock or transferred via a permanently pumped vacuum transport unit. A central motor driven manipulator with five degrees of freedom allows sample transfer and precise positioning of samples relative to beam and spectrometers. Computer controlled scanning of the samples under the synchrotron beam with µm accuracy allowing 2D laterally resolved XES and PES analyses has been developed by HMI. For the in-situ observation of wet chemical processes at the liquid/solid interface an XES wet cell with a 100 nm Si_3N_4 window is available.

CISSY has been built in network between the Hahn-Meitner-Institut, the University of Würzburg, BESSY und Shell Solar GmbH and is funded by BMWi and BMBF.

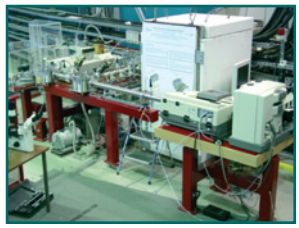

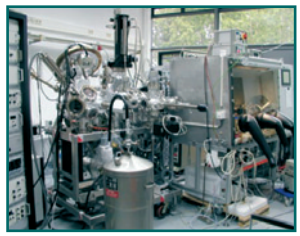

Contact:
Ulrich Schade
ulrich.schade@bessy.de

Karsten Holldack
karsten.holldack@bessy.de

Mike Sperling
mike.sperling@bessy.de

Christian-Herbert Fischer
fischer@hmi.de

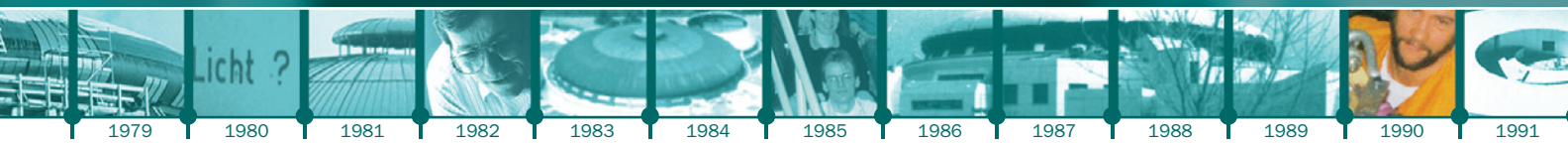

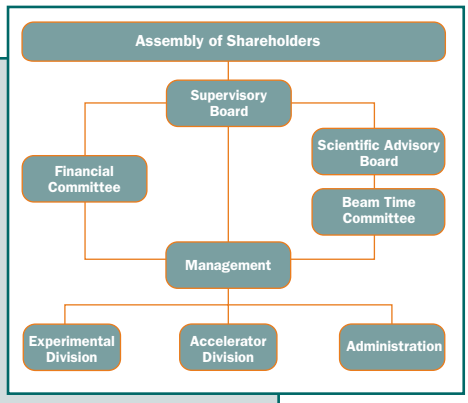

Supervisory Board:

Prof. Dr. J. Treusch (Chairman)	Forschungszentrum Jülich
Prof. Dr. E. Umbach (Vice Chairman)	Universität Würzburg
Min.Dir. Dr. H.F. Wagner	Bundesministerium für Bildung und Forschung
Prof. Dr. E. O. Göbel	PTB, Braunschweig
Prof. Dr. R. Maschuw	Forschungszentrum Karlsruhe
Dr. H. Braun	Max-Planck-Gesellschaft München
Frau Prof. Dr.-Ing. L. Blessing	Technische Universität Berlin
Prof. Dr. J. Schneider	DESY Hamburg
Dr.-Ing. P. Szent-Ivanyi	Bundesministerium für Wirtschaft und Arbeit, Berlin
Prof. Dr. M. Steiner	Hahn-Meitner-Institut, Berlin
Senatsdirig. W. Eckey	Senatsverwaltung für Wissenschaft, Forschung und Kultur Berlin

Scientific Advisory Committee:

Prof. Dr. R. Schlögl (Chairman)	Fritz-Haber-Institut, Berlin
Prof. E.J. Nordgren (Vice Chairman)	Universität Uppsala
Prof. D.S. Chemla	ALS Berkeley
Prof. Dr. T. Elsässer	Max-Born-Institut, Berlin
Dr. John Galayda	Stanford Synchrotron Radiation Laboratory (SSRL)
Prof. Dr. Adam Hitchcock	McMaster University Hamilton, Ontario
Priv.-Prof. Dr. Ilme Schlichting	Max-Planck-Institut für medizinische Forschung Heidelberg
Prof. Dr. Hans-Peter Steinrück	Universität Erlangen-Nürnberg
Prof. Dr. Günther Tränkle	Ferdinand-Braun-Institut für Höchstfrequenztechnik
Prof. Dr. Joachim Ullrich	Max-Planck-Institut für Kernphysik Heidelberg
Prof. Dr. Richard Walker	Rutherford Appleton Laboratory (Diamond) Chilton Didcot

Permanent Guests

Dr. Josef Feldhaus	HASYLAB/DESY Hamburg
Prof. Dr. Raimund Gerhardt-Multhaupt	Universität Potsdam
Prof. Dr. Helmuth Möhwald	Max-Planck-Institut für Kolloid- und Grenzflächenforschung
Prof. Dr. Jürgen Richter	Bundesministerium für Bildung und Forschung
Dr. R. Schuchhardt	Senatsverwaltung für Wissenschaft, Forschung und Kultur Berlin

Beam Time Committee

Prof. Dr. E. Rühl (Chairman)	Universität Würzburg
Prof. Dr. W. Wurth (Vice Chairman)	Universität Hamburg
Dr. D. Arvanitis	Universität Uppsala
Prof. Dr. S. Blügel	Forschungszentrum Jülich
Prof. Dr. T. Elsässer	Max-Born-Institut, Berlin
Prof. Dr. J. Fink	IFW Dresden
Prof. Dr. K. Horn	Fritz-Haber-Institut, Berlin
Prof. Dr. K.-H. Schartner	Universität Gießen
Prof. Dr. L. Singheiser	Forschungszentrum Jülich
Prof. Dr. Günther Tränkle	Ferdinand-Braun-Institut für Höchstfrequenztechnik

Subcommittee Protein Crystallography

Prof. Dr. R. Ficner	Universität Göttingen
Prof. Dr. P. Lindley	Universität Lissabon
Dr. M. Wilmanns	EMBL Hamburg

Financial Committee

S. Lettow (Chairman)	Forschungszentrum Karlsruhe
R. Kellermann (Vice Chairman)	Forschungszentrum Jülich
Dr. W. Buck	PTB, Berlin
M. Schleier	Max-Planck-Gesellschaft, München
Dr. R. Schuchardt	Senatsverwaltung für Wissenschaft, Forschung und Kultur Berlin
H. Görres	Bundesministerium für Bildung und Forschung

User Committee

Dr. Uwe Hergenhahn	MPI für Plasmaphysik, München
Dr. Wolfgang Braun	Paul-Drude-Institut, Berlin
Dr. Christian-Herbert Fischer	Hahn-Meitner-Institut, Berlin
Dr. Ralf Püttner	Freie Universität Berlin

Contact

Scientific Director

Prof. Dr. Dr. h.c. Wolfgang Eberhardt
Secretary: Ines Maupetit
phone +49 (0)30 / 6392 4633
fax +49 (0)30 / 6392 2989
wolfgang.eberhardt@bessy.de,
ines.maupetit@bessy.de

Technical Director

Prof. Dr. Eberhard Jaeschke
Secretary: Dr. Nikoline Hansen
phone +49 (0)30 / 6392 4651
fax +49 (0)30 / 6392 4632
eberhard.jaeschke@bessy.de,
nikoline.hansen@bessy.de

Administration

Thomas Frederking
Secretary: Katrin Rosenblatt
phone +49 (0)30 / 6392 2901
fax +49 (0)30 / 6392 2920
thomas.frederking@bessy.de,
katrin.rosenblatt@bessy.de

Beamtime Coordination

Dr. Walter Braun, Dr. Gerd Reichardt
Secretary: Stine Mallwitz
phone +49 (0)30 / 6392 2904
fax +49 (0)30 / 6392 4673
beamtime@bessy.de

User Office

Daniela Baum, Maha Dürr
phone +49 (0)30 / 6392 4734
fax +49 (0)30 / 6392 4746
useroffice@bessy.de

Public Relations

Dr. Heike Henneken,
Dr. Markus Sauerborn
phone +49 (0)30 / 6392 4921
fax +49 (0)30 / 6392 4972
pr@bessy.de

Credits:

For providing photographs and drawings we would like to thank:
3dworks visual
andidas.deviantart.net
Andrew Giddings
Armin Okulla
Bernhard Schurian
fischerAppelt
Ferdinand-Braun Institut für Höchstfrequenztechnik
Gastroeinrichter Peter Engel und Falk Schulze GmbH
House of Brick Technologies, LLC
Hybrid Medical Animations
Martin Basel
NTNU Info / Rune Petter Ness
Stephan Rentenberger
www.fitnesstrainingbyjon.com

Following BESSY staff members opened their 'historic archives':
Kai Godehusen, Franz Schäfers, Christian Jung, Walter Braun, Andreas Gaupp, Klaus Bürkmann-Gehrlein, Wolfram von Scheibner, Hans Bäcker, Helmuth Petersen †